

# STRUCTURE ACTIVITY RELATIONSHIPS IN PYRIDOXAL-5'-PHOSPHATE

## DEPENDENT ENZYMES

by

SANTIAGO LIMA

(Under the Direction of Robert S. Phillips)

### ABSTRACT

Pyridoxal-5'-phosphate (PLP) dependent enzymes are a large and catalytically diverse group of proteins primarily involved in the metabolism of amino acids, amino acid derived compounds, and amino sugars. In this work, three PLP-dependent enzymes, *Homo sapiens* kynureninase, *Pseudomonas dacunhae* L-aspartate- $\beta$ -decarboxylase, and *Pyrococcus furiosus* tryptophan synthase  $\beta$ -subunit homolog are studied using a variety of biophysical methods. The novel crystal structures for these enzymes are presented, along with the structure of a kynureninase-inhibitor complex, and the analysis of a number of mutants generated to study specific structure activity relationships in them. The results of these analyses reveal the interactions that contribute to substrate specificity in kynureninase, a novel oligomerization scheme and catalytically important residues in aspartate- $\beta$ -decarboxylase, and the elucidation of the kinetic properties of the *P. furiosus* tryptophan synthase  $\beta$ -subunit homolog.

INDEX WORDS: pyridoxal-5'-phosphate, kynureninase, L-kynurenine hydrolase, 3-hydroxykynurenine, 2HZP, L-aspartate-beta-decarboxylase, aspartate-4-decarboxylase, tryptophan synthase beta subunit homolog, trpb2, tryptophan synthase

**STRUCTURE ACTIVITY RELATIONSHIPS IN PYRIDOXAL-5'-PHOSPHATE  
DEPENDENT ENZYMES**

by

SANTIAGO LIMA

BS, The University of Georgia, 2001

A Dissertation Submitted to the Graduate Faculty of The University of Georgia in Partial  
Fulfillment of the Requirements for the Degree

DOCTOR OF PHILOSOPHY

ATHENS, GEORGIA

2008

© 2008

Santiago Lima

All Rights Reserved

**STRUCTURE ACTIVITY RELATIONSHIPS IN PYRIDOXAL-5'-PHOSPHATE  
DEPENDENT ENZYMES**

by

SANTIAGO LIMA

Major Professor: Robert S. Phillips  
Committee: Michael W. W. Adams  
Cory Momany  
Bi-Cheng Wang

Electronic Version Approved:

Maureen Grasso  
Dean of the Graduate School  
The University of Georgia  
May 2008

## DEDICATION

I would like to dedicate this dissertation to my parents and sister who have stood by and supported, always believed in me, and encouraged me to believe in myself. I would also like to dedicate this work to my advisor and friend Dr. Robert S. Phillips for his invaluable guidance, patience, encouragement, and dedication to teaching.

## ACKNOWLEDGEMENTS

The work contained in this dissertation is the fruit of hard work, luck, and extensive collaboration. I would like to thank Dr. Cory Momany for supplying me with a great experience in learning the techniques and theory behind macromolecular X-ray crystallography. I would also like to thank Dr. Michael W.W. Adams, for his fair and cunning scientific input to my research, and Dr. Bi-Cheng Wang for taking time out of his busy schedule to serve on my committee.

## TABLE OF CONTENTS

	Page
ACKNOWLEDGEMENTS .....	v
LIST OF TABLES .....	vii
LIST OF FIGURES .....	viii
INTRODUCTION AND LITERATURE REVIEW .....	1
CHAPTER	
1 Crystal Structure of <i>Homo sapiens</i> kynureninase .....	18
2 Crystal Structure of <i>Homo sapiens</i> Kynureninase-3-hydroxy-hippuric Acid Inhibitor Complex; Insights into the Molecular Basis of Kynureninase Substrate Specificity .....	57
3 The Crystal Structure of the <i>Pseudomonas dacunhae</i> L-Aspartate-Beta Decarboxylase Reveals a Novel Oligomeric Assembly for a Pyridoxal-5'-Phosphate Dependent Enzyme .....	82
4 Atomic Structure and Substrate Specificity of the <i>Pyrococcus furiosus</i> Tryptophan Synthase $\beta$ -Subunit Homolog .....	110
CONCLUSIONS.....	138

## LIST OF TABLES

	Page
Table 1.1: Summary of Crystallographic analysis.....	47
Table 2.1: Summary of Crystallographic Analysis.....	78
Table 2.2: Summary of L-kynurenine and 3-OH-DL-kynuenine kinetic constants for wild type and kynureninase mutants.....	79
Table 3.1: Summary of Crystallographic analysis.....	104
Table 4.1: Summary of Crystallographic analysis.....	130
Table 4.1: Summary of kinetic constants measured for tryptophan synthases form <i>S. typhimurium</i> and <i>P. furiosus</i> . ....	131

## LIST OF FIGURES

	Page
Figure 1.1: Ribbon drawing of the kynureninase biologically active unit with secondary structure elements colored in a blue to red progressing scheme. ....	48
Figure 1.2: Stereo ribbon drawing of the kynureninase monomer with secondary structure elements colored in a blue to red progressing scheme .....	49
Figure 1.3: Map calculated with likelihood-weighted 2Fo-Fc coefficients for the area surrounding the pyridoxal-5'-phosphate-Lys-276 internal aldimine complex.....	50
Figure 1.4: Stereo image of the kynureninase active site PLP hydrogen bonding interactions.....	51
Figure 1.5: Structural superposition between dimers of human and <i>Pseudomonas fluorescens</i> kynureninases. ....	52
Figure 1.6: Stereo image of 3-hydroxy-L-kynurenine docked with human kynureninase. ....	53
Figure 1.7: Ribbon drawing of the Hkyn small domain S20-S21 $\beta$ -hairpin and equivalent hairpins from the structures with PDB IDs 1qz9, 1m32, 1jf9, 1ibj, 1i29, 1h0c, 1fg3, 1d2f, 1bj4, and 2ch2. ....	54
Figure 1.8: Comparison of the superimposed small domains of aspartate aminotransferase in open and closed conformation with the <i>Homo sapiens</i> kynureninase and the <i>Pseudomonas fluorescens</i> kynureninase .....	55
Figure 1.9: Active site amino acid differences between human and <i>P. fluorescens</i> kynureninases in the vicinity of the 3-hydroxyl moiety of docked 3-hydroxy-L-kynurenine. ....	56
Figure 2.1: An electron density map showed continuous electron density for 3-HHA atoms .....	80

Figure 2.2: Stereo representation of the interactions that stabilize 3-HHA (colored green, ball and stick atoms) within the Homo sapiens kynureninase active site .....	81
Figure 3.1: ABDC monomer with successive secondary structure elements labeled.....	105
Figure 3.2: The ABDC active site is composed of residues contributed from two monomer chains related by a 2-fold axis of symmetry.....	106
Figure 3.3: Active sites of structurally superposed ABDC and <i>E. coli</i> AAT .....	107
Figure 3.4: Ribbon representation of the ABDC dodecamer with each monomer labeled. ....	108
Figure 3.5: Schematic illustrating the symmetry relationships between monomers in the ABDC particle.....	109
Figure 4.1: PfTrpB2 monomer with secondary structure elements labeled.....	132
Figure 4.2: A structural superposition between the <i>PfTrpB2</i> and <i>PfTrpB1</i> identifies substitutions among residues surrounding the PLP cofactor.....	133
Figure 4.3: The <i>StTrpAB1</i> complex has an intramolecular tunnel through which indole is diffused from the $\alpha$ -subunit to the $\beta$ -subunit.....	134
Figure 4.4: The <i>StTrpAB1</i> complex has an intramolecular tunnel through which indole is diffused from the $\alpha$ -subunit to the $\beta$ -subunit.....	135
Figure 4.5: Spectral changes associated with the sequential addition of 5 mM L-L-cys, and 0.1 mM indole, to a solution containing PfTrpB2.....	136
Figure 4.6: Initial rate vs [S] profiles for the L-ser/L-cys + indole condensation catalyzed by PfTrpB1, PfTrpAB1, StTrpAB1, and StTrpB1.....	137

## INTRODUCTION AND LITERATURE REVIEW

Pyridoxal-5'-phosphate (PLP) is the phosphate ester and catalytically active form of vitamin B6. Enzymes utilizing PLP as a cofactor are among the most catalytically diverse group of proteins, containing members in five of six (1) Enzyme Commission (2) (EC) groups, which equates to approximately 4% of the reactions catalogued in the EC (3). It is believed that up to 1.5 % of all prokaryotic genes encode for PLP-dependent enzymes (1). Many cellular processes involved in the biosynthesis of amino acids, amino acid-derived compounds, and amino sugars (4) are catalyzed by enzymes that utilize PLP as a cofactor. In humans, a number of diseases such as epilepsy, African sleeping sickness, and Parkinson's disease are treated by specifically targeting PLP-dependent enzymes (5-7). Also, a number of these proteins have been proposed as possible drug targets in the treatment of maladies including cancer (8), Alzheimer's disease (9, 10), AIDS related dementia (11, 12), Huntington's disease (13, 14), and malaria (15).

The catalytic versatility of PLP-catalyzed reactions arise from the cofactor's ability to stabilize  $\alpha$ -carbanionic intermediates generated during catalysis by delocalizing electrons into the PLP pyridine ring  $\pi$ -system. The majority of enzymes that utilize this prosthetic group covalently bind it *via* a Schiff base linkage with the  $\epsilon$  amino group of a strictly conserved active site lysine residue. This enzyme-PLP covalent adduct is commonly known as the internal aldimine and has characteristic spectroscopic properties that are indicative of the protonation state of the cofactor-enzyme complex. Incoming amino acid substrates undergo a transamination reaction via the formation of a geminal diamine to form a covalent complex with PLP that is referred to as the external aldimine.

Reaction specificity is controlled by the relative geometrical arrangement between substituents on the amino acid  $\alpha$  carbon and the cofactor-imine  $\pi$  system (16). By aligning the bond to be broken in a plane perpendicular to the imine-pyridine ring system,  $\sigma$ - $\pi$  bond overlap is maximized and the energy of the transition state is minimized (16). Upon cleavage of the scissile bond, PLP-dependent reactions proceed *via* formation of a resonance stabilized quinonoid intermediate (17, 18) that is central to most reactions catalyzed by these enzymes (19). In reactions in which the  $\alpha$ -proton is aligned in said manner, its removal leads to reactions such as racemization, cyclization,  $\beta$ -eliminations and replacement. Additionally, loss of the  $\alpha$  proton with reprotonation of the quinonoid species at C-4' produces a ketimine intermediate characteristic of transamination,  $\gamma$ -elimination, and replacement. Alignment of the  $\alpha$ -carboxylate and its subsequent elimination leads to the loss of CO<sub>2</sub> seen among  $\alpha$ -decarboxylases. Finally, the alignment of side chain atoms leads to reactions such as  $\beta$ -condensation and aldol cleavage.

Although PLP-dependent enzymes catalyze a large number chemically diverse reactions they are composed of five basic structural scaffolds (20). This is the primary basis of classification for enzymes within the PLP-dependent enzyme superfamily. Each “family” is named after the first member whose structure was solved and are thus named the aspartate aminotransferase (AAT) or  $\alpha$ -family (fold type I), the tryptophan synthase or  $\beta$ -family (fold type II), the alanine racemase family (fold type III), the D-amino acid aminotransferase family (fold type IV), and the glycogen phosphorylase family (fold type V). Fold type V enzymes are mechanistically different from other PLP-dependent enzymes since they utilize the phosphate moiety for proton transfer.

The primary focus of this dissertation is to elucidate previously unknown structures and answer specific questions regarding functional aspects of three PLP-dependent enzymes.

Specifically, the *Homo sapiens* kynureninase, *Pseudomonas dacunhae* L-aspartate- $\beta$ -decarboxylase, and the *Pyrococcus furiosus* tryptophan synthase  $\beta$ -subunit homolog are studied using a variety of biophysical methods.

Kynureninase has been recognized as an important pharmaceutical target (3, 21-24) since it is a member of a metabolic pathway implicated in the production of a potent neurotoxin, quinolinic acid (25). The etiology of a large number of neurodegenerative diseases has been correlated with the overproduction of this endogenous neurotoxic metabolite (9, 11, 12, 14, 26-30). As such, the primary aim of studying this enzyme was to provide essential components of the drug design process: a native crystal structure, an enzyme-inhibitor complex, and active site-ligand interactions critical to substrate specificity. In this work, the first cloning, recombinant expression, purification, characterization, crystallization, the first atomic structure of *H. sapiens* kynureninase, and the crystal structure of *H. sapiens* kynureninase complexed with the competitive inhibitor 3-hydroxyhippuric acid (3-HHA) are reported. Furthermore, data presented on several active site mutants clearly shows that residues involved in conveying substrate specificity to the *H. sapiens* kynureninase have been identified.

The *P. dacunhae* L-aspartate- $\beta$ -decarboxylase is an important structural target among PLP-dependent enzymes because of its oligomerization into dodecameric particles (31-33). Also, the catalytic cycle in these enzymes has been shown to result in the inversion of stereochemistry about the product's  $\beta$ -carbon; an uncommon reaction among PLP-dependent enzymes. This mechanism appears to require the involvement of two catalytic bases, the identity of which remained uncharacterized. In this work the cloning, recombinant expression, new crystallization conditions, and the first atomic structure of the dodecameric assembly are reported. Based on an analysis of the crystal structure, the role of the active site residue Arg-37 is evaluated as a

possible second catalytic base and data obtained from site-directed mutagenesis experiments provide some evidence to support such a role.

Finally, a variety of studies aimed at determining the metabolic function of tryptophan synthase  $\beta$ -subunit homolog is presented. These recently discovered homologs are almost exclusively found outside the architecture of the *trp* operon (34), and are found in the genomes of organisms containing full, incomplete, or none of the *trp* operon genes (35). Previous studies with a related tryptophan synthase  $\beta$ -subunit homolog from *Thermotoga maritima* suggested that these enzymes function as scavengers for indole escaping the canonical tryptophan synthase reaction (36). Although their data supports such a scenario, the analysis of the kinetic properties of the *P. furiosus* tryptophan synthase  $\beta$ -subunit homolog (PfTrpB2) in this work suggests otherwise. The data from this analysis indicates that these enzymes have a higher binding affinity for L-serine (approx. 10-fold) than previously reported (36), and furthermore, shows that these enzymes have a binding affinity for the amino acid L-cysteine (L-cys) similar to that of L-serine (L-ser). Results indicate that, unlike canonical tryptophan synthases, tryptophan synthase  $\beta$ -subunit homologs show no significant preference for L-cys or L-ser. This suggests that organisms containing the tryptophan synthase  $\beta$ -subunit homolog can utilize either amino acid for the biosynthesis of L-tryptophan (L-trp), a previously uncharacterized enzymatic reaction leading to the production of this essential metabolite.

In order to better define the substrate specificity of PfTrpB2, an L-ser/L-cys substrate specificity profile was established for the *P. furiosus* tryptophan synthase  $\alpha_2\beta_2$  complex (PfTrpAB1), the *P. furiosus* tryptophan synthase  $\beta_2$  subunit (PfTrpB1), the *Salmonella typhimurium*  $\alpha_2\beta_2$  tryptophan synthase complex (StTrpAB1), and the *S. typhimurium* tryptophan synthase  $\beta_2$  subunit (StTrpB1).

## Background

### Kynureninase

Mammalian kynureninase [E.C. 3.7.1.3] is a pyridoxal-5'-phosphate (PLP) dependent constitutive (37) enzyme that catalyzes the hydrolytic cleavage of 3-hydroxy-L-kynurenine to yield 3-hydroxyanthranilic acid and L-alanine (L-ala). Kynureninase belongs to the PLP-dependent AAT superfamily (20, 38) ( $\alpha$ -family). In mammals, it is a member of the catabolic cascade known as the "kynurenine pathway" (39) through which the majority of dietary tryptophan is hepatically degraded (22) and provides metabolites for the *de novo* biosynthesis of  $\text{NAD}^+$  in the absence of niacin (39, 40). In extrahepatic cells, kynurenine pathway genes are expressed in macrophages and microglia, although the primary metabolite produced in these cells appears to be quinolinic acid (QA) and not  $\text{NAD}^+$  (41, 42). QA is a known agonist of NMDA sensitive glutamergic ionotropic receptors and is thus an excitotoxin. It is also a known necrotic agent of cultured neuron cells (43) and prolonged exposure causes excitotoxic damage at concentrations ten times below physiological levels (44). Excessive quinolinate in CNS tissues resulting from the overstimulation of the kynurenine pathway is thought to contribute to the etiology of many neurodegenerative diseases including AIDS-related dementia, Alzheimer's, stroke, epilepsy, Huntington's disease, and amyotrophic lateral sclerosis (9, 11, 12, 14, 26-30). The increasing body of evidence implicating changes in normal concentrations of QA in CNS tissues with neurotoxicity has led to the development of the idea that altering the ratio of QA to other kynurenine pathway metabolites could provide a neuroprotective effect during the onset of such maladies (3, 21-24).

Two functional orthologs of kynureninase are known: a constitutive (37), primarily eukaryotic enzyme which catalyzes the hydrolysis of 3-OH-kyn and a prokaryotic inducible (37)

form which has a higher affinity for L-kynurenine (L-kyn) (45). Although both orthologs have been found to catalyze the hydrolysis of their non-cognate substrate, they do so at much slower rates and have lower binding affinities (45, 46). Indeed, a number of organisms are known to contain both orthologs (37). To date, the molecular basis of substrate specificity that allows these enzymes to differentiate between substrates has not been elucidated. Some insight into this mechanism was gained through docking studies with the native crystal structure of *H. sapiens* kynureninase and 3-OH-L-kyn as a ligand (45). These studies revealed that two active site residues, His-102 and Asn-333, could play an important role in substrate binding and specificity (45).

### **L-Aspartate- $\beta$ -Decarboxylase**

The *P. dacunhae* L-aspartate- $\beta$ -decarboxylase (ABDC) is a PLP-dependent enzyme that catalyzes the  $\beta$ -decarboxylation of L-aspartate (L-asp) to produce L-ala and CO<sub>2</sub>. This prokaryotic enzyme is known for its catalytic versatility (32, 33), its activation by  $\alpha$ -keto acids (33, 47-49), and its use in the industrial-scale biocatalytic synthesis of L-ala by immobilized *P. dacunhae* and other organisms (50, 51). Although some of the ABDC steady-state properties have been extensively studied, many details regarding its catalytic mechanism remain uncharacterized. Previous work has shown that the ABDC catalyzed decarboxylation of L-asp proceeds through an L-asp ketimine intermediate (52). ABDC must direct the  $\beta$ -decarboxylation of the L-asp ketimine to yield an enamine, which is subsequently re-protonated at C- $\beta$  in an inversion of stereochemistry mode (52, 53). However, to yield L-ala, ABDC must prevent ketimine hydrolysis and limit the production of the transamination product, oxaloacetate, to a small fraction of total turnovers (32). Although this implies a handful of mechanistic scenarios, the most likely appears to be one in which there are two bases involved in the

deprotonation/protonation steps (53). Assuming that, as in all other members of the AAT-family of PLP-dependent enzymes, the Schiff base forming active site lysine side chain abstracts and donates a proton to the  $\alpha$ -carbon and PLP C-4' (ketimine formation), then the identity of the second catalytic base is unknown.

The *in vivo* function of ABDC is poorly understood, but as with other decarboxylases, it is thought to function in combination with a dicarboxylate/monocarboxylate antiporter to establish a proton gradient across the membrane that can be used for ATP biosynthesis (54, 55). A similar mechanism is employed by *Escherichia coli* in which arginine or glutamate decarboxylation consumes scalar protons to regulate the intracellular pH and generate ATP (56). *In vitro* studies have shown that ABDC forms homo-dodecameric particles (31-33), has highest activity at pH 5.5, and partially dissociates into dimers with lower catalytic activity as the pH is increased (32). The industrial process used in the production of L-ala by immobilized cells expressing ABDC requires acidic pH values (pH 5.5) for optimal activity (50).

### **Tryptophan Synthase Beta Subunit Homolog**

Tryptophan synthase is a PLP-dependent enzyme that catalyzes the condensation of L-ser and indole to produce L-trp. This enzyme plays a pivotal role in the metabolism of prokaryotes and provides an essential metabolite to higher eukaryotes. Much of our understanding of protein allosteric and conformational regulation stem from decades of studying this enzymatic complex (57). The canonical tryptophan synthase reaction produces L-trp from indole-3-glycerophosphate and L-ser. Yet, the  $\alpha_2\beta_2$  complex can also utilize L-cys as a substrate to produce L-trp (58), but the reaction is much slower than that with L-ser (58, 59). L-Cys binding affinities for the mesophilic tryptophan synthase  $\alpha_2\beta_2$  or tryptophan synthase  $\beta$ -subunit have not been reported in the literature.

*P. furiosus* and many other *Archaea*, hyperthermophilic *Bacteria*, and some plants (60) possess two tryptophan synthase  $\beta$ -subunit genes that encode two separate yet closely related enzymes: the canonical tryptophan synthase  $\beta$ -subunit (TrpB1) and a tryptophan synthase  $\beta$ -subunit homolog (TrpB2) (35). In *P. furiosus*, the *trpB2* gene is located outside of a full set of *trp* operon genes (34), but some *Crenarchaeota*, *Pyrococcus horikoshii*, and hyperthermophilic *Bacteria* possess only *trpB2* and none of the other *trp* operon genes (35). Sequence based comparisons reveal that these enzymes are moderately homologous (28% identity between *P. furiosus* TrpBs), but TrpB1 proteins are on average 50 residues shorter than TrpB2s (35), and the regulatory residues involved in allosteric interactions with the tryptophan synthase  $\alpha$ -subunit (R141 and K167) are not conserved (35, 36). Thus, it is thought that TrpB2s have lost the ability to interact with tryptophan synthase  $\alpha$ -subunits (TrpA). In fact, a study with recombinant TrpA and TrpB2 from *T. maritima* revealed that these proteins do not associate to form an  $\alpha_2\beta_2$  complex, and TrpA does not increase the activity of TrpB2 (36).

TrpB2s are thought to function as either L-ser deaminases (35) or indole scavengers (36). L-Ser deaminase activity has been ascribed on the basis of a genomic analysis in which the absence of L-ser deaminase genes has been correlated with presence of *trpB2* genes (36). This function remains to be experimentally determined. An experimentally based approach determined that recombinant *T. maritima* TrpB2 (TmTrpB2) catalyzes the canonical tryptophan synthase reaction:  $\text{L-ser} + \text{indole} \rightarrow \text{H}_2\text{O} + \text{L-trp}$ , with a  $K_m$  of 50.2 mM and 0.7  $\mu\text{M}$  for L-ser and indole, respectively (36). Based on the low Michaelis constant for indole and low binding affinity for L-ser, it was concluded that the TmTrpB2 is a metabolic scavenging protein used to salvage indole escaping from the putative  $\alpha_2\beta_2$  reaction (36).

Several observations suggest that further investigation of the properties of TrpB2 are needed to understand the physiological role of these enzymes. First, intracellular concentrations of L-ser have been measured in bacteria and found not to exceed 5 mM (61). Thus, the high L-ser  $K_m$  of 50.2 mM (36) observed in TmTrpB2 implies that catalytic turnover into L-trp would rarely occur. Second, a sequence based phylogenetic analysis revealed that although TrpB2 and TrpB1 are closely related, they each represent a distinct family of proteins (35, 36). Third, studies involving the non-coding region upstream of the *Methanothermobacter thermoautotrophicus* TrpB2 (MtTrpB2) revealed the presence of a *trp* repressor protein (TrpY in *M. thermoautotrophicus*) binding site (62). *In vitro* transcription experiments involving the intergenic region immediately upstream of the MtTrpB2 gene showed that the *M. thermoautotrophicus* TrpY regulates the transcription of MtTrpB2 in direct response to L-trp concentrations (62). Thus, regulation of TrpB2 expression by tryptophan suggests that these proteins are likely to be involved in the tryptophan biosynthetic pathways.

## References

- (1) Percudani, R., and Peracchi, A. (2003) A genomic overview of pyridoxal-phosphate-dependent enzymes. *EMBO Rep* 4, 850-4.
- (2) (1992) Enzyme Nomenclature.
- (3) Amadasi, A., Bertoldi, M., Contestabile, R., Bettati, S., Cellini, B., di Salvo, M. L., Borri-Voltattorni, C., Bossa, F., and Mozzarelli, A. (2007) Pyridoxal 5'-phosphate enzymes as targets for therapeutic agents. *Curr Med Chem* 14, 1291-324.
- (4) He, X. M., and Liu, H. W. (2002) Formation of unusual sugars: mechanistic studies and biosynthetic applications. *Annu Rev Biochem* 71, 701-54.
- (5) Kleppner, S. R., and Tobin, A. J. (2001) GABA signalling: therapeutic targets for epilepsy, Parkinson's disease and Huntington's disease. *Expert Opin Ther Targets* 5, 219-39.
- (6) Lees, A. J. (1986) L-dopa treatment and Parkinson's disease. *Q J Med* 59, 535-47.
- (7) Wang, C. C. (1995) Molecular mechanisms and therapeutic approaches to the treatment of African trypanosomiasis. *Annu Rev Pharmacol Toxicol* 35, 93-127.
- (8) Snell, K., and Riches, D. (1989) Effects of a triazine antifolate (NSC 127755) on serine hydroxymethyltransferase in myeloma cells in culture. *Cancer Lett* 44, 217-20.
- (9) Guillemin, G. J., Brew, B. J., Noonan, C. E., Takikawa, O., and Cullen, K. M. (2005) Indoleamine 2,3 dioxygenase and quinolinic acid immunoreactivity in Alzheimer's disease hippocampus. *Neuropathol Appl Neurobiol* 31, 395-404.
- (10) Leonard, B. E. (2007) Inflammation, depression and dementia: are they connected? *Neurochem Res* 32, 1749-56.

- (11) Achim, C. L., Heyes, M. P., and Wiley, C. A. (1993) Quantitation of human immunodeficiency virus, immune activation factors, and quinolinic acid in AIDS brains. *J Clin Invest* 91, 2769-75.
- (12) Heyes, M. P., Brew, B., Martin, A., Markey, S. P., Price, R. W., Bhalla, R. B., and Salazar, A. (1991) Cerebrospinal fluid quinolinic acid concentrations are increased in acquired immune deficiency syndrome. *Adv Exp Med Biol* 294, 687-90.
- (13) Giorgini, F., Moller, T., Kwan, W., Zwillling, D., Wacker, J. L., Hong, S., Tsai, L. C., Cheah, C. S., Schwarcz, R., Guidetti, P., and Muchowski, P. J. (2008) Histone deacetylase inhibition modulates kynurenine pathway activation in yeast, microglia, and mice expressing a mutant huntingtin fragment. *J Biol Chem* 283, 7390-400.
- (14) Heyes, M. P., Swartz, K. J., Markey, S. P., and Beal, M. F. (1991) Regional brain and cerebrospinal fluid quinolinic acid concentrations in Huntington's disease. *Neurosci Lett* 122, 265-9.
- (15) Yuthavong, Y., Kamchonwongpaisan, S., Leartsakulpanich, U., and Chitnumsub, P. (2006) Folate metabolism as a source of molecular targets for antimalarials. *Future Microbiol* 1, 113-25.
- (16) Dunathan, H. C. (1966) Conformation and reaction specificity in pyridoxal phosphate enzymes. *Proc Natl Acad Sci U S A* 55, 712-6.
- (17) Schirch, L., and Jenkins, W. T. (1964) Serine Transhydroxymethylase. Properties Of The Enzyme-Substrate Complexes Of D-Alanine And Glycine. *J Biol Chem* 239, 3801-7.
- (18) Ulevitch, R. J., and Kallen, R. G. (1977) Studies of the reactions of lamb liver serine hydroxymethylase with L-phenylalanine: kinetic isotope effects upon quinonoid intermediate formation. *Biochemistry* 16, 5350-4.

- (19) Schneider, G., Kack, H., and Lindqvist, Y. (2000) The manifold of vitamin B6 dependent enzymes. *Structure* 8, R1-6.
- (20) Jansonius, J. N. (1998) Structure, evolution and action of vitamin B6-dependent enzymes. *Curr Opin Struct Biol* 8, 759-69.
- (21) Stone, T. W., Mackay, G. M., Forrest, C. M., Clark, C. J., and Darlington, L. G. (2003) Tryptophan metabolites and brain disorders. *Clin Chem Lab Med* 41, 852-9.
- (22) Schwarcz, R., and Pellicciari, R. (2002) Manipulation of brain kynurenines: glial targets, neuronal effects, and clinical opportunities. *J Pharmacol Exp Ther* 303, 1-10.
- (23) Stone, T. W., and Addae, J. I. (2002) The pharmacological manipulation of glutamate receptors and neuroprotection. *Eur J Pharmacol* 447, 285-96.
- (24) Tankiewicz, A., Pawlak, D., and Buczko, W. (2001) [Enzymes of the kynurenine pathway]. *Postepy Hig Med Dosw* 55, 715-31.
- (25) Stone, T. W., and Perkins, M. N. (1981) Quinolinic acid: a potent endogenous excitant at amino acid receptors in CNS. *Eur J Pharmacol* 72, 411-2.
- (26) Saito, K., Crowley, J. S., Markey, S. P., and Heyes, M. P. (1993) A mechanism for increased quinolinic acid formation following acute systemic immune stimulation. *J Biol Chem* 268, 15496-503.
- (27) Saito, K., Nowak, T. S., Jr., Markey, S. P., and Heyes, M. P. (1993) Mechanism of delayed increases in kynurenine pathway metabolism in damaged brain regions following transient cerebral ischemia. *J Neurochem* 60, 180-92.
- (28) Saito, K., Nowak, T. S., Jr., Suyama, K., Quearry, B. J., Saito, M., Crowley, J. S., Markey, S. P., and Heyes, M. P. (1993) Kynurenine pathway enzymes in brain: responses to ischemic brain injury versus systemic immune activation. *J Neurochem* 61, 2061-70.

- (29) Sei, S., Saito, K., Stewart, S. K., Crowley, J. S., Brouwers, P., Kleiner, D. E., Katz, D. A., Pizzo, P. A., and Heyes, M. P. (1995) Increased human immunodeficiency virus (HIV) type 1 DNA content and quinolinic acid concentration in brain tissues from patients with HIV encephalopathy. *J Infect Dis* 172, 638-47.
- (30) Sei, Y., Paul, I. A., Saito, K., Layar, R., Hartley, J. W., Morse, H. C., 3rd, Skolnick, P., and Heyes, M. P. (1996) Quinolinic acid levels in a murine retrovirus-induced immunodeficiency syndrome. *J Neurochem* 66, 296-302.
- (31) Bowers, W. F., Czubaroff, V. B., and Haschemeyer, R. H. (1970) Subunit structure of L-aspartate beta-decarboxylase from *Alcaligenes faecalis*. *Biochemistry* 9, 2620-5.
- (32) Wang, N. C., and Lee, C. Y. (2006) Molecular cloning of the aspartate 4-decarboxylase gene from *Pseudomonas* sp. ATCC 19121 and characterization of the bifunctional recombinant enzyme. *Appl Microbiol Biotechnol* 73, 339-48.
- (33) Tate, S. S., and Meister, A. (1971) L-aspartate-beta-decarboxylase: structure, catalytic activities, and allosteric regulation. *Adv Enzymol Relat Areas Mol Biol* 35, 503-43.
- (34) Xie, G., Keyhani, N. O., Bonner, C. A., and Jensen, R. A. (2003) Ancient origin of the tryptophan operon and the dynamics of evolutionary change. *Microbiol Mol Biol Rev* 67, 303-42, table of contents.
- (35) Xie, G., Forst, C., Bonner, C., and Jensen, R. A. (2002) Significance of two distinct types of tryptophan synthase beta chain in Bacteria, Archaea and higher plants. *Genome Biol* 3, RESEARCH0004.
- (36) Hettwer, S., and Sterner, R. (2002) A novel tryptophan synthase beta-subunit from the hyperthermophile *Thermotoga maritima*. Quaternary structure, steady-state kinetics, and putative physiological role. *J Biol Chem* 277, 8194-201.

- (37) Shetty, A. S., and Gaertner, F. H. (1975) Kynureninase-Type enzymes of *Penicillium roqueforti*, *Aspergillus niger*, *Rhizopus stolonifer*, and *Pseudomonas fluorescens*: further evidence for distinct kynureninase and hydroxykynureninase activities. *J Bacteriol* 122, 235-44.
- (38) Mehta, P. K., Hale, T. I., and Christen, P. (1993) Aminotransferases: demonstration of homology and division into evolutionary subgroups. *Eur J Biochem* 214, 549-61.
- (39) Soda, K., and Tanizawa, K. (1979) Kynureninases: enzymological properties and regulation mechanism. *Adv Enzymol Relat Areas Mol Biol* 49, 1-40.
- (40) Magni, G., Amici, A., Emanuelli, M., Orsomando, G., Raffaelli, N., and Ruggieri, S. (2004) Enzymology of NAD<sup>+</sup> homeostasis in man. *Cell Mol Life Sci* 61, 19-34.
- (41) Espey, M. G., Chernyshev, O. N., Reinhard, J. F., Jr., Namboodiri, M. A., and Colton, C. A. (1997) Activated human microglia produce the excitotoxin quinolinic acid. *Neuroreport* 8, 431-4.
- (42) Moffett, J. R., Els, T., Espey, M. G., Walter, S. A., Streit, W. J., and Namboodiri, M. A. (1997) Quinolate immunoreactivity in experimental rat brain tumors is present in macrophages but not in astrocytes. *Exp Neurol* 144, 287-301.
- (43) Chiarugi, A., Meli, E., and Moroni, F. (2001) Similarities and differences in the neuronal death processes activated by 3OH-kynurenine and quinolinic acid. *J Neurochem* 77, 1310-8.
- (44) Giulian, D., Vaca, K., and Noonan, C. A. (1990) Secretion of neurotoxins by mononuclear phagocytes infected with HIV-1. *Science* 250, 1593-6.
- (45) Lima, S., Khristoforov, R., Momany, C., and Phillips, R. S. (2007) Crystal structure of *Homo sapiens* kynureninase. *Biochemistry* 46, 2735-44.

- (46) Toma, S., Nakamura, M., Tone, S., Okuno, E., Kido, R., Breton, J., Avanzi, N., Cozzi, L., Speciale, C., Mostardini, M., Gatti, S., and Benatti, L. (1997) Cloning and recombinant expression of rat and human kynureninase. *FEBS Lett* 408, 5-10.
- (47) Chibata, I., Kakimoto, T., Kato, J., Shibatani, T., and Nishimura, N. (1968) On the activation mechanism of L-aspartate beta-decarboxylase from *Pseudomonas dacunhae* by alpha-ketoglutarate. *Biochem Biophys Res Commun* 32, 375-9.
- (48) Nishimura, J. S., Manning, J. M., and Meister, A. (1962) Studies on the mechanism of activation acid beta-decarboxylase by alpha-keto acids and pyridoxal 5'-phosphate. *Biochemistry* 1, 442-7.
- (49) Novogrodsky, A., Nishimura, J. S., and Meister, A. (1963) Transamination and beta-decarboxylation of aspartate catalyzed by the same pyridoxal phosphate-enzyme. *J Biol Chem* 238, 1903-5.
- (50) Fusee, M. C., and Weber, J. E. (1984) Immobilization by Polyurethane of *Pseudomonas dacunhae* Cells Containing L-Aspartate beta-Decarboxylase Activity and Application to L-Alanine Production. *Appl Environ Microbiol* 48, 694-698.
- (51) Yamakatsu, F., Kiyokazu, Y. (1983) Pressurized Reaction Method for Continuous Production of L-Alanine by Immobilized *Pseudomonas dacunhae* Cells. *J. Ferment. Technol.* 61, 587-591.
- (52) Rosenberg, R. M., and O'Leary, M. H. (1985) Aspartate beta-decarboxylase from *Alcaligenes faecalis*: carbon-13 kinetic isotope effect and deuterium exchange experiments. *Biochemistry* 24, 1598-603.
- (53) Chang, C. C., Laghai, A., O'Leary, M. H., and Floss, H. G. (1982) Some stereochemical features of aspartate beta-decarboxylase. *J Biol Chem* 257, 3564-9.

- (54) Dimroth, P., and Schink, B. (1998) Energy conservation in the decarboxylation of dicarboxylic acids by fermenting bacteria. *Arch Microbiol* 170, 69-77.
- (55) Abe, K., Ohnishi, F., Yagi, K., Nakajima, T., Higuchi, T., Sano, M., Machida, M., Sarker, R. I., and Maloney, P. C. (2002) Plasmid-encoded asp operon confers a proton motive metabolic cycle catalyzed by an aspartate-alanine exchange reaction. *J Bacteriol* 184, 2906-13.
- (56) Richard, H., and Foster, J. W. (2004) *Escherichia coli* glutamate- and arginine-dependent acid resistance systems increase internal pH and reverse transmembrane potential. *J Bacteriol* 186, 6032-41.
- (57) Miles, E. W. (2001) Tryptophan synthase: a multienzyme complex with an intramolecular tunnel. *Chem Rec* 1, 140-51.
- (58) Crawford, I. P., and Ito, J. (1964) Serine Deamination by the B Protein of *Escherichia Coli* Tryptophan Synthetase. *Proc Natl Acad Sci U S A* 51, 390-7.
- (59) Kayastha, A. M., and Miles, E. W. (1991) A colorimetric assay for a pyridoxal phosphate-dependent beta-replacement reaction with L-cysteine: application to studies of wild-type and mutant tryptophan synthase alpha 2 beta 2 complexes. *Anal Biochem* 193, 200-3.
- (60) Sato, S., Kotani, H., Nakamura, Y., Kaneko, T., Asamizu, E., Fukami, M., Miyajima, N., and Tabata, S. (1997) Structural analysis of *Arabidopsis thaliana* chromosome 5. I. Sequence features of the 1.6 Mb regions covered by twenty physically assigned P1 clones. *DNA Res* 4, 215-30.

- (61) Clark, V. L., Peterson, D. E., and Bernlohr, R. W. (1972) Changes in free amino acid production and intracellular amino acid pools of *Bacillus licheniformis* as a function of culture age and growth media. *J Bacteriol* 112, 715-25.
- (62) Xie, Y., and Reeve, J. N. (2005) Regulation of tryptophan operon expression in the archaeon *Methanothermobacter thermautotrophicus*. *J Bacteriol* 187, 6419-29.

## CHAPTER 1

CRYSTAL STRUCTURE OF *HOMO SAPIENS* KYNURENINASE<sup>1</sup>

---

<sup>1</sup> Reproduced with permission from Lima S, Khristoforov R, Momany C, Phillips RS. Crystal structure of *Homo sapiens* kynureninase. 2007. *Biochemistry*. 13;46(10):2735-44. Copyright 2007 American Chemical Society.

## Abstract

Kynureninase is a member of a large family of catalytically diverse but structurally homologous pyridoxal-5'-phosphate dependent enzymes known as the aspartate aminotransferase superfamily or  $\alpha$ -family. The *Homo sapiens* and other eukaryotic constitutive kynureninases preferentially catalyze the hydrolytic cleavage of 3-hydroxy-L-kynurenine to produce 3-hydroxyanthranilate and L-alanine, while L-kynurenine is the substrate of many prokaryotic inducible kynureninases. The human enzyme was cloned with an N-terminal hexahistidine tag, expressed, and purified from a bacterial expression system using Ni-metal ion affinity chromatography. Kinetic characterization of the recombinant enzyme reveals classic Michaelis-Menten behavior, with a  $K_m = 28.3 \pm 1.9 \mu\text{M}$ , and a specific activity of  $1.75 \mu\text{mol min}^{-1} \text{mg}^{-1}$  for 3-hydroxy-DL-kynurenine. Crystals of recombinant kynureninase were obtained that diffracted to  $2.0 \text{ \AA}$ , and the atomic structure of the PLP-bound holoenzyme was solved by molecular replacement using the *Pseudomonas fluorescens* kynureninase structure (PDB accession 1qz9) as the phasing model. A structural superposition with the *P. fluorescens* kynureninase revealed that these two structures resemble the "open" and "closed" conformations of aspartate aminotransferase. The comparison illustrates the dynamic nature of these proteins' small domains and reveals a role for Arg-434 similar to that in other AAT  $\alpha$ -family members. Docking of 3-hydroxy-L-kynurenine into the human kynureninase active site suggests that Asn-333 and His-102 are involved in substrate binding and molecular discrimination between inducible and constitutive kynureninase substrates.

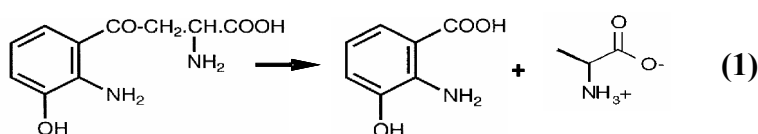
## Abbreviations

HEPES, 4-(2-hydroxyethyl)-1-piperazineethanesulfonic acid; Hkyn, *Homo sapiens* kynureninase; KPi, potassium phosphate; LB, Luria Bertrani Broth; MME, monomethylether;

PEG, polyethylene glycol; Pkyn, *Pseudomonas fluorescens* kynureninase; PLP: pyridoxal-5'-phosphate; KPi, potassium phosphate.

## Introduction

Mammalian kynureninase [E.C. 3.7.1.3] is a pyridoxal-5'-phosphate (PLP) dependent constitutive (1) enzyme that catalyzes the hydrolytic cleavage of 3-hydroxy-L-kynurenine to 3-hydroxyanthranilic acid and L-alanine (Eq. 1).



In contrast, prokaryotic inducible kynureninases preferentially hydrolyze L-kynurenine to yield anthranilic acid and L-alanine. Mammalian kynureninase is a member of the catabolic cascade known as the “kynurenine pathway” (2) through which the majority of dietary tryptophan is hepatically degraded (3), and provides for the de novo biosynthesis of NAD<sup>+</sup> in the absence of niacin (2, 4). In extrahepatic cells, kynurenine pathway genes are expressed in immune system cells such as macrophages, and microglia, although the primary metabolite produced in these cells appears to be quinolinic acid and not NAD<sup>+</sup> (5, 6). Quinolinic acid (QA) is a known agonist of NMDA sensitive glutamnergic ionotropic receptors (7) and is thus an excitotoxin. QA is a known necrotic agent of cultured neuron cells (8), and prolonged exposure causes excitotoxic damage at concentrations ten times below physiological levels (9). Excessive quinolinate in CNS tissues resulting from the overstimulation of the kynurenine pathway is thought to contribute to the etiology of many neurodegenerative diseases including AIDS-related dementia complex, Alzheimer's, stroke, epilepsy, and Huntington's disease (10-18). Since kynureninase acts at a metabolic branch point that directs metabolites to either the production of

quinolinate via kynureninase, or xanthurenic acid via 3-hydroxykynurenine transaminase (3), inhibitors of this enzyme could prevent the overproduction of quinolinate. Thus, inhibitors that specifically target constitutive kynureninases have potential therapeutic value. To this end, the availability of the three dimensional structure of human kynureninase is an important step for rational drug design.

Kynureninase belongs to the PLP-dependent aspartate aminotransferase superfamily fold (19, 20) (or  $\alpha$ -family), subgroup IVa (21). This catalytically diverse group shares very low sequence identity but retains significant structural homology (22). Only a few amino acid residues are conserved among all members: 1) the PLP-enzyme Schiff base forming lysine; 2) an active site aspartate; and 3) a substrate binding arginine invariantly located on a small domain  $\beta$ -hairpin loop (19). In aspartate aminotransferase, this arginine plays an important role in substrate binding and catalysis by stabilizing and orienting the substrate within the active site. Also, the small domains of aspartate aminotransferases are known to undergo conformational changes upon ligand binding (23).

In this work, we report the first cloning, expression, purification, characterization, and crystallization of *Homo sapiens* kynureninase (Hkyn) using a bacterial expression system and the atomic structure to 2.0 Å resolution.

## **Experimental Procedures**

### **Protein Expression and Purification**

The *Homo sapiens* kynureninase was cloned into a pET100 plasmid using a TopoTA-Kit (Invitrogen) after PCR amplification from a placental cDNA clone obtained from the American Type Culture Collection (ATCC MGC-5080; Genbank accession number U57721.gb-pr3) to generate an N-terminal hexahistidine recombinant protein fusion. The resulting plasmid was

sequenced to confirm identity with the Genbank cDNA sequence. The PCR oligonucleotide primers used for amplification were: 5'-GAGCCTTCATCTCTTGAGCTGCC-3' (forward), and 5'- GTTGCCCTAGAAAACACTGCTAA-3' (reverse). A single colony of *Escherichia coli* BL21 (DE3) cells transformed with the recombinant plasmid was inoculated into 1 L of ZYP-5052 medium (24) containing 100 mg L<sup>-1</sup> ampicillin and grown at 37 °C for 20 hours with shaking at 300-325 rpm. Prior to harvesting, the cultures were pre-chilled for 1 hour at 4 °C and then collected by centrifugation at 2500 × g for 15 minutes at 4 °C. Cell pellets were resuspended in 30 mL of ice-cold buffer (0.3 M NaCl, 0.05 M KPi, pH 7.0, and 0.1 mM PLP) and sonicated for four cycles of 1 minute intervals followed by 2 minutes on ice. Cell debris was removed by centrifugation for 20 minutes at 25,000 × g and 4 °C. The supernatant was allowed to stand at room temperature for 20 minutes followed by the drop-wise addition of four mL of a 2% protamine sulfate solution (in resuspension buffer), and the resultant cloudy solution was centrifuged for 40 minutes at 25,000 × g at 4 °C. The supernatant was applied to a Ni-CAM (Sigma) resin column pre-equilibrated with buffer A (0.3 M NaCl, 0.05 M KPi, pH 7.0, 0.1 mM PLP, 4 °C) at a rate of 0.5 mL min<sup>-1</sup> at 4 °C. After a 1 hour wash with buffer A (1.5 mL min<sup>-1</sup>), kynureninase was eluted from the column with a 360 minute 0% to 100% buffer B (0.3 M NaCl, 0.05 M KPi, pH 7.0, 0.1 mM PLP, 150 mM imidazole, 4 °C) linear gradient (0.5 mL min<sup>-1</sup>). SDS-PAGE analysis of fractions eluting from the column was used to determine appropriate samples to be pooled and concentrated. Pooled fractions were dialyzed for 6 hours at 4 °C in a 3.5 L solution containing 0.1 M KPi, pH 7.0, 0.1 mM PLP, and then exchanged, via two tenfold dilutions, into 0.05 M HEPES, pH 5.2, and 0.2 mM PLP using Amicon Centriprep centrifugal filter units (YM-30 membrane). Protein concentration was determined using a Bradford (Bio-Rad) assay (25).

## Kinetic Assay

Kynureninase activity was measured at 37 °C by following the absorbance change at  $\lambda_{\text{max}} = 370 \text{ nm}$  as 3-hydroxykynurenine ( $\Delta\epsilon = 4500 \text{ M}^{-1}\text{cm}^{-1}$ ) is converted to 3-hydroxyanthranilate and L-alanine in 30 mM KPi, pH 7.0, and 40  $\mu\text{M}$  PLP. Specific activity assays contained 70  $\mu\text{M}$  3-hydroxy-DL-kynurenine, 40  $\mu\text{M}$  PLP, and 30 mM KPi, pH 7.0.  $K_m$  measurements were performed in 5  $\mu\text{M}$  steps from 0  $\mu\text{M}$  to 100  $\mu\text{M}$  3-hydroxy-DL-kynurenine in quadruplicate assays.

## Crystallization, Structure Determination, and Refinement

High throughput crystallization trials were conducted at the Hauptman-Woodward Institute (26). Screenings were performed with a 11  $\text{mg mL}^{-1}$  kynureninase solution in several buffers: 1) 30 mM MOPS, pH 7, 0.2 mM PLP, 2) 30 mM KPi, pH 7.5, 0.2 mM PLP, 3) 50 mM HEPES, pH 5.2, 0.2 mM PLP, and 4) 30 mM MOPS, pH 7, 0.2 mM PLP, 10% Glycerol.

Kynureninase crystals were grown in-house at 23.5 °C using the microbatch under-oil method (27) by mixing 2  $\mu\text{L}$  of a 9.2  $\text{mg mL}^{-1}$  kynureninase solution in 50 mM HEPES, pH 5.2, 0.2 mM PLP with 2  $\mu\text{L}$  of 0.05 M  $\text{MgCl}_2$ , 0.1 M Tris-Cl, pH 8.0, 25% PEG 3000. Crystals were flash frozen in liquid nitrogen with cryoprotectant containing 0.055 M  $\text{MgCl}_2$ , 0.11 M Tris-Cl, pH 8.0, 33% PEG 3000. X-ray synchrotron data were collected (detector distance 200 mm, 200 frames, 1° oscillations, 5 second exposure,  $\lambda = 0.97934 \text{ \AA}$ ) at the Advanced Photon Source SBC-CAT beamline 19-BM in Argonne, IL (28). Data were processed, scaled, and merged using HKL2000 (29). The merged SCALEPACK (30) intensities were used as input for the MolRep (31) utility in the CCP4 crystallographic suite (32), and a suitable molecular replacement solution was identified using the *Pseudomonas fluorescens* (Pkyn) (PDB (33) accession code 1qz9 (21)) as a model (initial Rvalue = 55.7). All water molecules, hetero atoms, and pyridoxal-

5'-phosphate coordinates were deleted from the molecular replacement model. The electron density for the PLP cofactor was used to evaluate the success of phasing methods. Phases of the highest scoring MolRep solution and the Hkyn sequence were used as input for the automated building package RESOLVE (34) with default set parameters and no input model. The highest scoring RESOLVE solution was refined with Refmac5 (35) in the CCP4 suite with ARP/wARP (36, 37) automated water addition ( $3\sigma$  cutoff). Refined phases were subsequently used as input into the ARP/wARP automated free atom model building utility in CCP4. Two tandem RESOLVE-ARP/wARP cycles produced a kynureninase model covering approximately 83% of the predicted amino acid sequence. Manual building of the remainder of the model and PLP docking were carried out with the XtalView/Xfit (38) CCP4 utility, followed by restrained refinement in Refmac5. A final TLS refinement was used with the following residue segments: 6-52, 53-65, 66-101, 102-111, 112-134, 135-180, 181- 200, 201-252, 253-267, 268-277, 278-285, 286-291, 292-306, 307-329, 330-375, 376-391, 392-413, 414-460. TLS groups were defined based on secondary structure, and were chosen to maximize the improvement in Rfree. MolProbity (39) and Procheck (40) were used to identify errors during the building/refinement process and evaluate the quality of the final structure.

### **Structural Superpositions and Ligand Docking**

Structural superpositions were done using the Hkyn monomer as a reference model with STRAP (41) and the Iterative and Magic Fit utilities in the Swiss PDB viewer (SPDBV) (42). 3-Hydroxy-L-kynurenine was docked into the Hkyn dimer using the molecular docking algorithm Moldock (43) in the Molegro Virtual Docker. Active site cavities were identified using the Molegro Van der Waals molecular surface prediction algorithm with a grid resolution of 0.5 Å. Kynureninase and 3-hydroxy-L-kynurenine atoms were defined using the Molegro atom

definition tool. The pyridoxal-5'-phosphate was defined as a cofactor, and the protonation and hybridization state of individual PLP atoms were defined to correspond to the internal aldimine dipolar ionic tautomer. All water molecules were deleted from the model and hydrogens were added using the Molegro protonation wizard. Arg-434 was modeled to resemble the position of Arg-375 in 1qz9 with XtalView/Xfit. Side chain atoms in Arg-434, Asn-333\* (residues having \* are associated with a second subunit of the dimeric biological unit), Ser-75, and the 3-hydroxy-L-kynurenine 2-amino and 3-hydroxyl group were defined as hydrogen bond donors. The 3-hydroxy-L-kynurenine  $\alpha$ -carboxylate and  $\gamma$ -carbonyl were defined as hydrogen bond acceptors. A total of 50 docking runs with a population size of 200 were calculated over a 15 Å radius surrounding the predicted active site cavity, with a grid resolution of 0.2 Å, and a maximum of 5000 iterations per pose. Pre-positioned ligands were randomized in the predicted active site cavity prior to each docking run, and docking was constrained to the predicted active site cavity.

## **Results**

### **Protein Purification and Kinetic Analysis**

Although *Homo sapiens* kynureninase was expressed in *E. coli* cells from a pET vector under lac control, a pilot expression study revealed that the addition of IPTG or the use of Rosetta cells containing rare tRNAs did not increase the final yield. Also, a large pellet of insoluble protein, which has the same SDS-PAGE molecular weight as the soluble kynureninase fractions, results from each culture. No attempt was made to resolubilize the insoluble protein pellet. The final yield was only increased (by 2 mg per liter) when ZYP-5052 (24) was used as the growth media (as opposed to LB broth). The expression and purification from *E. coli* yields ~ 8.4 mg of crystallization purity grade protein from a 1 L culture. The recombinant enzyme has a

specific activity of  $1.75 \mu\text{mol min}^{-1} \text{mg}^{-1}$ , a  $k_{\text{cat}}$  of  $3.5 \text{ s}^{-1}$ , a  $K_{\text{m}}$  for 3-hydroxy-DL-kynurenine of  $28.3 \pm 1.9 \mu\text{M}$ , and a  $k_{\text{cat}}/K_{\text{m}}$  of  $2.5 \times 10^5 \text{ s}^{-1} \mu\text{M}^{-1}$  for 3-hydroxy-L-kynurenine.

## Crystallization

High-throughput screens of kynureninase in 50 mM HEPES, pH 5.2, and 0.2 mM PLP yielded two crystallization conditions that produced two distinct morphologies. Crystals grow under a range of pH values in HEPES buffers (5.2-7.5) but the best crystals grow with HEPES, pH 5.2. Exchanging the protein buffer from KPi, pH 7.0, to HEPES, pH 5.2, results in a 20%-30% loss of protein mass. Kynureninase is subsequently stable for several weeks at 4 °C in 50 mM HEPES, pH 5.2, 0.1 mM PLP. Crystallization solutions contained: A) 0.1 M tribasic KPi, 0.1 M Tris-Cl, pH 8.0, 40% PEG 4000, and B) 0.05 M MgCl<sub>2</sub>, 0.1 M Tris-Cl, pH 8.0, 25% PEG 3000. Crystals grown in solution A appeared after two days and were small (0.5 x 0.2 x 0.2 mm) pale yellow rhombohedra with Laue symmetry 4/m and cell dimensions  $a = b = 98.8$ ,  $c = 231.1$  Å,  $\alpha = \beta = \gamma = 90^\circ$ . Crystals grown in solution B appeared after two weeks and were dark yellow and block shaped (0.17 x 0.1 x 0.17 mm) with Laue symmetry 2/m, had cell constants  $a = 74.1$ ,  $b = 76.8$ ,  $c = 93.2$ ,  $\beta = 108.7$  Å, and belonged to space group C2. Only data collected with a single crystal grown with crystallization solution B is presented henceforth.

## Model Geometry

The final kynureninase model was refined to 2.0 Å with an  $R_{\text{Free}}$  and R value of 0.195 and 0.150, respectively, (see Table 1.1 for model statistics) with 98% of the cDNA predicted amino acid residues (residues 6-460) fitted to the electron density. An eight residue segment between helix H16 and  $\beta$ -strand S17 (residues 379-386) could not be modeled due to poor electron density and is not included in the PDB file. Cysteine-45 had additional electron density protruding from the  $\gamma$  sulfur atom which was modeled as a cysteine sulfenic acid. The structure

had good geometry with r.m.s. delta deviations from ideal bond lengths of 0.008 Å, and bond angles 1.135° with 97.3%, 2.5%, and 0.2% residues in the favorable, generously allowed, and disallowed regions of the Ramachandran plot, respectively. (Table 1.1). The conformation of the single residue in the disallowed region, Thr-353, appears to be forced into an unusual geometry by a strong hydrogen bond (2.50 Å) between its side chain  $\gamma$  oxygen and the Ala-352 carbonyl oxygen. Electron density is clearly visible between these two atoms. This residue is located on a three residue turn that connects the first (helix H15) and last (helix H16) helices of the large and small domains, respectively, and has excellent electron density at contour levels as high as 1.8  $\sigma$ . The C2 crystallographic unit cell contained one monomer per asymmetric unit, with approximately 53% bulk solvent, and there are 535 water molecules in the final model.

### **Overall Fold**

The biological dimer (Figure 1.1) can be generated by applying the crystallographic symmetry operator  $1-x, y, -z$  to the monomer. Monomers are related by a two-fold rotation axis located at the interface of the large domains. Evaluation of the crystal contacts between molecules revealed only a dimeric kynureninase form; no higher polymerization forms were identified. Each monomer (Figure 1.2) consists of a small domain (residues 9-74 and 354-462) and a large domain (residues 75-353), which have  $\alpha\beta$ -sandwich and Greek key  $\alpha\beta\alpha$  architecture, respectively. The large domain is composed of a seven stranded mixed  $\beta$ -pleated sheet of topology AGFEDBC ( $\beta$ -strands S5-S8, S10, and S11) surrounded by  $\alpha$ -helices H8-H14. The small domain is composed of a four stranded anti-parallel  $\beta$ -pleated sheet ( $\beta$ -strands S17, S18, S20, and S21) of topology ABED surrounded by  $\alpha$ -helices H17-H20. The organization of the secondary structure elements in the small and large domains is consistent with other PLP dependent  $\alpha$ -family members.

Important dimerization contacts are provided by: 1) a two helix bundle formed between residues on  $\alpha$ -helix H4 and its two-fold related counterpart, 2) interactions between residues on  $\beta$ -strand S2 with residues on  $\alpha$ -helix H4, and 3) hydrogen bonding between Ala-164/Asn-318\*, Ser-167/Trp-305\*, His-142/Val-303\*, Ser-174/Val-303\*. The active site is formed at the bottom of a large cavity found at the interface of the large and small domains; it is amphiphilic in nature and has dimensions of 10 Å x 23 Å wide and 16 Å deep. The large domain face of the active site is lined with the hydrophobic side chains of Tyr-226, Phe-225, Leu-310\*, Phe-314\*, Met-316\*, Trp-305\*, and Phe-165, which form a large hydrophobic patch directly above the PLP cofactor. On the opposite side of the active site cleft, the small domain face contains the charged side chains of Gln-402, Asp-426, Arg-434, Arg-428, and Asn-429. The bottom of the active site is lined with the side chains of Ser-75 and His-102\*.

### **PLP-Binding Site**

The electron density returned from the molecular replacement solution showed continuous density between the  $\epsilon$  nitrogen of Lys-276 and the 4' carbon atom of the PLP cofactor (Figure 1.3). This observation is consistent with the presence of an enzyme-PLP internal aldimine complex and follows the observed spectroscopic characteristics of the active enzyme which has a 422 nm absorption maximum. The pyridoxal-5'phosphate molecule is stabilized and properly oriented at the monomer-monomer interface via extensive hydrogen bonding with residues contributed by two-fold related monomer chains (Figure 1.4). Hydrogen bonding between PLP phosphate oxygens and the side chains of residues involved in monomer-monomer contacts (Trp-305\*/Ser-167, Asn-333\*/Gly-278, Asn-333\*/Tyr-275) coordinate residues from both monomer chains within the active site. PLP-phosphate oxygens are within hydrogen bonding distance of atoms on Trp-305\*, Tyr-275, Asn-333\*, Ser-332\*, and Thr-138. Also, a

water bridge appears to coordinate one of the PLP-oxygens with the main chain amide nitrogen of Leu-137. The coenzyme pyridine ring is stabilized via  $\pi$ - $\pi$  stacking interactions with the phenyl ring of Phe-165. Phe-165 is conserved in all kynureninases and it is likely that these enzymes stabilize the PLP pyridine ring through  $\pi$  stacking with the side chain of a phenylalanine residue. The PLP pyridine nitrogen is hydrogen bonded with the side chains of Asp-168 and Asp-250, which are strictly conserved among kynureninases. Density can be observed between the  $\delta$  oxygen of Asp-168 and the PLP pyridine nitrogen. The  $\delta$  oxygens of Asp-168 and Asp-250 share a strong hydrogen bond (2.59 Å) and electron density can be seen extending between these atoms. Aspartate-250 is the expected conserved aspartate involved in PLP binding and maintaining the PLP pyridinium nitrogen protonated (44) among  $\alpha$ -family members. The PLP phenolic 3' oxygen is stabilized by hydrogen bonds with the His-253  $\delta$  nitrogen (2.95 Å) and the Lys-276-PLP aldimine NH ( $\zeta$  nitrogen -3' oxygen distance 2.58 Å). The interactions of Asp-250 and His-253 with PLP atoms fix the pyridine ring as the dipolar ionic tautomer, resulting in the 422 nm absorption peak. The active site is highly solvated with two well ordered water molecules interacting with one of the PLP-phosphate oxygens, and another with the PLP 3' oxygen. Also, water molecules connect active site residues of the large and small domains through a continuous string of seven waters between the  $\delta$  oxygen and nitrogen atoms of Asn-333\*, the His-102\*  $\epsilon$  nitrogen, the main chain carbonyl oxygen of Ser-75, across the active site cavity and passing directly over the aldimine NH towards the His-253  $\epsilon$  nitrogen, and ending at the main chain carbonyl oxygen of Phe-225 in the small domain. Four of the water molecules closest to the side chains of Asn-333\* and His-102\* occupy a large space in the active site that is devoid of any amino acid side chains.

### Comparison with the *Pseudomonas fluorescens* Kynureninase

*Homo sapiens* kynureninase shares 26% sequence identity with the *Pseudomonas fluorescens* ortholog, and a structural superposition reveals a high level of homology with a 1.2 Å<sup>2</sup> R.M.S.D. over 317 amino acid residues. Human kynureninase has an additional  $\alpha$ -helix (helix H1) that is part of a 25 amino acid extension at the N-terminus. There are three additional loops in Hkyn: 1) a fourteen amino acid loop connecting  $\beta$ -strand S2 and  $\beta$ -strand S3 (residues 52-65), 2) a ten amino acid loop between helix H11 and  $\beta$ -strand S7 (residues 191-200), and 3) a nine amino acid loop between helix H16 and  $\beta$ -strand S17 (378-387). For the most part, these extensions are found exclusively in constitutive kynureninase orthologs. Residues that play a role in stabilizing the PLP cofactor are well conserved. However, residues surrounding the PLP-phosphate moiety are much less conserved and include the following variations: Thr<sub>Pkyn</sub>96 to Leu<sub>Hkyn</sub>137, Ser<sub>Pkyn</sub>97 to Thr<sub>Hkyn</sub>138, Thr<sub>Pkyn</sub>131 to Ser<sub>Hkyn</sub>167, Gly<sub>Pkyn</sub>281\* to Ser<sub>Hkyn</sub>332\*, and Thr<sub>Pkyn</sub>282\* to Asn<sub>Hkyn</sub>333\*. Absolutely conserved active site residues include Phe-165, Asp-168, Asp-250, His-253, Cys-273, Tyr-275, Lys-276, Arg-434, and Trp-305\*.

The structural superposition of the Hkyn with Pkyn reveals differences in the quaternary structures not related to the primary structures. These high-order variations lie within elements of the small domain and in a large domain loop between  $\beta$ -strands S15 and S16 (residues 310-320), henceforth referred to as  $\beta$ -strand S15-S16loop, that extends above the active site cavity (Figure 1.5). Conformational differences in the small domain are observed in the  $\beta$ -hairpin formed by  $\beta$ -strands S20 and S21. This hairpin, the S20-S21  $\beta$ -hairpin, contains two arginines conserved among kynureninases and other  $\alpha$ -family members (Arg<sub>Hkyn</sub>434 and Arg<sub>Hkyn</sub>428). Of these, Arg<sub>Hkyn</sub>434, is known to be dynamically and catalytically important in substrate binding and catalysis (45). The side chain  $\zeta$  carbons of these arginines are separated in the superpositioned

structures by 5.9 Å (between Arg<sub>Hkyn</sub>434 and Arg<sub>Pkyn</sub>375) and 11.18 Å (between Arg<sub>Hkyn</sub>428 and Arg<sub>Pkyn</sub>369), respectively. In Hkyn, the side chain of Arg-434 is thoroughly stabilized at the small/large domain interface with hydrogen bonds to the backbone carbonyls of Lys-427 and Tyr-226, through a water bridge to the conserved Asp-426, and by a hydrogen bond with the side chain of Arg-428. In Pkyn, the Arg-375 side chain is also extensively hydrogen bonded, but is instead stabilized within the active site cavity with hydrogen bonds to Asp-367 (equivalent to Asp<sub>Hkyn</sub>426), Tyr-176, with the PLP-aldimine through a chloride ion, and with atoms on a PEG molecule. The Pkyn Arg-375 guanidino nitrogens are thus much closer (by 6.5 Å) to the PLP-Lys-276 imine bond than in the Hkyn structure. The Hkyn and Pkyn S20-S21 β-hairpins are approximately 11.2° apart if measured from the Pkyn PLP-Lys aldimine. At their maximum separation point, α-carbons within this β-hairpin (of the conserved Pro<sub>Hkyn</sub>430 and Pro<sub>Pkyn</sub>371) are 5.9 Å away (Figure 1.5). Behind the S20-S21 β-hairpin, residues on helix H17 and β-strand S18 are 5.8 Å away (between α carbons of Pro<sub>Hkyn</sub>410 and Pro<sub>Pkyn</sub>350) from those of their prokaryotic counterparts (Figure 1.5). Also, the small domain helices H16 and helix H18 are each separated from their prokaryotic counterparts by 2.7 Å (between α carbons of Leu<sub>Hkyn</sub>371 and Leu<sub>Pkyn</sub>320) and 3.7 Å (between α carbons of Ile<sub>Hkyn</sub>457 and Ile<sub>Pkyn</sub>398), respectively. These conformational changes bring the entire small domain of the bacterial kynureninase closer to the Lys-276-PLP atoms and large domain active site residues.

Large domain residues that line the active site cavity also exhibit considerable differences between kynureninase crystal structures. The Phe<sub>Hkyn</sub>314 side chain (Figure 1.5) is found within the active site cavity, 14.8 Å from its prokaryotic counterpart (Phe<sub>Pkyn</sub>263), although Phe<sub>Pkyn</sub>263 was observed to have poor electron density in the bacterial structure (46). Here, the side chain of Phe<sub>Hkyn</sub>314 forms part of a large hydrophobic patch directly above the PLP-phosphate moiety

with the side chains of Ile-110\*, Phe-165, Trp-305\*, Phe-306\*, and Met-316\*. The side chains of Arg-313\* and Met-316\* are 7.5 Å and 5.5 Å away from their prokaryotic counterparts, respectively (not shown).

### **Docking of 3-Hydroxykynurenine into the Hkyn Active Site**

Each Molegro output pose was evaluated based on MolDock score, protein interaction, hydrogen bonding, and affinity interaction energies. The pose with the best overall energy values with these criteria had values (in kJ/mol) of -114.5, -124.7, -18.9, and -25.8, respectively. This pose is positioned within the active site cavity with the  $\alpha$ -amino moiety within hydrogen bonding distance of the side chains of small domain residues Arg-434, and Ser-75. The aromatic ring moiety is centered among the side chains of His-102\*, Ile-110\*, Trp-305\*, Phe-306\*, Phe-314\*, Asn-333\*, and Tyr-275 (Figure 1.6). The main chain carbonyl oxygen of Ser-75 is also within hydrogen bonding distance of the aromatic ring 2-amino group, whereas the 3-hydroxy group is within 2.9 Å of the Asn-333\*  $\delta$  nitrogen.

### **Discussion**

Previously, the human enzyme was expressed in sf9 insect cells using a baculovirus expression vector (47), and in COS-1 cells transfected with human kynureninase cDNA (46). Until now, its expression has not been reported using a bacterial expression system. The  $K_m$  values, and specific activity for 3-hydroxykynurenine that have been reported for the constitutive forms of kynureninase range from 3  $\mu$ M (47) to 49  $\mu$ M (46), and 0.16  $\mu$ mol  $\text{min}^{-1}$   $\text{mg}^{-1}$  from sf9 cells (47) to 5.5  $\mu$ mol  $\text{min}^{-1}$   $\text{mg}^{-1}$  for the enzyme expressed in COS-1 cells (47), respectively. The Michaelis constant ( $K_m = 28.3$   $\mu$ M), and specific activity (1.75  $\mu$ mol  $\text{min}^{-1}$   $\text{mg}^{-1}$ ) of our enzyme for 3-hydroxykynurenine agree best with that for enzyme expressed in COS-1 cells (47). We find this to be a good indicator that the expression of the human enzyme in a bacterial system is

functionally comparable to that from a eukaryotic expression system. We also determined the  $K_m$  of the human enzyme for the bacterial substrate ( $493 \pm 46 \mu\text{M}$ ), L-kynurenine, which agrees well with that reported for the human enzyme expressed in COS-1 (48) cells. All of our data were fit with HYPERO (46), Prism (GraphPad), and EnzFitter (Biosoft), and found to exhibit classical Michaelis-Menten behavior, which also contrasts with reports of sigmoid kinetic behavior from the enzyme expressed in sf9 cells (49). Attempts to fit our data to a Hill equation were unsuccessful. We measured the kinetic properties of a pseudo-native enzyme (with the hexahistidine tag proteolitically removed) and found no change in  $K_m$  and only a slight loss of activity (less than 3%). This enzyme had classic Michaelis-Menten behavior as well.

Like other members of the PLP-dependent  $\alpha$ -family, kynureninase appears to undergo conformational changes during catalysis. In this work we identify two regions in the small and large domains that could play a role in opening and closing the active site cavity: the small domain S20-S21  $\beta$ -hairpin, and the large domain S15-S16loop. The S20-S21  $\beta$ -hairpin in particular emerges as a dynamic region since a structural superposition between Hkyn and the structures of Pkyn (PDB ID 1qz9), 2-aminoethylphosphonate transaminase (PDB ID 1m32) (50), NifS (PDB ID 1jf9) (51), cystathionine beta-lyase (PDB ID 1ibj) (52), CsdB (PDB ID 1i29) (53), alanine:glyoxylate aminotransferase (PDB ID 1h0c) (54), histidinol phosphate aminotransferase (PDB ID 1fg3) (55), malY (PDB ID 1d2f) (56), serine hydroxymethyltransferase (PDB ID 1bj4) (57), and 3-hydroxykynurenine transaminase (PDB ID 2ch2) (57) reveals that the difference in the S20-S21  $\beta$ -hairpin conformational states observed between kynureninases is also clearly visible with other members of the  $\alpha$ -family (Figure 1.7). Based on the structural superposition, it appears that the conformation of the conserved Arg-434 in Hkyn is a function of the positioning of the small domain, in particular that of the S20-S21  $\beta$ -hairpin. Furthermore, the conformational

changes required to position the Hkyn S20-S21  $\beta$ -hairpin, Arg-434, and small domain elements closer to active site residues (thus resembling the structures of 1qz9) would be very similar to the movements observed between aspartate aminotransferase open (PDB ID 1ama) (58) and closed (PDB ID 9aat) states. Although the small domains of kynureninases and aspartate aminotransferases do not superimpose well, in part due to a difference in length between the small-large domain linker  $\alpha$ -helix (32 residues in aspartate aminotransferase versus 21 residues in kynureninase), the relative motion that must be undertaken by the entire small domain is very similar between the AAT open/closed and Pkyn/Hkyn pairs (Figure 1.8). Even though the small domain movements in aspartate aminotransferase are much more pronounced, it is possible that neither the Pkyn or Hkyn structures demonstrate a fully closed/open state, but rather an intermediate between them. Thus, the investigation of new kynureninase conformational states presents an interesting avenue of research. It is also possible that the second crystal morphology of kynureninase crystals grown in solution A might contain this different conformational state. It is important to note that these conditions would require some optimization in order to produce crystals with desirable diffraction properties.

The two kynureninase structures taken together suggest that the Arg<sub>Hkyn</sub>434/Arg<sub>Pkyn</sub>375 side chain is dynamic near the vicinity of the PLP aldimine bond. This conserved residue plays an important role in the substrate binding and catalysis of other PLP  $\alpha$ -family members. Site directed mutagenesis studies with aspartate aminotransferase and serine hydroxymethyltransferase have shown that this residue is important for both substrate specificity and regulating the conformational changes that accompany substrate binding in these enzymes. Arginine to lysine mutants of serine hydroxymethyltransferase have a 15-fold reduction in affinity and 0.03% of the wild type catalytic activity (59). Arginine to alanine mutants do not

bind substrate or have catalytic activity (60). Also, aspartate aminotransferase arginine to aspartate mutants have catalytic properties that are several orders of magnitude slower than wild type (23). The structural superposition between these kynureninase orthologs also suggests that it is reasonable to presume it is involved in substrate binding as well. Human kynureninase crystals shatter within seconds of exposure to a mother solution containing 100  $\mu\text{M}$  3-hydroxy-DL-kynurenine. Thus, we speculate that substrate binding causes a conformational change that breaks crystal contacts and causes these crystals to shatter. This conformational change is likely to be initiated by an interaction between the substrate's  $\alpha$  carboxyl group and the Arg-434 guanidino nitrogens, as is seen in aspartate aminotransferase (61). This is an important step in the closure mechanism since aspartate aminotransferase arginine to alanine mutants cannot adopt fully closed conformational states (62). Subsequently, the substrate's ring can occupy an amphiphilic pocket near the PLP-phosphate moiety between the charged side chains of Ser-75, His-102\*, Tyr-275, Asn-333\* and the hydrophobic side chains of Ile-110\*, Phe-306\*, Phe-314\*, and Trp-305\* (Figure 1.6). Substrate binding within the active site would tether the S20-21  $\beta$ -hairpin, and consequently the rest of the small domain, to the large domain through the side chain of Arg-434 and stabilize the closed state until product release. The binding of substrate to both small and large domain residues would place a certain amount of strain on substrate bonds which would be released as the substrate is cleaved. In this way the large and small domains act as a spring loaded catalytic unit that puts strain on the substrate bonds and facilitates hydrolysis.

The docking of 3-hydroxy-L-kynurenine in the kynureninase active site reveals that substrate  $\alpha$ -carboxylate oxygens are likely to form hydrogen bonds with the side chain of Arg-434. The docking also suggests that the 2-amino and 3-hydroxyl moieties of the substrate are likely to be within hydrogen bonding distance to atoms on Asn-333\*, Ser-75, and His-102\*, and

in a favorable distal quadrupole  $\pi$ - $\pi$  stacking interaction with the side chain of the conserved Trp-305\*. Several atoms in the kynureninase-3-hydroxy-L-kynurenine docking solution occupy the positions of atoms on a PEG molecule found in the active site of 1qz9 (not shown). The Moldock docking algorithm positions the  $\alpha$  nitrogen of 3-hydroxy-L-kynurenine in close proximity to the PLP-Lys-276 Schiff base aldimine as required to form the 3-hydroxy-L-kynurenine external aldimine, which is the first intermediate in the kynureninase catalytic mechanism (62). 3-Hydroxy-L-kynurenine is also properly oriented such that the  $\alpha$  carbon can be properly protonated by Lys-276 (21) in subsequent catalytic steps to form the appropriate product enantiomer (L-alanine). Also, the position of the top scoring docking pose from our calculations is oriented within the active site in a similar fashion to that of 4-(2-aminophenyl)-4-oxobutanoic acid in the crystal structure of *A. gambiae* 3-hydroxykynurenine transaminase (PDB ID 2ch2) (57) (superimposed figure in supplementary material). In both cases,  $\alpha$  carboxylate atoms are near small domain residues, whereas the hydrophobic ring moiety is anchored on the large domain side of the active site cavity.

Inducible kynureninases preferentially catalyze the hydrolytic cleavage of kynurenine, which is not hydroxylated at the 3' position. On the other hand, constitutive orthologs preferentially utilize 3-hydroxykynurenine as a substrate. Currently, there is a poor understanding of the molecular basis of the discrimination process between these two very similar molecules. The problem is further complicated by the fact that these enzymes have active sites that are highly conserved. Many of these conserved residues are found near the pyridoxal-5'-phosphate cofactor and there are currently no substrate or inhibitor kynureninase complex crystal structures to help identify residues involved in substrate differentiation. It is thus difficult to predict with certainty which residues convey molecular specificity. However, a structural

superposition of the docked Hkyn-3-hydroxy-L-kynurenine structure with Pkyn, reveals contacts that can aid in directing experiments to identify these residues (Figure 1.9). Specifically, the Trp<sub>Pkyn</sub>69\* side chain phenyl group and the  $\gamma$  carbon of Thr<sub>Pkyn</sub>282\* form a hydrophobic patch unfavorable for hydrogen bonding with the 3-hydroxyl moiety of 3-hydroxykynurenine. These groups are more suitable to accommodate the kynurenine 3' methyne carbon. On the other hand, the  $\delta$  nitrogen of Asn<sub>Hkyn</sub>333\* and the smaller His<sub>Hkyn</sub>102\* side chains form an environment in human kynureninase that would allow for this group (3-hydroxyl) to interact favorably with their side chains and not be sterically hindered (by Trp-69\* in Pkyn). Interestingly, these two point mutations are conserved among constitutive and inducible kynureninases, with inducible kynureninases having a Thr-Trp pair whereas constitutive orthologs contain the Asn-His pair. Based on these deductions, we have designed site-directed mutagenesis experiments to determine whether these residues play a role in substrate binding and specificity.

### **Acknowledgements**

We would like to thank the Hauptman-Woodward Institute for their instrumental role in identifying crystallization conditions. We would also like to thank the staff at the SBC-CAT beamline 19-BM at the Advanced Photon Source, Argonne, IL for their assistance during data collection.

### **Supporting Information Available**

Human kynureninase coordinates are available from the Protein Data Bank, PDB ID code 2HZP. A figure of a structural superposition between Hkyn-3-hydroxy-L-kynurenine and 3-hydroxykynurenine transaminase (PDB ID 2ch2) (57) complexed with 4-(2-aminophenyl)-4-oxobutanoic acid is also available. This material is available free of charge via the Internet at <http://pubs.acs.org>.

## References

- (1) Shetty, A. S., and Gaertner, F. H. (1975) Kynureninase-Type enzymes of *Penicillium roqueforti*, *Aspergillus niger*, *Rhizopus stolonifer*, and *Pseudomonas fluorescens*: further evidence for distinct kynureninase and hydroxykynureninase activities. *J Bacteriol* 122, 235-44.
- (2) Soda, K., and Tanizawa, K. (1979) Kynureninases: enzymological properties and regulation mechanism. *Adv Enzymol Relat Areas Mol Biol* 49, 1-40.
- (3) Schwarcz, R., and Pellicciari, R. (2002) Manipulation of brain kynurenines: glial targets, neuronal effects, and clinical opportunities. *J Pharmacol Exp Ther* 303, 1-10.
- (4) Magni, G., Amici, A., Emanuelli, M., Orsomando, G., Raffaelli, N., and Ruggieri, S. (2004) Enzymology of NAD<sup>+</sup> homeostasis in man. *Cell Mol Life Sci* 61, 19-34.
- (5) Espey, M. G., Chernyshev, O. N., Reinhard, J. F., Jr., Namboodiri, M. A., and Colton, C. A. (1997) Activated human microglia produce the excitotoxin quinolinic acid. *Neuroreport* 8, 431-4.
- (6) Moffett, J. R., Els, T., Espey, M. G., Walter, S. A., Streit, W. J., and Namboodiri, M. A. (1997) Quinolinic acid immunoreactivity in experimental rat brain tumors is present in macrophages but not in astrocytes. *Exp Neurol* 144, 287-301.
- (7) Stone, T. W., and Perkins, M. N. (1981) Quinolinic acid: a potent endogenous excitant at amino acid receptors in CNS. *Eur J Pharmacol* 72, 411-2.
- (8) Chiarugi, A., Meli, E., and Moroni, F. (2001) Similarities and differences in the neuronal death processes activated by 3OH-kynurenine and quinolinic acid. *J Neurochem* 77, 1310-8.

- (9) Giulian, D., Vaca, K., and Noonan, C. A. (1990) Secretion of neurotoxins by mononuclear phagocytes infected with HIV-1. *Science* 250, 1593-6.
- (10) Guillemain, G. J., Brew, B. J., Noonan, C. E., Takikawa, O., and Cullen, K. M. (2005) Indoleamine 2,3 dioxygenase and quinolinic acid immunoreactivity in Alzheimer's disease hippocampus. *Neuropathol Appl Neurobiol* 31, 395-404.
- (11) Achim, C. L., Heyes, M. P., and Wiley, C. A. (1993) Quantitation of human immunodeficiency virus, immune activation factors, and quinolinic acid in AIDS brains. *J Clin Invest* 91, 2769-75.
- (12) Heyes, M. P., Brew, B., Martin, A., Markey, S. P., Price, R. W., Bhalla, R. B., and Salazar, A. (1991) Cerebrospinal fluid quinolinic acid concentrations are increased in acquired immune deficiency syndrome. *Adv Exp Med Biol* 294, 687-90.
- (13) Heyes, M. P., Swartz, K. J., Markey, S. P., and Beal, M. F. (1991) Regional brain and cerebrospinal fluid quinolinic acid concentrations in Huntington's disease. *Neurosci Lett* 122, 265-9.
- (14) Saito, K., Crowley, J. S., Markey, S. P., and Heyes, M. P. (1993) A mechanism for increased quinolinic acid formation following acute systemic immune stimulation. *J Biol Chem* 268, 15496-503.
- (15) Saito, K., Nowak, T. S., Jr., Markey, S. P., and Heyes, M. P. (1993) Mechanism of delayed increases in kynurenine pathway metabolism in damaged brain regions following transient cerebral ischemia. *J Neurochem* 60, 180-92.
- (16) Saito, K., Nowak, T. S., Jr., Suyama, K., Quearry, B. J., Saito, M., Crowley, J. S., Markey, S. P., and Heyes, M. P. (1993) Kynurenine pathway enzymes in brain: responses to ischemic brain injury versus systemic immune activation. *J Neurochem* 61, 2061-70.

- (17) Sei, S., Saito, K., Stewart, S. K., Crowley, J. S., Brouwers, P., Kleiner, D. E., Katz, D. A., Pizzo, P. A., and Heyes, M. P. (1995) Increased human immunodeficiency virus (HIV) type 1 DNA content and quinolinic acid concentration in brain tissues from patients with HIV encephalopathy. *J Infect Dis* 172, 638-47.
- (18) Sei, Y., Paul, I. A., Saito, K., Laya, R., Hartley, J. W., Morse, H. C., 3rd, Skolnick, P., and Heyes, M. P. (1996) Quinolinic acid levels in a murine retrovirus-induced immunodeficiency syndrome. *J Neurochem* 66, 296-302.
- (19) Mehta, P. K., Hale, T. I., and Christen, P. (1993) Aminotransferases: demonstration of homology and division into evolutionary subgroups. *Eur J Biochem* 214, 549-61.
- (20) Jansonius, J. N. (1998) Structure, evolution and action of vitamin B6-dependent enzymes. *Curr Opin Struct Biol* 8, 759-69.
- (21) Momany, C., Levnikov, V., Blagova, L., Lima, S., and Phillips, R. S. (2004) Three-dimensional structure of kynureninase from *Pseudomonas fluorescens*. *Biochemistry* 43, 1193-203.
- (22) Paiardini, A., Bossa, F., and Pascarella, S. (2004) Evolutionarily conserved regions and hydrophobic contacts at the superfamily level: The case of the fold-type I, pyridoxal-5'-phosphate-dependent enzymes. *Protein Sci* 13, 2992-3005.
- (23) Jager, J., Moser, M., Sauder, U., and Jansonius, J. N. (1994) Crystal structures of *Escherichia coli* aspartate aminotransferase in two conformations. Comparison of an unliganded open and two liganded closed forms. *J Mol Biol* 239, 285-305.
- (24) Studier, F. W. (2005) Protein production by auto-induction in high density shaking cultures. *Protein Expr Purif* 41, 207-34.

- (25) Bradford, M. M. (1976) A rapid and sensitive method for the quantitation of microgram quantities of protein utilizing the principle of protein-dye binding. *Anal Biochem* 72, 248-54.
- (26) Luft, J. R., Collins, R. J., Fehrman, N. A., Lauricella, A. M., Veatch, C. K., and DeTitta, G. T. (2003) A deliberate approach to screening for initial crystallization conditions of biological macromolecules. *J Struct Biol* 142, 170-9.
- (27) Chayen, N. E., Shaw Stewart, P. D., and Blow, D. M. (1992) Microbatch crystallization under oil-a new technique allowing many small-volume crystallization trials. *J. Crystal Growth* 122, 176-180.
- (28) Use of the Advanced Photon Source was supported by the U. S. Department of Energy, O. o. S., Office of Basic Energy Sciences, under Contract No. W-31-109-Eng-38.
- (29) Otwinowski, Z., and W., M. (1997) Processing of X-ray Diffraction Data Collected in Oscillation Mode. *Methods in Enzymology* 276, 307-326.
- (30) Otwinowski, Z., and and Minor, W. (1997) Processing of X-ray Diffraction Data Collected in Oscillation Mode. *Methods Enzymol* 276, 307-326.
- (31) Vagin, A., and Teplyakov, A. (1997) MOLREP: an automated program for molecular replacement. *J. Appl. Cryst.* 30, 1022-1025.
- (32) Collaborative Computational Project, N. (1994) The CCP4 Suite: Programs for Protein Crystallography. *Acta Cryst D*50.
- (33) Berman, H. M., Westbrook, J., Feng, Z., Gilliland, G., Bhat, T. N., Weissig, H., Shindyalov, I. N., and Bourne, P. E. (2000) The Protein Data Bank. *Nucleic Acids Res* 28, 235-42.

- (34) Terwilliger, T. C. (2003) Automated main-chain model building by template matching and iterative fragment extension. *Acta Crystallogr D Biol Crystallogr* 59, 38-44.
- (35) Murshudov, G. N., Vagin, A. A., and Dodson, E. J. (1997) Refinement of macromolecular structures by the maximum-likelihood method. *Acta Crystallogr D Biol Crystallogr* 53, 240-55.
- (36) Lamzin, V. S., Perrakis, A., and Wilson, K. S. (2001) The ARP/WARP suite for automated construction and refinement of protein models. In *Int. Tables for Crystallography, Vol. F*, Dordrecht, Kluwer Academic Publishers, The Netherlands.
- (37) Perrakis, A., Morris, R., and Lamzin, V. S. (1999) Automated protein model building combined with iterative structure refinement. *Nat Struct Biol* 6, 458-63.
- (38) McRee, D. E. (1999) XtalView/Xfit--A versatile program for manipulating atomic coordinates and electron density. *J Struct Biol* 125, 156-65.
- (39) Lovell, S. C., Davis, I. W., Arendall, W. B., 3rd, de Bakker, P. I., Word, J. M., Prisant, M. G., Richardson, J. S., and Richardson, D. C. (2003) Structure validation by C $\alpha$  geometry: phi,psi and C $\beta$  deviation. *Proteins* 50, 437-50.
- (40) Morris, A. L., MacArthur, M. W., Hutchinson, E. G., and Thornton, J. M. (1992) Stereochemical quality of protein structure coordinates. *Proteins* 12, 345-64.
- (41) Gille, C., and Frommel, C. (2001) STRAP: editor for STRuctural Alignments of Proteins. *Bioinformatics* 17, 377-8.
- (42) Guex, N., and Peitsch, M. C. (1997) SWISS-MODEL and the Swiss-PdbViewer: an environment for comparative protein modeling. *Electrophoresis* 18, 2714-23.
- (43) Thomsen, R., and Christensen, M. H. (2006) MolDock: a new technique for high-accuracy molecular docking. *J Med Chem* 49, 3315-21.

- (44) Alexander, F. W., Sandmeier, E., Mehta, P. K., and Christen, P. (1994) Evolutionary relationships among pyridoxal-5'-phosphate-dependent enzymes. Regio-specific alpha, beta and gamma families. *Eur J Biochem* 219, 953-60.
- (45) Han, G. W., Schwarzenbacher, R., Page, R., Jaroszewski, L., Abdubek, P., Ambing, E., Biorac, T., Canaves, J. M., Chiu, H. J., Dai, X., Deacon, A. M., DiDonato, M., Elsliger, M. A., Godzik, A., Grittini, C., Grzechnik, S. K., Hale, J., Hampton, E., Haugen, J., Hornsby, M., Klock, H. E., Koesema, E., Kreusch, A., Kuhn, P., Lesley, S. A., Levin, I., McMullan, D., McPhillips, T. M., Miller, M. D., Morse, A., Moy, K., Nigoghossian, E., Ouyang, J., Paulsen, J., Quijano, K., Reyes, R., Sims, E., Spraggon, G., Stevens, R. C., van den Bedem, H., Velasquez, J., Vincent, J., von Delft, F., Wang, X., West, B., White, A., Wolf, G., Xu, Q., Zagnitko, O., Hodgson, K. O., Wooley, J., and Wilson, I. A. (2005) Crystal structure of an alanine-glyoxylate aminotransferase from *Anabaena* sp. at 1.70 Å resolution reveals a noncovalently linked PLP cofactor. *Proteins* 58, 971-5.
- (46) Walsh, H. A., and Botting, N. P. (2002) Purification and biochemical characterization of some of the properties of recombinant human kynureninase. *Eur J Biochem* 269, 2069-74.
- (47) Toma, S., Nakamura, M., Tone, S., Okuno, E., Kido, R., Breton, J., Avanzi, N., Cozzi, L., Speciale, C., Mostardini, M., Gatti, S., and Benatti, L. (1997) Cloning and recombinant expression of rat and human kynureninase. *FEBS Lett* 408, 5-10.
- (48) Cleland, W. W. (1979) Statistical analysis of enzyme kinetic data. *Methods Enzymol* 63, 103-38.

- (49) Clausen, T., Kaiser, J. T., Steegborn, C., Huber, R., and Kessler, D. (2000) Crystal structure of the cystine C-S lyase from *Synechocystis*: stabilization of cysteine persulfide for FeS cluster biosynthesis. *Proc Natl Acad Sci U S A* 97, 3856-61.
- (50) Lima, C. D. (2002) Analysis of the *E. coli* NifS CsdB protein at 2.0 Å reveals the structural basis for perselenide and persulfide intermediate formation. *J Mol Biol* 315, 1199-208.
- (51) Breiting, U., Clausen, T., Ehlert, S., Huber, R., Laber, B., Schmidt, F., Pohl, E., and Messerschmidt, A. (2001) The three-dimensional structure of cystathionine beta-lyase from *Arabidopsis* and its substrate specificity. *Plant Physiol* 126, 631-42.
- (52) Mihara, H., Fujii, T., Kato, S., Kurihara, T., Hata, Y., and Esaki, N. (2002) Structure of external aldimine of *Escherichia coli* CsdB, an IscS/NifS homolog: implications for its specificity toward selenocysteine. *J Biochem (Tokyo)* 131, 679-85.
- (53) Zhang, X., Roe, S. M., Hou, Y., Bartlam, M., Rao, Z., Pearl, L. H., and Danpure, C. J. (2003) Crystal structure of alanine:glyoxylate aminotransferase and the relationship between genotype and enzymatic phenotype in primary hyperoxaluria type 1. *J Mol Biol* 331, 643-52.
- (54) Sivaraman, J., Li, Y., Larocque, R., Schrag, J. D., Cygler, M., and Matte, A. (2001) Crystal structure of histidinol phosphate aminotransferase (HisC) from *Escherichia coli*, and its covalent complex with pyridoxal-5'-phosphate and l-histidinol phosphate. *J Mol Biol* 311, 761-76.
- (55) Clausen, T., Schlegel, A., Peist, R., Schneider, E., Steegborn, C., Chang, Y. S., Haase, A., Bourenkov, G. P., Bartunik, H. D., and Boos, W. (2000) X-ray structure of MalY from

- Escherichia coli*: a pyridoxal 5'-phosphate-dependent enzyme acting as a modulator in mal gene expression. *Embo J* 19, 831-42.
- (56) Nakai, T., Okada, K., Akutsu, S., Miyahara, I., Kawaguchi, S., Kato, R., Kuramitsu, S., and Hirotsu, K. (1999) Structure of *Thermus thermophilus* HB8 aspartate aminotransferase and its complex with maleate. *Biochemistry* 38, 2413-24.
- (57) Rossi, F., Garavaglia, S., Giovenzana, G. B., Arca, B., Li, J., and Rizzi, M. (2006) Crystal structure of the *Anopheles gambiae* 3-hydroxykynurenine transaminase. *Proc Natl Acad Sci U S A* 103, 5711-6.
- (58) McPhalen, C. A., Vincent, M. G., Picot, D., Jansonius, J. N., Lesk, A. M., and Chothia, C. (1992) Domain closure in mitochondrial aspartate aminotransferase. *J Mol Biol* 227, 197-213.
- (59) Delle Fratte, S., Iurescia, S., Angelaccio, S., Bossa, F., and Schirch, V. (1994) The function of arginine 363 as the substrate carboxyl-binding site in *Escherichia coli* serine hydroxymethyltransferase. *Eur J Biochem* 225, 395-401.
- (60) Almo, S. C., Smith, D. L., Danishefsky, A. T., and Ringe, D. (1994) The structural basis for the altered substrate specificity of the R292D active site mutant of aspartate aminotransferase from *E. coli*. *Protein Eng* 7, 405-12.
- (61) Graber, R., Kasper, P., Malashkevich, V. N., Sandmeier, E., Berger, P., Gehring, H., Jansonius, J. N., and Christen, P. (1995) Changing the reaction specificity of a pyridoxal-5'-phosphate-dependent enzyme. *Eur J Biochem* 232, 686-90.
- (62) Koushik, S. V., Moore, J. A., 3rd, Sundararaju, B., and Phillips, R. S. (1998) The catalytic mechanism of kynureninase from *Pseudomonas fluorescens*: insights from the

effects of pH and isotopic substitution on steady-state and pre-steady-state kinetics.  
Biochemistry 37, 1376-82.

**Table 1.1** Summary of Crystallographic analysis.

Space Group	C2
Resolution range (outer shell), Å	88.39-2.00 (2.08-2.01)
No of reflections (outer shell)	31583 (2269)
Redundancy (outer shell)	3.7 (3.3)
% of Reflections with $I > 3\sigma$ (outer shell)	82 (53.9)
$R_{\text{sym}}$ (outer shell)	0.055 (0.264)
$R_{\text{factor}}$ (outer shell)	0.150 (0.186)
$R_{\text{free}}$ (outer shell)	0.195 (0.255)
Mean B value	21.97 Å <sup>2</sup>
r.m.s delta. from ideal geometry:	
Bond angles	1.135°
Bond distances	0.008 Å
Ramachandran plot residues in favored/allowed/disallowed (%) regions	97.3/2.5/0.2

$R_{\text{free}}$  calculated with 5.1% of total data that was excluded from refinement.

**Figure 1.1.** Ribbon drawing of the kynureninase biologically active unit with secondary structure elements colored in a blue to red progressing scheme. The dimer can be generated by applying the crystallographic symmetry operator  $1-x, y, -z$  to the monomer.

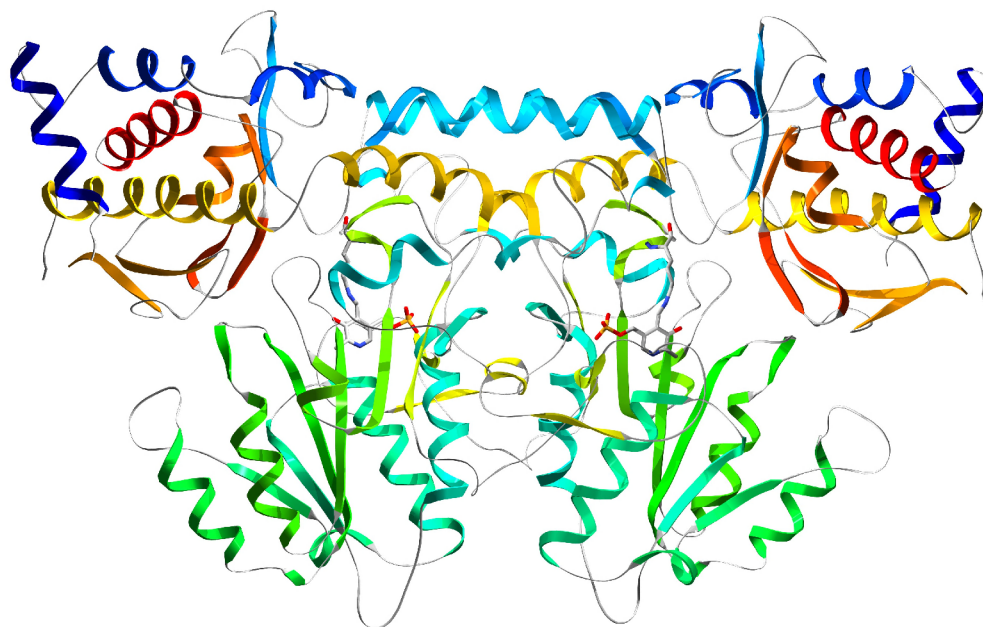


**Figure 1.2.** Stereo ribbon drawing of the kynureninase monomer with secondary structure elements colored in a blue to red progressing scheme.  $\beta$ -Strands are labeled with the prefix S,  $\alpha$ -helices with the prefix H. The pyridoxal-5'-phosphate cofactor is drawn in CPK scheme and can be seen in the middle portion of the monomer between  $\beta$ -strand S8 and  $\beta$ -strand S11. The large domain is colored green, aquamarine, and yellow (H15, S15, and S16). Small domain elements are colored red, dark blue, orange, and yellow (H16).

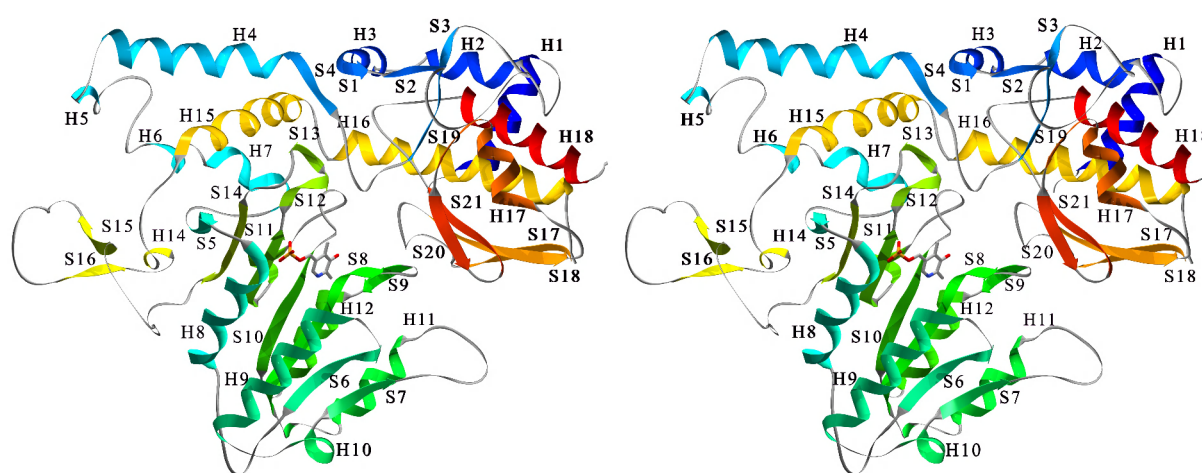


**Figure 1.3.** Map calculated with likelihood-weighted 2Fo-Fc coefficients for the area surrounding the pyridoxal-5'-phosphate-Lys-276 internal aldimine complex (contoured at  $1.5\sigma$ ). The active site is well solvated and several water molecules can be observed near the side chains of Asn-333\*, Asp-168, and Tyr-275. Other active site residues have been omitted for clarity. Residues contributed from the symmetry related monomer are labeled with an asterisk (\*).

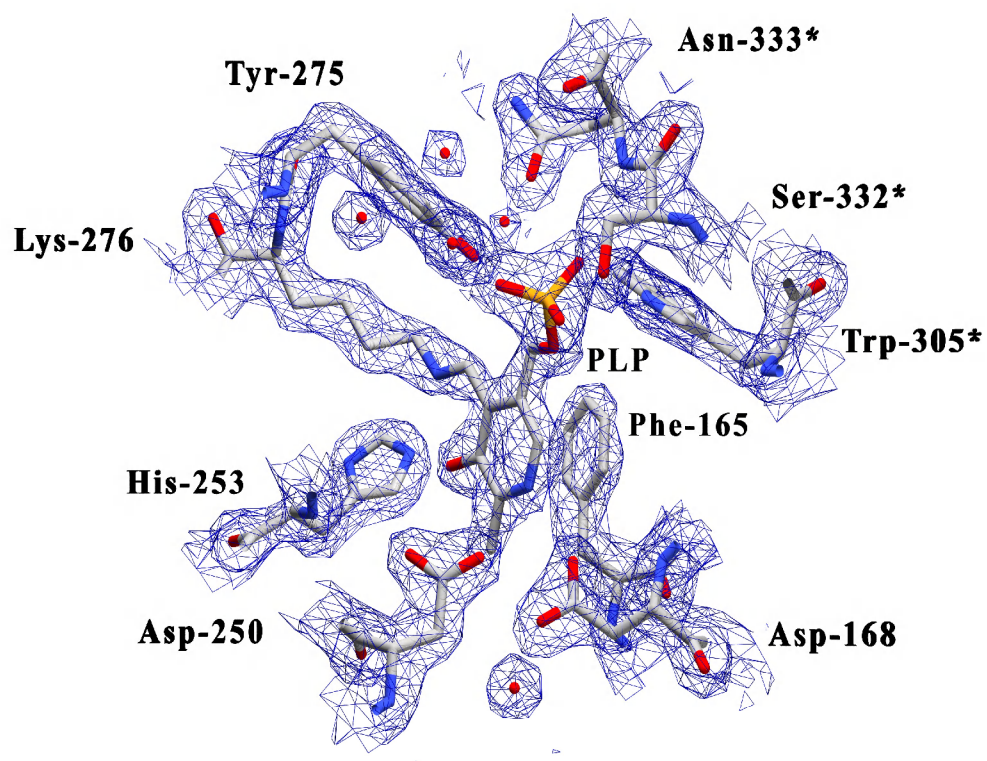


**Figure 1.4.** Stereo image of the kynureninase active site PLP hydrogen bonding interactions. Hydrogen bonds were drawn using a 3.55 Å cutoff. Residues contributed from the symmetry related monomer are labeled with an asterisk (\*).

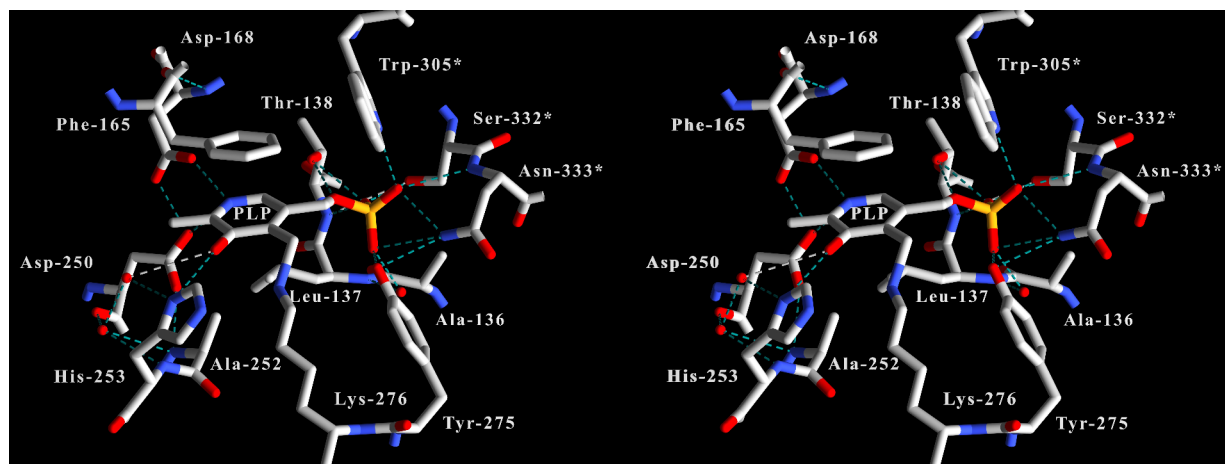


**Figure 1.5.** Structural superposition between dimers of human (ribbons and labels blue, atoms CPK) and *Pseudomonas fluorescens* (ribbons and labels green, atoms CPK) kynureninases. For clarity, only *P. fluorescens* residues Phe-263\*, Arg-375, Pro-371, Pro-350 and their human equivalents Phe-314\*, Arg-434, Pro-430, and Pro-410 are labeled. Only distances between conserved residues are shown and are in angstroms. Residues contributed from the symmetry related monomer are labeled with an asterisk (\*). Unlabeled residues surrounding the pyridoxal-5'-phosphate cofactor (PLP) are all contributed from the human chain and are displayed for perspective only.

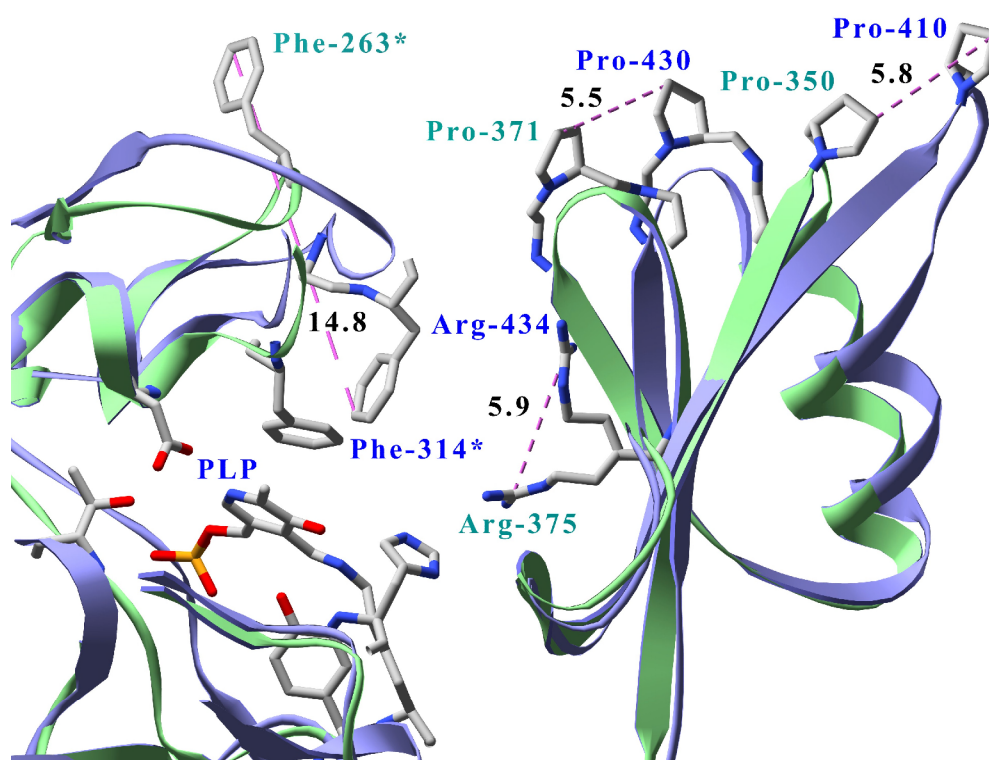


**Figure 1.6.** Stereo image of 3-hydroxy-L-kynurenine docked with human kynureninase. Human kynureninase bonds and labels are colored white with CPK colored atoms. 3-hydroxy-L-kynurenine (3-HK) bonds and labels are colored blue. Residues contributed from the symmetry related monomer are labeled with an asterisk (\*).

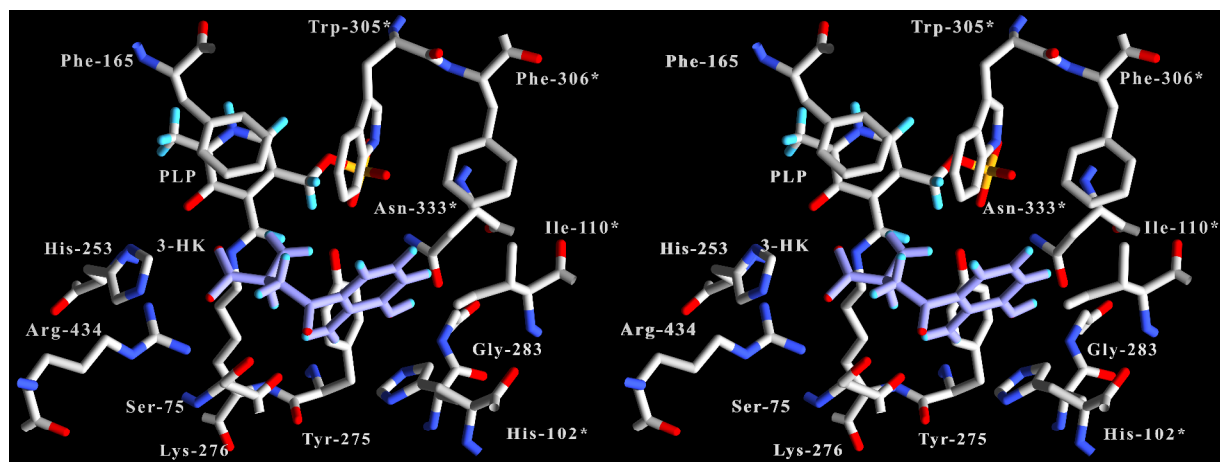


**Figure 1.7.** A) Ribbon drawing of the Hkyn small domain S20-S21  $\beta$ -hairpin (red) and equivalent hairpins (gray) from the structures with PDB IDs 1qz9, 1m32, 1jf9, 1bj, 1i29, 1h0c, 1fg3, 1d2f, 1bj4, and 2ch2. All structures were superimposed using STRAP with the Hkyn monomer as the reference model. B) view as in (A) rotated 90 degrees. The Hkyn Arg-434 is colored red and all other equivalent arginine residues are colored gray.

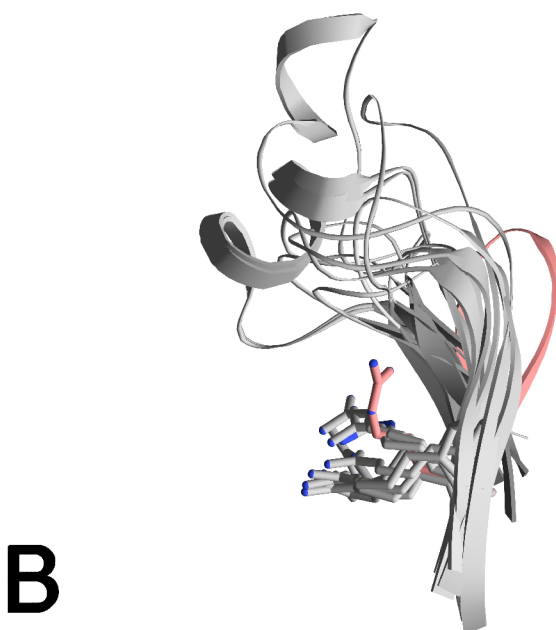
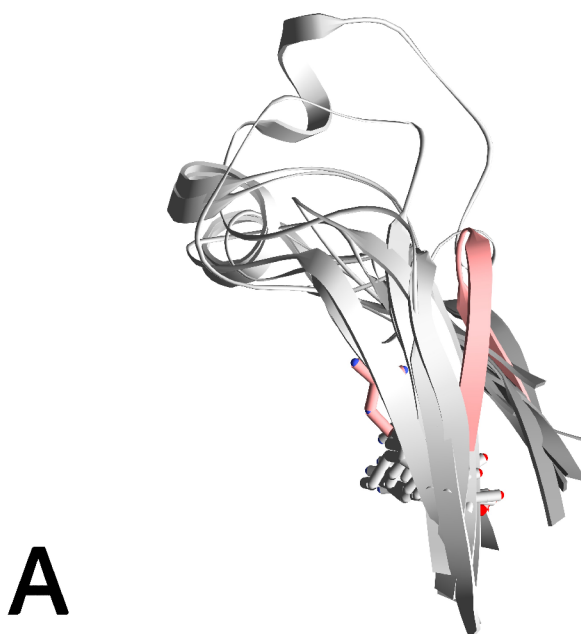


**Figure 1.8.** Comparison of the superimposed small domains of aspartate aminotransferase in open (PDB ID 1ama, colored dark red) and closed (PDB ID 9aat, colored light red) with the *Homo sapiens* kynureninase (colored dark green) and the *Pseudomonas fluorescens* kynureninase (PDB ID 1qz9, colored light green).

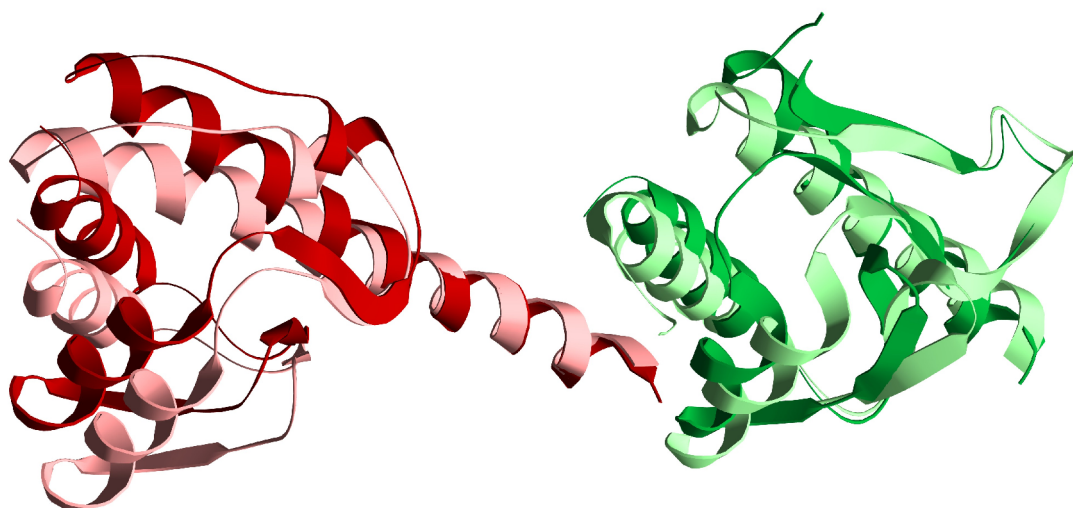
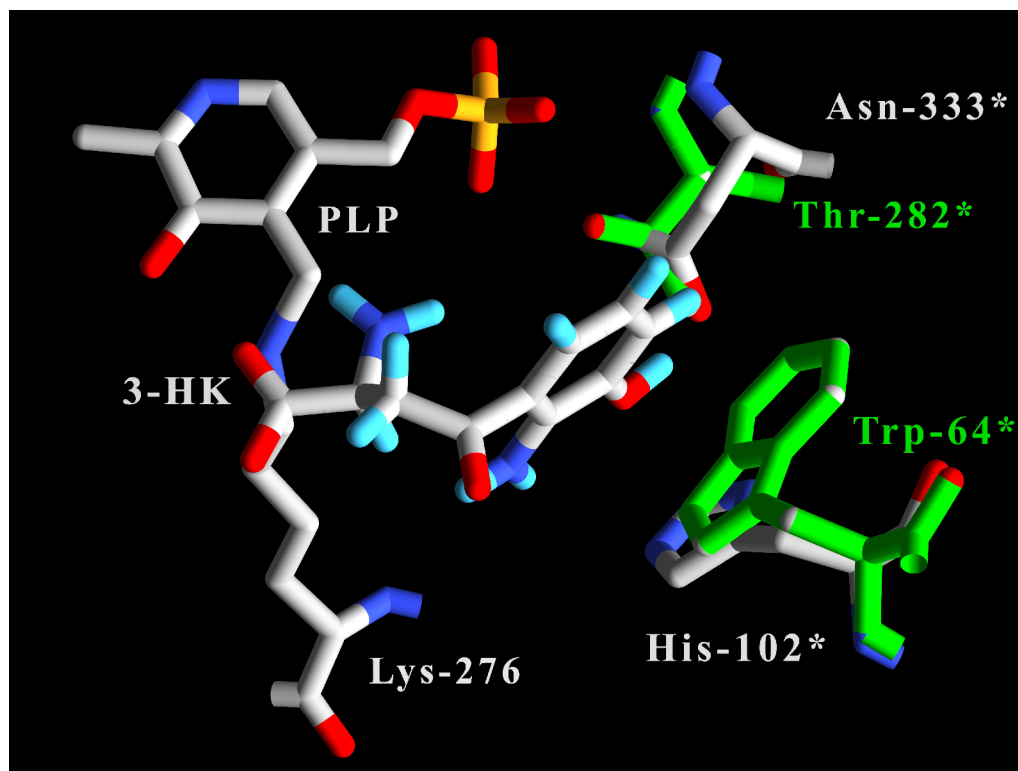


**Figure 1.9.** Active site amino acid differences between human and *P. fluorescens* kynureninases in the vicinity of the 3-hydroxyl moiety of docked 3-hydroxy-L-kynurenine (3-HK). 3-hydroxy-L-kynurenine and Hkyn labels and bonds are colored white with CPK-colored atoms. Pkyn residues and labels are colored green. Residues contributed from the symmetry related monomer are labeled with an asterisk (\*).



## CHAPTER 2

CRYSTAL STRUCTURE OF *HOMO SAPIENS* KYNURENINASE-3-HYDROXYHIPPURIC  
ACID INHIBITOR COMPLEX; INSIGHTS INTO THE MOLECULAR BASIS OF  
KYNURENINASE SUBSTRATE SPECIFICITY<sup>2</sup>

---

<sup>2</sup>Santiago Lima, Sunil Kumar, Vijay Gawandi, Cory Momany, and Robert S. Phillips. To be submitted to *Journal of Medicinal Chemistry*.

## Abstract

*Homo sapiens* kynureninase is a pyridoxal-5'-phosphate dependent enzyme that catalyzes the hydrolytic cleavage of 3-hydroxykynurenine to yield 3-hydroxyanthranilate and L-alanine. In mammals, it is a member of the tryptophan catabolic pathway that leads to the *de novo* biosynthesis of NAD<sup>+</sup>, commonly known as the kynurenine pathway. This metabolic cascade is notable for the formation of quinolinic acid, an excitotoxin whose agonistic effect on glutamate sensitive NMDA receptors has been correlated with the etiology of neurodegenerative disorders such as AIDS-related dementia and Alzheimer's disease. It is thought that inhibiting kynurenine pathway enzymes can decrease quinolinic acid levels and correct some of the pathophysiological conditions characteristic of these diseases. Our laboratory has synthesized a novel kynureninase competitive inhibitor, 3-hydroxyhippuric acid. We have co-crystallized it with human kynureninase and solved the atomic structure to 1.7 Å resolution. Based on a structural analysis of the complex, we designed a series of kynureninase His-102, Ser-332, and Asn-333 mutants. These mutants showed complete reversal of binding affinity between 3-hydroxykynurenine and the prokaryotic substrate, L-kynurenine, thus defining the primary residues contributing to substrate specificity in these enzymes. Furthermore, the complex reveals important restraints for *in silico* inhibitor design and pharmacophore library screening

## Keywords

3-hydroxykynurenine, aminotransferase, inhibitor complex, kynureninase, kynurenine L-hydrolase, L-kynurenine, PLP, pyridoxal-5'-phosphate,

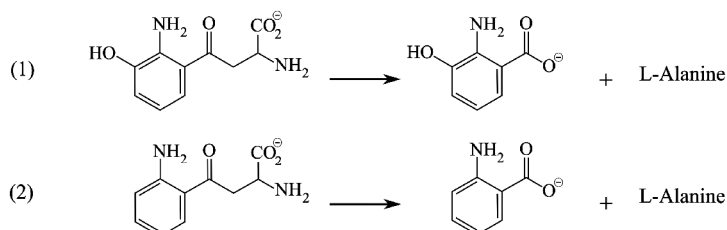
## Introduction

In mammals, the essential amino acid L-tryptophan is a precursor for metabolites such as the neurotransmitter serotonin, the hormone melatonin, nicotinic acid, and NAD<sup>+</sup>, with the latter

two being the primary metabolic fate of dietary tryptophan. The catabolic cascade that leads to the *de novo* biosynthesis of nicotinic acid and NAD<sup>+</sup>, commonly known as the kynurenine pathway (1), is notable for intermediates with important neuroactive properties. Kynureninase, the third enzyme along the kynurenine pathway, is a pyridoxal-5'-phosphate (PLP) dependent enzyme that catalyzes the hydrolytic cleavage of 3-hydroxy-L-kynurenine (3-OH-kyn) to yield 3-hydroxyanthranilic acid and L-alanine (Eq 1). One further kynurenine pathway enzyme, 3-hydroxyanthranilate-3,4-dioxygenase, metabolizes 3-hydroxyanthranilic acid, the product of which undergoes a non-enzymatic rearrangement leading to the formation of quinolinic acid (2). Quinolinic acid has endogenous neurotoxic activity (3) that is mediated *via* its agonist effect on glutamate sensitive NMDA ionotropic receptors (4), and its excitotoxic effect has been correlated with the etiology of many neurodegenerative diseases including AIDS-related dementia (5, 6), Huntington's disease (7, 8), amyotrophic lateral sclerosis (9), and Alzheimer's disease (10, 11). The increasing body of evidence implicating changes in normal concentrations of quinolinic acid in CNS tissues with neurotoxicity has led to the development of the idea that altering the ratio of quinolinic acid to other kynurenine pathway metabolites could provide a neuroprotective effect during the onset of such maladies (12-15). Thus, our goal was to provide a robust template that can be used for rational and *in silico* drug design, as well as complex pharmacophore library screening. Here we report the crystal structure of *Homo sapiens* kynureninase (Hkyn) complexed with 3-hydroxyhippuric acid (3-HHA), a competitive inhibitor of kynureninase. The complex reveals important enzyme-ligand interactions that should be considered for the design and screening of novel kynureninase inhibitors.

Two functional orthologs of kynureninase are known: a constitutive (16), primarily eukaryotic enzyme, which catalyzes the hydrolysis of 3-OH-kyn, and a primarily prokaryotic

inducible (16) form, which catalyzes the hydrolysis of L-kynurenine (L-kyn) to yield hydroxyanthranilic acid and L-ala (Eq. 2). Although both orthologs have been found to catalyze the hydrolysis of their non-cognate substrate, they do so at much slower rates and have lower binding affinities (17, 18). Indeed, a number of organisms are known to contain both orthologs (16). To date, the molecular basis of substrate specificity that allows these enzymes to differentiate between substrates has not been elucidated. Some insight into this mechanism was gained through docking studies with the native structure of *H. sapiens* kynureninase and 3-OH-L-kyn as the target ligand (18). These revealed that two active site residues, His-102 and Asn-333, could play an important role in substrate binding and specificity (18). We now present experimental evidence supporting this hypothesis.



## Materials and Methods.

### Crystallization, Data Collection, and Molecular Replacement

Kynureninase was expressed and purified as previously described (18). Complexed kynureninase-3-hydroxyhippuric acid crystals were grown at 25 °C by mixing (1:1 ratio) a kynureninase solution (9 mg mL<sup>-1</sup> in 50 mM HEPES, pH 5.1, and 0.1 mM PLP) with a crystallization solution containing 0.05 M MgCl<sub>2</sub>, 0.1 M Tris (pH 8.0), 25% PEG 3000, and 350 μM 3-HHA. Dark yellow crystals appeared after four to five weeks and grew to dimensions of 0.075 mm x 0.05 mm x 0.015 mm. These crystals were flash frozen in liquid nitrogen with

cryoprotectant containing 1 mM 3-HHA, 55 mM MgCl<sub>2</sub>, 110 mM Tris (pH 8), 33% PEG 3000. These crystals had space group C2 with cell constants  $a=74.44$  Å,  $b=77.12$  Å,  $c=94.55$  Å,  $\beta=109.35$ . X-ray synchrotron data were collected ( $\lambda = 1.007$  Å, 200 frames, 1° oscillations) at the Advanced Photon Source beamline 19-ID (19) and were processed and scaled with HKL3000 (20). The merged SCALEPACK (20) intensities were used as input for the molecular replacement program Phaser (21) using the *H. sapiens* kynureninase (PDB accession code 2HZP) (Hkyn) coordinates as the phasing model. All water, hetero, and PLP coordinates were deleted from the input model. The molecular replacement solution and kynureninase-3-HHA complex were refined with Refmac5 (22). Water addition was done with ARP/wARP (23). The PLP cofactor and 3-HHA were manually introduced with COOT (24). TLS (25) refinement was performed with the following groups: 6-37, 38-45, 46-120, 121-190, 191-213, 214-357, 358-375, 376-412, 413-460. The 3-HHA model and library description were created with the CCP4i Monomer Library Sketcher (26). Molprobity (27) was used to evaluate the quality of the final model.

### **Inhibition Kinetics**

3-HHA was evaluated for its ability to inhibit the reaction between Hkyn and its cognate substrate, 3-hydroxykynurenine. Assays were performed at 37 °C by following the absorbance change at 370 nm as 3-hydroxykynurenine is converted to 3-hydroxyanthranilic acid and L-Alanine ( $\Delta\epsilon = 4500$  M<sup>-1</sup> cm<sup>-1</sup>). Assays contained 30 mM potassium phosphate (pH 8.0), and 40 μM PLP at 37 °C. Data were fit to a competitive inhibition model with Hypero(28).

### **Site directed mutagenesis**

Mutants were created using the QuickChange<sup>®</sup> site-directed mutagenesis kit (Stratagene). The following mutants were created and sequenced to confirm the desired codon change:



product (15.5 g, 0.079 mol). Yield was 65%. <sup>1</sup>H-NMR ppm (400 MHz, CDCl<sub>3</sub>) δ 1.29 (t, 3H), 4.21 (m, 2H), 7.96 (dd, 1H), 7.57 (d, 1H), 7.72 (d, 1H), 7.74 (m, 1H), 9.61 (s, 1H).

### **3-Ethoxycarbonyloxybenzoic acid (3) (30)**

3-Methoxycarbonyloxybenzaldehyde (6 g, 0.03 mol) was dissolved in DMF (0.1 M). Oxone (19 g, one equiv) was added and the mixture was stirred at room temperature for 3 hours. The reaction was monitored by TLC and 1 N HCl was used to dissolve the salts. The crude product was extracted into ethylacetate (50 mL), the organic extract washed with 1N HCl (3×15 mL) and brine (2×10 mL), and then dried over Na<sub>2</sub>SO<sub>4</sub>. 3-Ethoxycarbonyloxybenzoic acid (**3**) was obtained and purified by silica gel column chromatography (60:40 EtOAc/Hexane). Isolated yield was 63% (3.86 g, 0.009 mol). <sup>1</sup>H-NMR ppm (400 MHz, CDCl<sub>3</sub>) δ 1.29 (t, 3H), 4.21 (m, 2H), 7.93 (dd, 1H), 7.63 (d, 1H), 8.02 (d, 1H), 8.06 (m, 1H), 12.54 (s, 1H).

### **3-Ethoxycarbonyloxybenzoyl chloride (4)**

To 3.0 g (0.15 mol) of 3-methoxycarbonyloxybenzoic acid in dry dichloromethane, one equivalent of oxalyl chloride in 0.2 M dichloromethane was added dropwise and the mixture was stirred for 5 hours at room temperature. The crude 3-methoxycarbonyloxybenzoyl chloride (**4**, 2.35 g, 0.01 mol) was collected after evaporation of excess solvent and reagent. Yield was 68%. <sup>1</sup>H-NMR ppm (400 MHz, CDCl<sub>3</sub>) δ 1.29 (t, 3H), 4.21 (m, 2H), 7.93 (dd, 1H), 7.66 (d, 1H), 7.96 (d, 1H), 8.00 (m, 1H).

### **Synthesis of 3-hydroxyhippuric acid (5) (31)**

The finely powdered 3-methoxycarbonyloxybenzoyl chloride (1.7 gm, 0.007 mol) was added to 0.6 g of glycine in 20 mL of 0.5 N NaOH. Subsequently, 1N NaOH was continuously added to the solution over a period of 15 minutes. The hydroxybenzoylglycine was extracted

with ethylacetate (3 × 15 mL). Crude product was obtained after evaporation of ethylacetate, and then re-crystallized in a 50% ethanol-water solvent system.

Final product yield was 0.8 g (48.33%) and analysis was carried out by <sup>1</sup>H-NMR and mass spectrometer. <sup>1</sup>H-NMR (DMSO-d<sub>6</sub>) δ 3.87 (d, 2H), 6.88-6.91 (m, 3H), 7.21-7.25 (m, 1H), 8.68 (t, 1H), 9.6 (s, 1H), 12.6 (s, 1H). MS (MH)<sup>+</sup> = 196.

## Results and Discussion

### 3-Hydroxyhippuric Acid Synthesis

3-Hydroxy-hippuric acid was synthesized from 3-hydroxy benzaldehyde (**1**) as the starting material. The hydroxyl group in (**1**) was first protected with ethylchloroformate to obtain 3-ethoxycarbonyloxy benzaldehyde (**2**). The aldehyde group in (**2**) was then oxidized to carboxylic acid (**3**) using oxone as the sole oxidizing agent. Oxidation of the aldehyde with oxone is a highly effective, easy to work up, one pot reaction. Oxone is also very stable, non-toxic, and has non-polluting byproducts as compared to transition metal oxidants used for the above type reactions. The carboxylic acid group in (**3**) was then converted to its more reactive chloride derivative, 3-ethoxycarbonyloxybenzoyl chloride (**4**). Finally, deprotection of the hydroxyl group of (**4**), and formation of 3-hydroxy-hippuric acid (**5**) was achieved in one single step by the reaction of acid chloride (**4**) with glycine in the presence of sodium hydroxide.

### 3-Hydroxyhippuric Acid Inhibition

Previous efforts to derivatize kynureninase crystals with substrate analogs (data not shown) had proven ineffective due to severe crystal cracking upon exposing crystals to the derivatization solution. Substituted hippurates were chosen for derivatization because these compounds can mimic the L-kyn/3-OH-kyn external aldimine Michaelis complex without forming a covalent adduct with PLP. Thus, avoiding the structural rearrangements associated

with substrate binding (32), common among PLP-dependent aminotransferases, which can lead to crystal cracking during derivatization. Of the substituted hippurates tested, 2-amino-3-hydroxyhippuric acid (synthesis not shown) proved to be significantly unstable and could not be used to derivatize crystals or measure its competitive inhibition constant accurately. 2-Aminohippuric acid did not inhibit the reaction between kynureninase and 3-OH-kyn at a concentration of 1 mM. 3-Hydroxyhippuric acid was the most stable of the substituted hippurates tested and was thus chosen for the co-crystallization experiments. This compound was found to be a competitive inhibitor of 3-hydroxy-DL-kynurenine with an inhibition constant ( $K_i$ ) of 60  $\mu\text{M}$ .

### **Kynureninase-3-Hydroxyhippuric Acid Inhibitor Complex**

Statistics for the refined model are presented in Table 2.1. The structure contained one monomer per asymmetric unit and had good geometry with 441/1 residues in the allowed/disallowed regions of the Ramachandran plot. The final model was refined to an  $R_{\text{value}}$  of 0.152,  $R_{\text{free}}$  value of 0.189, and covers 96% of the predicted amino acid sequence with 668 water molecules included in the final structure. The biologically active unit (dimer) can be generated by applying the crystallographic symmetry operator  $1-x, y, -z$  to the monomer. The regions between residues 1-5, 377-387, and 442-446 could not be modeled due to poorly ordered electron density. These regions had disordered electron density in the native kynureninase structure as well (18). Electron density could be seen extending between the  $\epsilon$  amino group of Lys-276 and the C-4' of PLP; an observation consistent with a kynureninase-PLP internal aldimine covalent adduct. Positive density for the 3-HHA molecule could be clearly observed in a difference electron density map ( $F_o-F_c$ ) calculated from the unrefined molecular replacement solution. Upon docking the 3-HHA molecule, electron density for 3-HHA atoms improved and

became continuous (Figure 2.1). Further refinement revealed the presence of a water molecule (water 669) in difference electron density maps within a short distance of the C2 atom of the 3-HHA aromatic ring. Refinement of water 669 and 3-HHA at full occupancy produced density for both molecules at negative contour levels in a difference electron density map. Upon adjustment of occupancies to 20% (water 669) and 80% (3-HHA), no residual positive or negative density ( $<3\sigma$ ) could be observed for either molecule. Interestingly, water 669 occupies a position relative to 3-HHA similar to that which would be occupied by a substituent at the 2-position of the 3-HHA aromatic ring. Water 669 is stabilized by hydrogen bonds to the hydroxyl group of Tyr-275 (2.90 Å) and the  $\delta$  NH<sub>2</sub> group of Asn-333\* (3.19 Å) (\* denotes residues on the two-fold symmetry related monomer). Thus, this partial occupancy water molecule reveals some of the interactions that are likely to stabilize the 2-substituent on the aromatic ring, such as the 2-amino group in 3-OH-kyn and L-kynurenine.

The 3-HHA molecule is stabilized within the kynureninase active site by interactions with residues from both monomer chains. The aromatic ring moiety of 3-HHA lies in the active site pocket between the side chains of Ile-110\*, His-102\*, Tyr-275, Trp-305\*, Phe-306\*, Phe-314\*, and Asn-333\* (Figure 2.2). Trp-305\* and Phe-314\* stabilize 3-HHA *via* alignment of their molecular quadrupole moments towards the aromatic ring (3.53 Å and 3.73 Å, respectively) and sandwich it with a  $\pi$ -stacking interaction against the side chain of His-102\*. Trp-305 is strictly conserved in kynureninases of eukaryotic and prokaryotic origin. Interestingly, Trp-305\* also participates in cofactor stabilization by hydrogen bonding through its side chain pyrrole nitrogen with a PLP (phosphate moiety) oxygen. Among PLP-dependent aminotransferases, the external aldimine scissile bond must be aligned perpendicular to the plane of the cofactor ring system in order to minimize the energy of the upcoming transition state (33). Thus, maintaining the

appropriate geometry between cofactor and substrate in order to maximize  $\sigma$ - $\pi$  overlap of the breaking bond with the cofactor  $\pi$ -system is crucial to catalysis. This complex reveals that Trp-305\* likely plays a key role in maintaining the geometry of the external aldimine covalent adduct, and subsequent intermediates, by interacting with both substrate and cofactor. Moreover, Trp-305\* is held firmly in position, relative to both cofactor and ligand, by two flanking quadrupole  $\pi$ -stacking interactions with the side chains of Phe-165 and Phe-306\*. Phe-165 is a crucial active site residue since it participates in cofactor stabilization by  $\pi$ -stacking with the pyridine ring moiety of PLP. Phe-165 is stabilized in this position by one further quadrupole  $\pi$ -stacking interaction with the side chain of Phe-225. Phe-165, Trp-305\*, and Phe-314\* are strictly conserved among kynureninases, regardless of their substrate specificity. Furthermore, all kynureninases have either a histidine or tryptophan residue at the bottom of the active site cavity to provide a  $\pi$ -stacking interaction to the substrate ring moiety.

Other interactions that stabilize 3-HHA include hydrogen bonding between the 3-hydroxyl ring substituent and the side chain  $\delta$  oxygen of Asn-333\* (3.54 Å). Also, the 3-HHA carbonyl oxygen is involved in a hydrogen bond with the hydroxyl oxygen of Tyr-275 (3.77 Å) and the 3-HHA amide nitrogen is within hydrogen bonding distance to the Ser-75  $\gamma$  oxygen (3.63 Å). On the other side of the active site cavity, and near the Lys-276-PLP internal aldimine imine bond, the 3-HHA carboxylate oxygens are electrostatically stabilized *via* bonds with the guanidino nitrogens of Arg-434 (2.98 Å and 3.06 Å), the  $\epsilon$  nitrogen of His-253 (2.74 Å), and with the  $\gamma$  oxygen of Ser-75 (2.88 Å). The interaction between the carboxylate of 3-HHA, which is the equivalent to the  $\alpha$ -carboxylate of L-enantiomer substrates, with the strictly conserved Arg-434 is well characterized among members of the PLP-dependent aspartate aminotransferase superfamily, and is crucial to catalysis (32, 34, 35).

A structural superposition of native (PDB accession code **2HZZ**) and 3-HHA complexed kynureninase reveals no major structural conformational changes. However, the side chains of residues Tyr-226, Arg-428, and Arg-434 showed side chain conformational differences associated with the presence of 3-HHA. Specifically, Arg-434 forms an electrostatic bond with the carboxylate oxygens of 3-HHA. In order to do so, the Arg-434 guanidino nitrogens must move 7.7 Å from the position observed in native Hkyn (18). Consistent with the partial occupancy for 3-HHA, the difference electron density map suggests two conformational states for the side chain of Arg-434: a high occupancy state (80%) in which the side chain interacts with the carboxylate oxygens in 3-HHA, and a low occupancy state (20%) in which no ligand is present in the active site and the Arg-434 side chain conformation resembles that of native Hkyn. Similarly, Tyr-226 and Arg-428 showed additional density in a difference electron density map, suggesting that these residues must adopt different conformations in order to accommodate 3-HHA in the active site cavity. Interestingly, these residues do not directly contact ligand atoms, yet they line the surface of an interdomain channel that leads to the active site cavity. Thus, these residues appear to be dynamically involved in substrate binding by allowing access to the active site. The position of these residues' side chains in ligand bound kynureninase places them at 4.4 Å (between hydroxyl oxygens of Tyr-226) and 3.7 Å (between guanidino nitrogens of Arg-428) from those in native kynureninase

### **Kinetic Characterization of Kynureninase Mutants**

Mutants were analyzed for their ability to hydrolyze L-kynurenine and 3-hydroxy-DL-kynurenine. The results are summarized in Table 2. 3-OH-kyn  $K_m$  and  $V_{max}$  values for N333T and S332G/N333T mutants could not be accurately determined as rates for high concentrations of 3-hydroxy-DL-kynurenine showed significant substrate, or possibly D-enantiomer inhibition.

Moreover, these data could not be accurately fit with a substrate inhibition model. Thus,  $K_m$  values for these mutants (N333T and S332G/N333T) are estimated as greater than the last 3-OH-kyn concentration at which hydrolysis rates were still increasing in a linear fashion. The  $k_{cat}/K_m$  values for these mutants were calculated by estimating the second order rate constant ( $V/K_m$ ) along the linear portion of a  $v$  vs.  $[S]$  plot. Subsequently, the estimated  $K_m$  and  $k_{cat}/K_m$  values were used to calculate the upper limit of  $k_{cat}$ . Kynureninase H102W/N333T and H102W/S332G/N333T mutants did not have any measurable activity in an assay containing 3-OH-kyn at a concentration of  $600 \times 10^{-6}$  M and  $3.72 \times 10^{-5}$  M kynureninase. Thus, these values were used to estimate a theoretical upper limit for  $k_{cat}/K_m$  by making 3-OH-kyn  $K_m = 600 \times 10^{-6}$  M and  $V_{max} = 0.0001$  mAU  $\text{min}^{-1}$ .

Characterization of the kinetic properties of the kynureninase N333T mutant revealed a 9-fold decrease in L-kyn  $k_{cat}$  but no change in binding affinity. Yet, this mutant had weaker 3-OH-kyn binding (7-fold less) and hydrolyzed it at a rate at least  $1.1 \times 10^3$  times slower than wild type (Wt) kynureninase. Thus, this mutation affects 3-OH-kyn binding and reduces its catalytic efficiency ( $k_{cat}/K_m$ ) by a factor of  $6 \times 10^3$ , whereas the  $K_m$  for L-kyn is not affected and  $k_{cat}/K_m$  is reduced only 9-fold. These results suggest that the non-polar interaction between the 3-methylene of L-kyn and the  $\gamma$  carbon of Thr-333 does not solely control the L-kyn binding affinity. Contrarily, the hydrogen bond formed between the 3-OH group in 3-OH-kyn and the  $\gamma$  hydroxyl of Asn-333 appears to be an important determinant for 3-OH-kyn binding.

Isolation and characterization of kynureninase single mutant H102W was not possible since it could not be purified from the soluble cellular extract and appeared entirely in the insoluble protein fraction. We did not attempt to solubilize and re-fold protein from the inclusion bodies that resulted from these cultures. This pellet was of identical apparent SDS-PAGE

molecular weight as Wt kynureninase. However, combination of H102W and N333T mutations restored the expression of soluble protein to levels similar to that of Wt kynureninase. These results are consistent with the observation that kynureninases contain pairings of residues at this position that are consistently his/asn or trp/thr pairs (18). Characterization of the kynureninase mutant H102W/N333T revealed a small increase in binding affinity for L-kyn (1.5 fold), yet a sufficiently large change in  $k_{cat}/K_m$  for 3-OH-kyn that resulted in the lack of any measurable activity with this substrate. The net effect was a decrease in catalytic efficiency towards 3-OH-kyn by a factor of at least  $7.5 \times 10^6$  when compared to that of Wt kynureninase, although this number in principle could be significantly larger since no activity could be measured. Thus, removing the hydrogen bonding partner at the  $\gamma$  position of Asn-333, increasing the local non-polar environment, and introducing a large bulky side chain (Trp-102) effectively act to exclude any 3-OH-kyn binding at the concentrations measured. This suggests that these residues (Asn-333 and His-102) are the primary substrate specificity contacts for the 3-substituent on the kynurenine aromatic ring. Yet, these mutations appear not restore any of the catalytic potential for L-kyn since these mutants are 30-fold less efficient at hydrolyzing this substrate than the Wt enzyme, suggesting that further mutations in the surrounding shell of residues must be performed to restore catalytic activity. In order to further probe which residues contribute to catalytic efficiency we introduced a third mutation, S332G, a residue showing a conserved pattern among orthologs utilizing L-kyn or 3-OH-kyn similar to that of His-102 and Asn-333. A serine residue is conserved at this position among 3-OH-kyn hydrolyzing kynureninases, whereas kynureninases from organisms lacking the 3-OH-kyn metabolite contain a conserved glycine. The residue at this position hydrogen bonds through the backbone amide nitrogen with one of the PLP phosphate moiety oxygens, and in the complex presented here it does not hydrogen bond or

have electrostatic contacts with atoms in 3-HHA. H102W/S332G/N333T mutants had the strongest binding affinity and catalytic efficiency towards L-kyn of all mutants studied and showed no activity with 3-OH-kyn. H102W/S332G/N333T mutants had a 6-fold improvement in  $k_{\text{cat}}/K_{\text{m}}$  over H102W/N333T mutants, thus restoring catalytic efficiency to one third of that measured with Wt enzyme. From these results, we infer that the increased backbone elasticity provided by Gly-332 imparts flexibility to the interaction between Thr-333 and the bulky side chain of Trp-102, allowing a better fit of L-kyn within the mutant Hkyn active site cavity. Furthermore, this suggests that two shells of residues surrounding ligand atoms determine catalytic efficiency. One shell of residues directly contacts ligand atoms and the other contributes to the geometrical arrangement of the active site and plays a dynamic role in catalysis as opposed to a mechanistic one.

## Conclusion

Currently, a number of kynureninase inhibitors have been reported in the literature (36-41). Yet, their design is purely mechanistic in nature due to a lack of knowledge regarding the primary substrate binding mode and substrate-enzyme interactions required for *in silico* directed drug design. The *H. sapiens* kynureninase-3-HHA complex reveals important restraints for the design and screening of novel substrate analogs and kynureninase inhibitors. First, the following atoms should be designated as hydrogen bonding partners for ligand atoms: the side chain  $\delta$  oxygen of Asn-333\*, the side chain hydroxyl oxygen of Tyr-275, and the  $\gamma$  oxygen of Ser-75. Second, hydrophobic interactions should be maintained between aromatic substituents on screened ligands and the side chains of Ile-110\*, Trp-305\*, Phe-306\*, and Phe-314\*. 3-HHA-kynureninase interactions clearly show that a strong quadrupole molecular alignment occurs between the side chains of Trp-305\*, Phe-314\*, and the aromatic ring moiety of 3-HHA, as well

as ligand  $\pi$ -stacking against the side chain of His-102\*. Third, electrostatic and/or hydrogen bonding interactions should be assigned between ligand atoms and the guanidino nitrogens of Arg-434 and the imidazole nitrogen atoms of His-253. Fourth, our results clearly show that His-102 and Asn-333 are the substrate specificity conveying residues regarding substituents at the 3 position of the aromatic ring. As such, the interaction between these residues and ligand atoms should be used as a one of the primary forms of binding mode evaluation in docking studies. Furthermore, scoring of docked poses should consider the interaction between ligand atoms and Arg-434 side chain atoms as a strong indicator of acceptable docking since this form of stabilization is known to be crucial in ligand binding and stabilization throughout the PLP-dependent aspartate aminotransferase family of enzymes.

### **Acknowledgements**

Results shown in this report are derived from work performed at Argonne National Laboratory, Structural Biology Center at the Advanced Photon Source. Argonne is operated by UChicago Argonne, LLC, for the U.S. Department of Energy, Office of Biological and Environmental Research under contract DE-AC02-06CH11357.

## References

- (1) Soda, K., and Tanizawa, K. (1979) Kynureninases: enzymological properties and regulation mechanism. *Adv Enzymol Relat Area Mol Biol* 49, 1-40.
- (2) Colabroy, K. L., and Begley, T. P. (2005) The pyridine ring of NAD is formed by a nonenzymatic pericyclic reaction. *J Am Chem Soc* 127, 840-1.
- (3) Schwarcz, R., Whetsell, W. O., Jr., and Mangano, R. M. (1983) Quinolinic acid: an endogenous metabolite that produces axon-sparing lesions in rat brain. *Science* 219, 316-8.
- (4) Stone, T. W., and Perkins, M. N. (1981) Quinolinic acid: a potent endogenous excitant at amino acid receptors in CNS. *Eur J Pharmacol* 72, 411-2.
- (5) Heyes, M. P., Brew, B., Martin, A., Markey, S. P., Price, R. W., Bhalla, R. B., and Salazar, A. (1991) Cerebrospinal fluid quinolinic acid concentrations are increased in acquired immune deficiency syndrome. *Adv Exp Med Biol* 294, 687-90.
- (6) Achim, C. L., Heyes, M. P., and Wiley, C. A. (1993) Quantitation of human immunodeficiency virus, immune activation factors, and quinolinic acid in AIDS brains. *J Clin Invest* 91, 2769-75.
- (7) Heyes, M. P., Swartz, K. J., Markey, S. P., and Beal, M. F. (1991) Regional brain and cerebrospinal fluid quinolinic acid concentrations in Huntington's disease. *Neurosci Lett* 122, 265-9.
- (8) Giorgini, F., Moller, T., Kwan, W., Zwillig, D., Wacker, J. L., Hong, S., Tsai, L. C., Cheah, C. S., Schwarcz, R., Guidetti, P., and Muchowski, P. J. (2008) Histone deacetylase inhibition modulates kynurenine pathway activation in yeast, microglia, and mice expressing a mutant huntingtin fragment. *J Biol Chem* 283, 7390-400.

- (9) Guillemin, G. J., Meininger, V., and Brew, B. J. (2005) Implications for the kynurenine pathway and quinolinic acid in amyotrophic lateral sclerosis. *Neurodegener Dis* 2, 166-76.
- (10) Leonard, B. E. (2007) Inflammation, depression and dementia: are they connected? *Neurochem Res* 32, 1749-56.
- (11) Guillemin, G. J., Brew, B. J., Noonan, C. E., Takikawa, O., and Cullen, K. M. (2005) Indoleamine 2,3 dioxygenase and quinolinic acid immunoreactivity in Alzheimer's disease hippocampus. *Neuropathol Appl Neurobiol* 31, 395-404.
- (12) Stone, T. W., Mackay, G. M., Forrest, C. M., Clark, C. J., and Darlington, L. G. (2003) Tryptophan metabolites and brain disorders. *Clin Chem Lab Med* 41, 852-9.
- (13) Schwarcz, R., and Pellicciari, R. (2002) Manipulation of brain kynurenines: glial targets, neuronal effects, and clinical opportunities. *J Pharmacol Exp Ther* 303, 1-10.
- (14) Stone, T. W., and Addae, J. I. (2002) The pharmacological manipulation of glutamate receptors and neuroprotection. *Eur J Pharmacol* 447, 285-96.
- (15) Tankiewicz, A., Pawlak, D., and Buczko, W. (2001) [Enzymes of the kynurenine pathway]. *Postepy Hig Med Dosw* 55, 715-31.
- (16) Shetty, A. S., and Gaertner, F. H. (1975) Kynureninase-Type enzymes of *Penicillium roqueforti*, *Aspergillus niger*, *Rhizopus stolonifer*, and *Pseudomonas fluorescens*: further evidence for distinct kynureninase and hydroxykynureninase activities. *J Bacteriol* 122, 235-44.
- (17) Toma, S., Nakamura, M., Tone, S., Okuno, E., Kido, R., Breton, J., Avanzi, N., Cozzi, L., Speciale, C., Mostardini, M., Gatti, S., and Benatti, L. (1997) Cloning and recombinant expression of rat and human kynureninase. *FEBS Lett* 408, 5-10.

- (18) Lima, S., Khristoforov, R., Momany, C., and Phillips, R. S. (2007) Crystal structure of Homo sapiens kynureninase. *Biochemistry* 46, 2735-44.
- (19) Use of the Advanced Photon Source was supported by the U. S. Department of Energy, O. o. S., Office of Basic Energy Sciences, under Contract No. W-31-109-Eng-38.
- (20) Otwinowski, Z., and W., M. (1997) Processing of X-ray Diffraction Data Collected in Oscillation Mode. *Methods in Enzymology* 276, 307-326.
- (21) McCoy, A. J., Grosse-Kunstleve, R. W., Storoni, L. C., and Read, R. J. (2005) Likelihood-enhanced fast translation functions. *Acta Crystallogr D Biol Crystallogr* 61, 458-64.
- (22) Murshudov, G. N., Vagin, A. A., and Dodson, E. J. (1997) Refinement of macromolecular structures by the maximum-likelihood method. *Acta Crystallogr D Biol Crystallogr* 53, 240-55.
- (23) Lamzin, V. S., Perrakis, A., and Wilson, K. S. (2001) The ARP/WARP suite for automated construction and refinement of protein models. In *Int. Tables for Crystallography, Vol. F*, Dordrecht, Kluwer Academic Publishers, The Netherlands.
- (24) Emsley, P., and Cowtan, K. (2004) Coot: model-building tools for molecular graphics. *Acta Crystallogr D Biol Crystallogr* 60, 2126-32.
- (25) Winn, M. D., Isupov, M. N., and Murshudov, G. N. (2001) Use of TLS parameters to model anisotropic displacements in macromolecular refinement. *Acta Crystallogr D Biol Crystallogr* 57, 122-33.
- (26) Collaborative Computational Project, N. (1994) The CCP4 Suite: Programs for Protein Crystallography. *Acta Cryst D*50.

- (27) Davis, I. W., Leaver-Fay, A., Chen, V. B., Block, J. N., Kapral, G. J., Wang, X., Murray, L. W., Bryan Arendall, W., 3rd, Snoeyink, J., Richardson, J. S., and Richardson, D. C. (2007) MolProbity: all-atom contacts and structure validation for proteins and nucleic acids. *Nucleic Acids Res.*
- (28) Cleland, W. W. (1979) Statistical analysis of enzyme kinetic data. *Methods Enzymol* 63, 103-38.
- (29) Dalgliesh, C. E., Mann, F. G. (1947) Synthesis of  $\beta$ -(3, 4-dihydroxyphenyl)-N-methylserine (adrenalinecarboxylic acid). *Journal of the Chemical Society*, 658-62.
- (30) Travis, B. R. S., M.; Hollist, G. O.; Borhan, B. (2003) Facile Oxidation of Aldehydes to Acids and Esters with Oxone. *Organic Letters* 5, 1031-1034.
- (31) Acheson, R. M. B., D. A.; Brettle, R.; Harris, A. M. (1960) Synthesis of some acylglycines and related oxazolones. *Journal of the Chemical Society*, 3457-61.
- (32) Jager, J., Moser, M., Sauder, U., and Jansonius, J. N. (1994) Crystal structures of *Escherichia coli* aspartate aminotransferase in two conformations. Comparison of an unliganded open and two liganded closed forms. *J Mol Biol* 239, 285-305.
- (33) Dunathan, H. C. (1966) Conformation and reaction specificity in pyridoxal phosphate enzymes. *Proc Natl Acad Sci U S A* 55, 712-6.
- (34) Delle Fratte, S., Iurescia, S., Angelaccio, S., Bossa, F., and Schirch, V. (1994) The function of arginine 363 as the substrate carboxyl-binding site in *Escherichia coli* serine hydroxymethyltransferase. *Eur J Biochem* 225, 395-401.
- (35) Almo, S. C., Smith, D. L., Danishefsky, A. T., and Ringe, D. (1994) The structural basis for the altered substrate specificity of the R292D active site mutant of aspartate aminotransferase from *E. coli*. *Protein Eng* 7, 405-12.

- (36) Walsh, H. A., O'Shea, K. C., and Botting, N. P. (2003) Comparative inhibition by substrate analogues 3-methoxy- and 3-hydroxydesaminokynurenine and an improved 3 step purification of recombinant human kynureninase. *BMC Biochem* 4, 13.
- (37) Walsh, H. A., Leslie, P. L., O'Shea, K. C., and Botting, N. P. (2002) 2-Amino-4-[3'-hydroxyphenyl]-4-hydroxybutanoic acid; a potent inhibitor of rat and recombinant human kynureninase. *Bioorg Med Chem Lett* 12, 361-3.
- (38) Heiss, C., Anderson, J., and Phillips, R. S. (2003) Differential effects of bromination on substrates and inhibitors of kynureninase from *Pseudomonas fluorescens*. *Org Biomol Chem* 1, 288-95.
- (39) Fitzgerald, D. H., Muirhead, K. M., and Botting, N. P. (2001) A comparative study on the inhibition of human and bacterial kynureninase by novel bicyclic kynurenine analogues. *Bioorg Med Chem* 9, 983-9.
- (40) Chiarugi, A., Carpenedo, R., Molina, M. T., Mattoli, L., Pellicciari, R., and Moroni, F. (1995) Comparison of the neurochemical and behavioral effects resulting from the inhibition of kynurenine hydroxylase and/or kynureninase. *J Neurochem* 65, 1176-83.
- (41) Carpenedo, R., Chiarugi, A., Russi, P., Lombardi, G., Carla, V., Pellicciari, R., Mattoli, L., and Moroni, F. (1994) Inhibitors of kynurenine hydroxylase and kynureninase increase cerebral formation of kynurenate and have sedative and anticonvulsant activities. *Neuroscience* 61, 237-43.

**Table 2.1:** Summary of Crystallographic Analysis

space group	<i>C</i> 2
resolution range (outer shell) Å	89.09-1.65 (1-65.1-693)
no. of reflections (outer shell)	55445 (2993)
R <sub>factor</sub> (outer shell)	0.15419 (0.251)
R <sub>free</sub> <sup>a</sup> (outer shell)	0.19001 (0.342)
R <sub>sym</sub> (outer shell)	0.052 (0.0387)
mean <i>B</i> value (Å <sup>2</sup> )	16.592
rmsd from ideal geometry	
bond angles (deg)	1.067
bond distances (Å)	0.007
Ramachandran plot residues (%)	97.06/2.71/0.23
in favored/allowed/disallowed regions	

<sup>a</sup>R<sub>free</sub> calculated with 5.1% of the total data that were excluded from refinement.

**Table 2.2.** Summary of L-kynurenine and 3-OH-DL-kynurenine kinetic constants for wild type and kynureninase mutants.

Enzyme	L-Kynurenine			3-OH-DL-Kynurenine			k <sub>cat</sub> /K <sub>m</sub> Ratio
	K <sub>m</sub> (M)	k <sub>cat</sub> (s <sup>-1</sup> )	k <sub>cat</sub> /K <sub>m</sub> (M <sup>-1</sup> s <sup>-1</sup> )	K <sub>m</sub> (M)	k <sub>cat</sub> (s <sup>-1</sup> )	k <sub>cat</sub> /K <sub>m</sub> (M <sup>-1</sup> s <sup>-1</sup> )	
Wt	495x10 <sup>-6</sup>	230x10 <sup>-3</sup>	465	28.3x10 <sup>-6</sup>	3.5	1.23x10 <sup>5</sup>	3.78x10 <sup>-3</sup>
N333T	499x10 <sup>-6</sup>	26x10 <sup>-3</sup>	52.1	>200x10 <sup>-6</sup>	<3.9x10 <sup>-3</sup>	19.8*	2.63
S332G N333T	540x10 <sup>-6</sup>	17x10 <sup>-3</sup>	31.4	>510x10 <sup>-6</sup>	<10.9x10 <sup>-3</sup>	21.5*	1.46
H102W N333T	327x10 <sup>-6</sup>	7x10 <sup>-3</sup>	21.4	N/A	N/A	<0.0165 <sup>§</sup>	>1.36x10 <sup>3</sup>
H102W S332G N333T	143.3x10 <sup>-6</sup>	18x10 <sup>-3</sup>	125.6	N/A	N/A	<0.0165 <sup>§</sup>	>7.61x10 <sup>3</sup>

\*Values k<sub>cat</sub>/K<sub>m</sub> for these mutants were calculated by estimating the second order rate constant (V/K<sub>m</sub>) along the linear portion of a v vs. [S] plot.

§These mutants did not have any measurable activity in an assay containing 3-OH-kyn at a concentration of 600 x 10<sup>-6</sup> M and 3.72 x 10<sup>-5</sup> M kynureninase. Thus, these values were used to estimate a theoretical upper limit for k<sub>cat</sub>/K<sub>m</sub> by making 3-OH-kyn K<sub>m</sub> = 600 x 10<sup>-6</sup> M and V<sub>max</sub> = 0.0001 mAU min<sup>-1</sup>

**Figure 2.1.** An electron density map showed continuous electron density for 3-HHA atoms (green bonds, ball and stick atoms, CPK coloring).

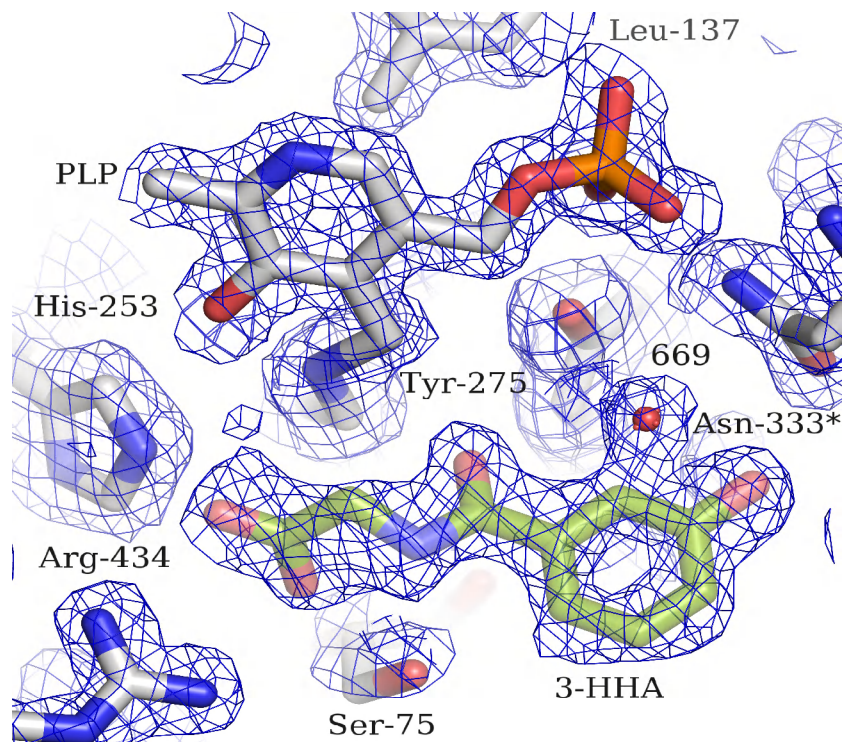
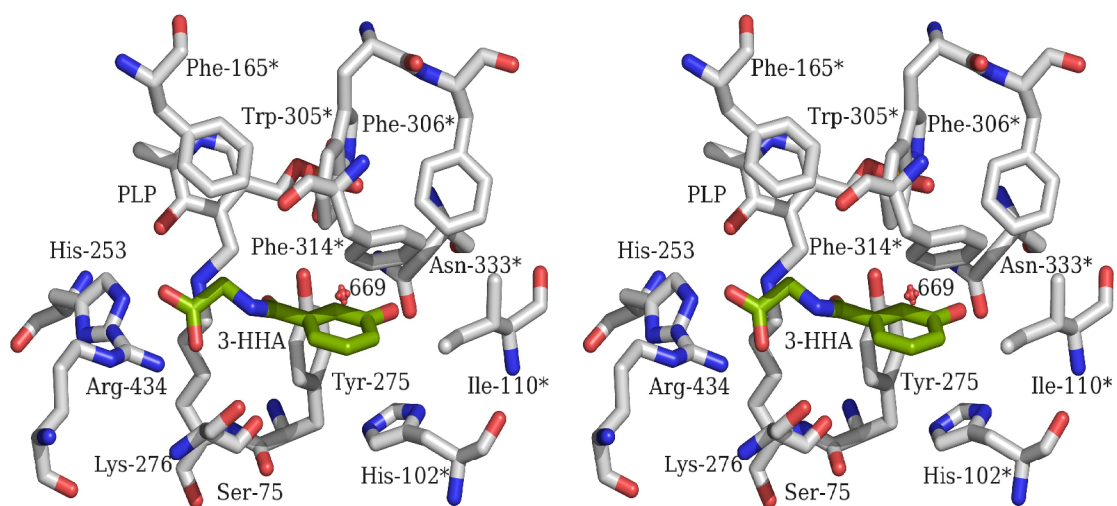


**Figure 2.2.** Stereo representation of the interactions that stabilize 3-HHA (colored green, ball and stick atoms) within the Homo sapiens kynureninase active site. Residues contributed from the symmetry related monomer are labeled with an asterisk (\*).



## CHAPTER 3

THE CRYSTAL STRUCTURE OF THE *PSEUDOMONAS DACUNHAE* L-ASPARTATE-B-  
DECARBOXYLASE REVEALS A NOVEL OLIGOMERIC ASSEMBLY FOR A  
PYRIDOXAL-5'-PHOSPHATE DEPENDENT ENZYME<sup>3</sup>

---

<sup>3</sup> Santiago Lima, Bakthavatsalam Sundararaju, Christina Huan Huan Huang, Roman Khristoforov, Cory Momany, and Robert S. Phillips. To be submitted to *Journal of Molecular Biology*

## Abstract

The *Pseudomonas dacunhae* L-aspartate- $\beta$ -decarboxylase (ABDC, aspartate 4-decarboxylase, aspartate 4-carboxylase, E.C. 4.1.1.12) is a pyridoxal-5'-phosphate (PLP) dependent enzyme that catalyzes the  $\beta$ -decarboxylation of L-aspartate to produce L-alanine and CO<sub>2</sub>. This catalytically versatile enzyme is known to form functional dodecamers at its catalytically optimal pH and is thought to work in conjunction with an L-asp/L-ala antiporter to establish a proton gradient across the membrane that can be used for ATP biosynthesis. We have solved the atomic structure of ABDC to 2.0 Å resolution using SAD phasing. The structure reveals that ABDC oligomerizes as a homododecamer in a novel mode using a domain unique among PLP-dependent enzymes. ABDC has highest structural homology with members of the aspartate aminotransferase subfamily of PLP-dependent enzymes. Based on the structure of the ABDC active site we have characterized an Arg-37 mutant to evaluate its role as a second catalytic base in the ABDC mechanism.

## Abbreviations

AAT, Aspartate aminotransferase; ABDC, Aspartate- $\beta$ -Decarboxylase; PLP, pyridoxal-5'-phosphate;

## Keywords

aspartate-beta-decarboxylase; PLP; aminotransferase; ABDC; dodecamer; vitamin B6

## Introduction

The *Pseudomonas dacunhae* L-aspartate- $\beta$ -decarboxylase (ABDC) is a pyridoxal-5'-phosphate (PLP) dependent enzyme that catalyzes the  $\beta$ -decarboxylation of L-aspartate (L-asp) to produce L-alanine (L-ala) and CO<sub>2</sub>. This prokaryotic enzyme is known for its catalytic versatility (1,2), its activation by  $\alpha$ -keto acids (1,3-5), and its use in the industrial-scale

biocatalytic synthesis of L-ala by immobilized *P. dacunhae* and other organisms (6,7). Although some of the ABDC steady-state properties have been extensively studied, many details regarding its catalytic mechanism remain uncharacterized. Previous work has shown that the ABDC catalyzed decarboxylation of L-asp proceeds through an L-asp ketimine intermediate (8). To yield L-ala, ABDC must prevent ketimine hydrolysis and limit the production of the transamination product, oxaloacetate, to a small fraction of total turnovers (2). Instead, ABDC must direct the  $\beta$ -decarboxylation of the L-asp ketimine to yield an L-ala enamine, which is subsequently re-protonated at C- $\beta$  with an unusual inversion of stereochemistry (8,9). Although this implies a handful of mechanistic scenarios, the most likely appears to be one in which there are two bases involved in the deprotonation/protonation steps (9). Assuming that, as in all other members of the AAT-family of PLP-dependent enzymes, the Schiff base forming active site lysine side chain abstracts and donates a proton to the  $\alpha$ -carbon and PLP C-4' (ketimine formation), then the identity of the second catalytic base is unknown. In this report we evaluate the role of the active site residue Arg-37 as a possible second catalytic base in the ABDC mechanism.

The *in vivo* function of ABDC in *P. dacunhae* is poorly understood, but as with other degradative decarboxylases, it is thought to function in combination with a dicarboxylate/monocarboxylate antiporter to establish a proton gradient across the membrane that can be used for ATP biosynthesis (10,11). Similar mechanisms are employed by *E.coli* in which arginine or glutamate decarboxylation consumes scalar protons to regulate the intracellular pH and generate ATP (12). *In vitro* studies have shown that ABDC forms homododecameric particles, has highest activity at pH 5.5, and partially dissociates into dimers with lower catalytic activity as the pH increases (2).

Although crystallization conditions for ABDC were first reported in 1969 (13), no structures have been made available. In this work we present the cloning, new crystallization conditions, and the structure of the dodecameric assembly to 2.0 Å resolution.

## Results

### Protein Purification, Crystallization, Crystal Harvesting

Although the purification of recombinant ABDC from a one liter culture yields approximately 60 mg of soluble crystallization-grade protein, a large amount of insoluble protein with an SDS-PAGE apparent molecular weight (data not shown) identical to soluble ABDC is produced during the expression of ABDC in *E. coli* BL21(DE3). We did not attempt to optimize the growth conditions to increase the yield of soluble ABDC or solubilize the inclusion bodies that resulted from each culture. ABDC extracts readily precipitate if the protein concentration exceeds 13-15 mg mL<sup>-1</sup>.

A large number (>20) of crystallization conditions were identified during high throughput crystallization trials. Of these, five conditions were reproduced in house and found to yield crystals that grew very large in size (>1 x 1 x 1 mm) and had poor diffraction properties –i.e. mosaicity  $\geq 1.25^\circ$  per  $0.5^\circ$  oscillation, low resolution, large and irregular spot size (data not shown). The crystallization conditions used to grow crystals, for which data is presented in this manuscript, were identified by combining two high throughput conditions and adding glycerol at varying concentrations. For most ABDC crystals, we observed a significant improvement of the diffraction properties such as lower mosaicity, sharpened spot size and shape, and improved resolution (data not shown) when the protein crystals were grown with increasing amounts of glycerol. In the absence of glycerol, poorly diffracting crystals form within five minutes of mixing protein and precipitant solutions. Although crystallization conditions used for the

crystallographic studies contained 10% glycerol, ABDC will crystallize (albeit more slowly) in glycerol concentrations that exceed 20%. X-ray data collection at room temperature (25 °C) revealed that ABDC crystals were very sensitive to changes in the concentrations of additives in the mother solution. The crystallization conditions used for the structure determination will produce ABDC crystals that can grow very large in size (up to 1 x 1 x 1 mm), but these large crystals were sensitive to the flash freezing process. We found that small (0.2 x 0.2 x 0.2 mm) ABDC crystals tolerated freezing best. Moreover, ABDC crystals had to be introduced to cryoprotectant conditions very slowly (in 1  $\mu$ L increments) with at least 5-10 minutes of equilibration time at each step. It was necessary to premix the cryoprotectant with an equal volume of the well mother liquor before adding the mixture back to the crystal.

### **Model Quality**

26 amino acids at the N-terminus and the last six C-terminal residues could not be modeled due to poor electron density for these regions. Thus, the final model covers 93% of the amino acid sequence derived from the DNA and contains 316 waters with one PLP molecule per monomer. The final model has good geometry with 494/2 in the allowed/ disallowed regions of the Ramachandran plot, and was refined to a  $R_{\text{free}}$  and  $R_{\text{value}}$  of 0.24123 and 0.18479 (See Table 3.1 for crystallographic statistics).

### **Subunit Structure**

Each ABDC monomer contains one pyridoxal-5'-phosphate molecule covalently bound *via* a Schiff base linkage with Lys-315 (Fig 3.1) and is composed of three major domains: a large, small, and oligomerization domain. The large domain (residues 131-404) contains a seven-stranded anti-parallel  $\beta$ -sheet ( $\beta$ -strands S1, S7, S6, S5, S4, S2, S3) surrounded by  $\alpha$ -helices ( $\alpha\beta\alpha$  architecture). The small domain (residues 1-44 and 405-533) contains a two-stranded antiparallel

$\beta$ -sheet ( $\beta$ -strands S8, S9) flanked by  $\alpha$ -helices on one side ( $\alpha\beta$  architecture). The organization of the secondary structure elements in the large and small domains of ABDC is consistent with that of members of the aspartate aminotransferase family of PLP-dependent enzymes (14). The remaining residues (residues 45-130) participate in the formation of the oligomerization domain, which is composed of four sequential amphiphilic  $\alpha$ -helices ( $\alpha$ -helices H2-H5) forming a tightly packed bundle with a hydrophobic core of strictly conserved residues (Phe-57, Ile-83, Phe-87, Leu-103, Val-110, Phe-121, Met-125). A BLAST analysis (15,16) with the full length ABDC amino acid sequence (E-value cutoff 0.01) revealed that it contains the putative conserved aspartate/tyrosine/aromatic aminotransferase (COG0436) and the aminotransferase class I and II domains (pfam 00155). A PDB-wide structure-structure similarity search with SSM (17,18) identified members of the aspartate aminotransferase subfamily of PLP-dependent transferases ( $\alpha$ -family) to be the most structurally homologous to ABDC. SSM ranked aspartate aminotransferase (PDB accession no. **1BJW**, Z-score = 9.3) as the closest match, with glutamine aminotransferase (PDB accession no. **1V2D**, Z-score = 9.2) and alanine aminotransferase (PDB accession no. **1XI9**, Z-score = 8.8) second and third, respectively. A structural superposition between these aminotransferases and ABDC revealed that the following active site residues are conserved (ABDC residue numbering): Gly-38, Tyr-134\*, Tyr-207, Asn-256, Asp-286, Tyr-289, Lys-315, Arg-323, and Arg-497 (\* denotes a residue contributed by the two-fold symmetry related monomer). A Conserved Domain Database (CDD) (19) search showed that ABDC does not contain the PLP-dependent  $\alpha$ -decarboxylase (pfam00282) or the arginine/lysine/ornithine decarboxylase conserved domains (COG1982, pfam02176). Moreover, the ABDC consensus sequence Ser-Phe-Ser-Lys(PLP) does not match that of the “canonical”  $\alpha$ -decarboxylase (20) motif Ser-X-His-Lys(PLP). Thus, ABDC lacks the conserved histidine critical for  $\alpha$ -

decarboxylase activity that is known to have several roles during the decarboxylase catalytic cycle including reprotonation of C- $\alpha$  (20). BLAST analysis (E-value cutoff 0.01) using the oligomerization domain sequence only (residues 45-130), followed by a sequence alignment (not shown), showed that this region is highly conserved among ABDCs. The analysis revealed this region to be annotated within the conserved domain PRK09275 (which broadly covers aspartate aminotransferases) in the National Center for Biotechnology Information (NCBI) CDD. Yet the structural alignment with aspartate aminotransferases (AAT) reveals that AATs do not contain this segment of highly conserved residues (ABDC residues 45-130). Moreover, the PDB-wide homology search with SSM and the NCBI database search revealed that this segment of residues is unique to ABDC and not found in any other PLP-dependent enzyme. Indeed, the SSM structure similarity search found only marginally homologous folds (E-value > 1) among the DNA binding domains of transcriptional regulators and DNA binding proteins. These results suggest that a CDD entry specific to the aspartate- $\beta$ -decarboxylases can be assigned to this segment (*P. dacunhae* ABDC residues 45-130).

### **Active Site**

The ABDC active site (Fig. 3.2) is formed at the interface of large and small domains in adjacent monomers related by a two-fold axis of symmetry. Electron density for active site residues was well ordered and could be clearly observed extending between the  $\epsilon$  carbon of Lys-315 and the PLP 4' carbon, an observation consistent with the presence of a PLP-enzyme internal aldimine complex. Interactions that stabilize the phosphate oxygens of the PLP cofactor include hydrogen bonds with side chain and main chain atoms of residues Arg-37, Tyr-134\*, Gly-174, Thr-175, Ser-312, Ser-314, and Arg-323. Also, the PLP imidazolium nitrogen forms a strong hydrogen bond with the side chain of Asp-286 (2.40 Å), which is the expected  $\alpha$ -family

conserved aspartate involved in maintaining the dipolar ionic tautomer of PLP among  $\alpha$ -family members (22). The same carboxylate oxygen in Asp-286 that hydrogen bonds with PLP nitrogen also forms a hydrogen bond with the side chain of Tyr-207 (2.69 Å). This salt bridge/hydrogen bond with an adjacent side chain aids in the stabilization of the positive charge at the PLP imidazolium nitrogen among AATs (23). The other Asp-286 carboxylate oxygen participates in a hydrogen bond with the main chain amide nitrogen of Val-288 (3.27 Å). Val-288 and Phe-204 sandwich the aromatic ring of the cofactor, whereas the PLP 3' oxygen forms hydrogen bonds with the side chain atoms of Asn-256 (2.73 Å) and Tyr-289 (2.99 Å). Tyr-289 is in an extended hydrogen bond network with Tyr-441 (2.58 Å), which in turn is hydrogen bonded with the main chain amide nitrogen of Gly-38 (3.10 Å) and the carbonyl oxygen of Gly-36 (3.56 Å). These hydrogen bonds assist in tethering an N-terminal domain loop succeeding  $\alpha$ -helix H1 to the active site, and thus position Arg-37 directly over the *re*-side of the Lys-315-PLP covalent adduct. One of the side chain guanidino nitrogens of Arg-37 is stabilized by a strong hydrogen bond (2.54 Å) with the PLP ester linkage oxygen, and with the Tyr-134 side chain hydroxyl group. Residues Arg-37, Tyr-134, Gly-174, Thr-175, Tyr-207, Asn-256, Asp-286, Tyr-289, Val-288, Ser-312, Ser-314, and Arg-323 are strictly conserved among ABDCs.

### **Comparison Between ABDC and AAT Active Sites**

A structural alignment between *E. coli* AAT (PDB accession no. **1X2A**) and ABDC reveals their active sites are highly homologous (Fig. 3.3), yet some amino acid substitutions exist between residues surrounding the PLP cofactor: (AAT/ABDC residue numbering) His-143/Tyr-207, Trp-140/Phe-204, Ala-224/Val-288, and Phe-360/Tyr-441. Also, AAT does not contain a residue equivalent to the ABDC Arg-37, yet the adjacent residue Gly-38, which is thought to contribute to the ground state destabilization of the Michaelis complex in AAT (24), is

conserved. The alignment with AAT reveals that Arg-37 side chain atoms closely overlay with atoms of the  $\beta$ -carboxylate in the AAT PLP-D-glutamate complex. This geometrical arrangement between Arg-37 side chain atoms and external aldimine atoms is also seen with other ligand bound AAT structures (PDB accession nos. **1GCK**, **1BKG**) (not shown) and those of the glutamine aminotransferase (PDB accession no. **1V2F**) (not shown). Other active site amino acids conserved between ABDC and AAT include those that are known to bind the  $\alpha$  and  $\beta$  carboxylates of incoming and bound substrates in AAT: Arg-292 and Arg-386 (ABDC equivalent residues Arg-375 and Arg-497), as well as the AAT Tyr-225 (Tyr-289 in ABDC). Interestingly, an *E. coli* AAT triple Y225R/R292K/R386A mutant has been shown to preferentially catalyze an L-asp  $\beta$ -decarboxylase reaction even though these mutations eliminate identity with the ABDC active site (25). This suggests that the hydrogen bond/electrostatic interactions contributed by these residues are not essential to  $\beta$ -decarboxylase activity. The alignment also reveals that ABDC active site residues must undergo a conformational change to accommodate incoming ligands. This is clearly the case since the conformation of the ABDC Arg-375 and Arg-497 side chains greatly differ from those of the ligand bound AAT. Moreover, it is likely that Arg-37 must also undergo a conformational change during catalysis since it occludes access to the PLP-Lys-315 aldimine linkage.

### **Dodecamer Assembly**

Analysis of crystal contacts revealed that the basic oligomeric unit is a twelve subunit (dodecamer) assembly of ABDC monomers (monomers A-L) (Fig. 3.4) with overall 223 symmetry (Fig. 3.5). The particle has a diameter of 156 Å with a 24 Å diameter central cavity void of side chains. Each dodecamer can be described as a spherical particle assembled through the association of six dimers (A-B, C-D, E-F, G-H, I-J, K-L) *via* their oligomerization domains

and monomer-monomer contacts. Each dimer is flanked by four others. High intra-particle symmetry allows the illustration of all oligomerization interactions through the description of contacts between monomer chains A-C and B-C. These chains (A, B, and C) form a trimeric interface that contains a complex hydrogen bonding network between the chain C  $\alpha$ -helix H4, a chain C loop inter-connecting  $\alpha$ -helices H2 and H3, and the last  $\alpha$ -helix on chain B. Specifically, hydrogen bonds exist between chain B residues Asn-504, Glu-505, Tyr-506 and chain C residues Asp-112 and Gln-113. Chain C residues Gln-113, Asp-112, Tyr-109, and Ser-108, and Lys-105 also form hydrogen bonds/electrostatic interactions with chain A residues Ser-65, Tyr-66, and Ser-67. Thus, this region contains important oligomerization contacts that link three chains together. Other chains A and C contacts outside this region occur between residues Met-69 and Met-402; Asn-70 and Asp-403; Arg-86 and Glu-88; and Arg-89 and Glu-88, respectively. Furthermore, there are chains B and C contacts between residues Gln-414 and Glu-404; Arg-418 with Arg-154 and Glu-404; Arg-425 and Asp-159, Ile-161, Ser-163, respectively. Hydrogen bonds occurring specifically between elements of the oligomerization domains are involved in the formation of three major structural elements that contribute to particle assembly: **1**) a three helix bundle formed by H3  $\alpha$ -helices related by a three fold axis of symmetry parallel to the axis of the bundle (Fig. 3.5); primary interactions stabilizing the bundle are mediated by hydrogen bonds between the side chains of Arg-89 on each chain participating in the bundle with the side chains of Glu-93 on adjacent chains (Fig. 3.5), **2**) a two helix bundle formed by H2  $\alpha$ -helices related by a two-fold axis of symmetry running perpendicular to the axis of the bundle, and **3**) a network of hydrogen bonds between residues at the end of  $\alpha$ -helix H2 and mid section residues of  $\alpha$ -helix H4. Each oligomerization domain interface has 223 symmetry. Interestingly, the two helix bundle formed by H2  $\alpha$ -helices contributes both to dimerization contacts (by forming a two

helix bundle with its symmetry related twin) and to oligomerization contacts by hydrogen bonding with residues on a neighboring H4  $\alpha$ -helix. The two helix bundle formed by two-fold symmetry related H2  $\alpha$ -helices is a common dimerization motif among AAT-family members.

### **ABDC Wild Type and R37A Mutant Kinetic Characterization**

Our kinetic analysis at pH 7 showed that wild type (Wt) ABDC had a  $K_M = 4.37$  mM and a  $k_{cat} = 4.34$  s<sup>-1</sup> for L-asp, and the R37A mutant had a  $K_M = 16.89$  mM and  $k_{cat} = 0.7$  s<sup>-1</sup> for L-asp. These values correspond to a  $k_{cat}/K_M$  ratio between Wt and R37A ABDC of 23.8. The activity of Wt ABDC is consistent with other reports in which the enzyme activity was measured at pH 7 (2).

### **Discussion**

Previous studies (9) have shown that the ABDC catalyzed decarboxylation of L-asp inverts the configuration of L-ala C- $\beta$  protons while retaining absolute configuration about C- $\alpha$ , suggesting that two bases are involved (9). One base required for the removal/addition of the  $\alpha$ -proton on the *si*-side of the external aldimine/quinonoid intermediate, while the second base adds a proton to C- $\beta$  on the *re*-side of the enamine. Assuming that the Schiff base forming lysine abstracts the  $\alpha$ -proton and reprotonates at C-4' to form the ketimine intermediate, as do other members of the PLP-dependent aminotransferase family, the identity of the second base remains unknown.

In the crystal structure presented in this report, the *re*-side of the PLP cofactor and the aldimine nitrogen are closely flanked by the side chain of the strictly conserved Arg-37, making Arg-37 a likely candidate for the second catalytic base. The kinetic analysis showed that R37A mutants have a 24-fold reduction in  $k_{cat}/K_m$  for L-asp as compared to Wt ABDC, which indicates that this residue plays some role in catalysis. Yet, a number of different scenarios can be

considered that are consistent with these results: 1) Arg-37 is not directly involved in reprotonating the enamine and thus a very large change in catalytic efficiency is not observed, 2) the mutation affects the catalytic cycle at a non-rate limiting step, or 3) protonation at the enamine C- $\beta$  is much faster than the rate-limiting step, and the mutation does not affect this rate sufficiently to be observed in the steady state. Further characterization of ABDC is needed to confirm these possibilities.

Within the extended group of PLP-dependent transferases, the biodegradative ornithine, arginine, and lysine decarboxylases associate into large complexes (27-30). Although arginine and lysine decarboxylases are known to form decamers, only the hexameric structure of a putative lysine decarboxylase from *Bacillus subtilis* (PDB accession no. **1T35**) and crystallization conditions for the *E. coli* arginine decarboxylase (31) have been reported. Among PLP-dependent aminotransferase family members, the only structure of a large oligomeric assembly available is that of the *Lactobacillus* 30a ornithine decarboxylase (ODC) (32). In ODC, the twelve subunits arrange as a ring-like structure of concentric side-by-side dimers through the interaction of an ODC unique “wing” domain (33) (pfam03709). Although similar to ABDC in overall monomer and active site composition (twelve in both), the ODC particle is intrinsically different from ABDC in terms of internal symmetry (six-fold in ODC) and dimer-dimer contacts. Moreover, ODC oligomerization contacts are primarily mediated by adjacent “wing” domains, contrasting with the extended hydrogen bonding networks formed by dimer-dimer contacts and dedicated oligomerization domain contacts in ABDC. In terms of sequence identity, the “wing” and ABDC oligomerization domains retain no significant sequence homology to one another.

Structure-structure and sequence based comparisons reveal that ABDC is most closely related to aspartate aminotransferase-like enzymes and not PLP-dependent decarboxylases.

However, no PLP-dependent aminotransferase contains a domain homologous to the ABDC oligomerization domain, nor does any aminotransferase use an oligomerization scheme similar to that used by this enzyme.

Conformational and structural details in this crystal structure do not clearly reveal the functional role of the dodecameric assembly with respect to catalysis. Although it has been previously determined that ABDC will partially dissociate into a mixture of dodecamer/dimers and lose activity as the pH is increased to neutrality (2), it is not clear whether this effect is primarily due to a pH dependence on catalytic activity or if the effect is due to a structural rearrangement of the particle into a low activity conformational state. It is also possible that the modular assembly/disassembly of ABDC in response to pH changes is a form of regulation by intracellular proton concentrations- all controlled by interactions between residues within the oligomerization domain.

## **Materials and Methods**

### **Recombinant protein cloning, expression, and purification**

The *Pseudomonas dacunhae* L-aspartate- $\beta$ -decarboxylase was cloned into a pET100 plasmid using a TopoTA-Kit (Invitrogen) after PCR amplification from a clone obtained from the American Type Culture Collection (ATCC no. 40134) to generate a native recombinant protein. The PCR oligonucleotide primers used for PCR amplification were: 5'-TGAAGGAGGAGTTGCGAGATGAGC-3' (forward), and 5'-GTAAGCCTTGAAGTCCTCGCCGTC-3' (reverse). The resulting plasmid was sequenced to confirm identity with the ATCC DNA sequence. A single colony of *E. coli* BL21 (DE3) cells transformed with the recombinant plasmid was inoculated into 1 L of ZYP-5052 medium (12) containing 100 mg L<sup>-1</sup> ampicillin and grown at 37 °C for 24 hours with shaking at 300-325 rpm.

Prior to harvesting, the cultures were pre-chilled for 1 hour at 4 °C and then collected by centrifugation at  $2500 \times g$  for 15 minutes at 4 °C. Cell pellets were resuspended in 30 mL of ice-cold buffer (50 mM Na-Acetate, pH 6, and 0.1 mM PLP) and sonicated for four cycles of 1 minute intervals followed by 2 minutes on ice. Cell debris was removed by centrifugation for 20 minutes at  $25,000 \times g$  at 4 °C. The supernatant was allowed to stand at room temperature for 20 minutes followed by the drop-wise addition of four mL of a 2% protamine sulfate solution (in resuspension buffer), and the resultant cloudy solution was centrifuged for 40 minutes at  $25,000 \times g$  at 4 °C. The supernatant was brought to 40% ammonium sulfate saturation, allowed to equilibrate for 30 minutes at 4 °C, and centrifuged for 40 minutes at  $25,000 \times g$  at 4 °C. The supernatant was then diluted twenty-fold with resuspension buffer, concentrated (Amicon Centriprep YM-50 centrifugal filter units), and applied to a 75 x 2.5 cm. Sepharose CL-6B resin (Sigma) gel filtration column pre-equilibrated with buffer (50 mM Na-Acetate, pH 6, 0.1 mM PLP, 4 °C) and eluted at a flow rate of  $0.1 \text{ mL minute}^{-1}$  at 4 °C. SDS-PAGE analysis of fractions eluting from the column was used to determine appropriate samples to be pooled and concentrated. Protein concentration was determined using the Bradford (Bio-Rad) assay.

### **Crystallization, data collection, SAD phasing, and molecular replacement**

High-throughput crystallization trials were conducted at the Hauptman-Woodward Institute (<http://www.hwi.buffalo.edu/>) (34). ABDC crystals were grown at 23.5 °C using the microbatch under-oil method (35) by mixing in a 1:1 ratio, a  $10.5 \text{ mg mL}^{-1}$  ABDC solution in 50 mM Na-Acetate, pH 6, and 0.1 mM PLP with a solution containing 100 mM  $\text{MgCl}_2$ , 100 mM Tris (pH 8.5), 25% PEG 400, 10% glycerol. Crystals appeared after three to four weeks. Platinum derivatized crystals were produced by soaking ABDC crystals overnight in a saturated dichloro(2,2':6',2''-terpyridine)-platinum(II) dihydrate solution in 25 mM Na-Acetate (pH 6), 50

mM MgCl<sub>2</sub>, 50 mM Tris (pH 8.5), 12.5% PEG 400, 2.5% glycerol. Crystals were flash-frozen in liquid nitrogen with cryoprotectant containing 25 mM Na-Acetate (pH 6), 55 mM MgCl<sub>2</sub>, 55 mM Tris (pH 8.5), 30% PEG 400, 20% glycerol. These crystals belonged to spacegroup I23 and had cell constants  $a=b=c=150.45$  Å. Single wavelength anomalous X-ray synchrotron data were collected at the Advanced Photon Source SBC-CAT beamline 19-BM in Argonne, IL (36). Data were processed, scaled, and merged using HKL3000 (37). The merged SCALEPACK (37) intensities were used as input for the SHELX C/D/E modules (38,39) in the CCP4i crystallographic suite (40). Refined phase coefficients calculated in SHELX E, the five platinum heavy atom sites, and the ABDC sequence were input into RESOLVE (41), which produced a model containing approximately 85% of the ABDC amino acid sequence. Manual building of the structure was performed using COOT (20), and water addition and refinement were carried out with ARP/wARP (42) and Refmac5 (43). All subsequent data sets were solved by molecular replacement using Phaser (44). MolProbity (45) was used to identify errors during the building and refinement process and to evaluate the quality of refined structures.

### Site Directed Mutagenesis

ABDC mutant R37A was prepared using the Stratagene QuickChange<sup>®</sup> Site-Directed Mutagenesis Kit. The forward primer was (mutated bases bold and underlined) 5'-CTCATGCTCAATGCGGGG**GCT**GGCAATCCCAATTTTCTGG-3', and the reverse primer was 5'-CCAGAAAATTGGGATTGCC**AG**CCCCCGCATTGAGCATGAG-3'. The resulting plasmid was sequenced to verify the base changes, and R37A mutants were expressed and purified as described.

### **Enzymatic Assay**

ABDC activity was measured by following the absorbance change at  $\lambda_{\text{max}} = 340$  nm as  $\text{NAD}^+$  is converted to NADH by L-alanine oxidation with alanine dehydrogenase ( $\Delta\epsilon = 6200 \text{ M}^{-1} \text{ cm}^{-1}$ ). Alanine dehydrogenase was purified as previously described (46). Assays were performed at 37 °C and contained 50 mM potassium phosphate (pH 7), 20 mM  $\text{NAD}^+$ , an excess of alanine dehydrogenase (in non-rate limiting amount) to ABDC (rate limiting), and varying concentrations of L-asp (pH 7).

### **Acknowledgments**

We are grateful to the staff at the Hauptman-Woodward Institute for performing the high-throughput crystallization screens and the staff at the Structural Biology Centre Collaborative Access Team (SBC-CAT) 19-BM beamline (Advanced Photon Source, Argonne National Laboratory) for assistance in X-ray data collection and the use of their facility. Use of the Advanced Photon Source was supported by the US Department of Energy, Office of Science, and Office of Basic Energy Sciences under Contract No. W-31-109-Eng-38.

## References

- (1) Tate, S. S., and Meister, A. (1971) L-aspartate-beta-decarboxylase: structure, catalytic activities, and allosteric regulation. *Adv Enzymol Relat Areas Mol Biol* 35, 503-43.
- (2) Wang, N. C., and Lee, C. Y. (2006) Molecular cloning of the aspartate 4-decarboxylase gene from *Pseudomonas* sp. ATCC 19121 and characterization of the bifunctional recombinant enzyme. *Appl Microbiol Biotechnol* 73, 339-48.
- (3) Chibata, I., Kakimoto, T., Kato, J., Shibatani, T., and Nishimura, N. (1968) On the activation mechanism of L-aspartate beta-decarboxylase from *Pseudomonas dacunhae* by alpha-ketoglutarate. *Biochem Biophys Res Commun* 32, 375-9.
- (4) Nishimura, J. S., Manning, J. M., and Meister, A. (1962) Studies on the mechanism of activation acid beta-decarboxylase by alpha-keto acids and pyridoxal 5'-phosphate. *Biochemistry* 1, 442-7.
- (5) Novogrodsky, A., Nishimura, J. S., and Meister, A. (1963) Transamination and beta-decarboxylation of aspartate catalyzed by the same pyridoxal phosphate-enzyme. *J Biol Chem* 238, 1903-5.
- (6) Fusee, M. C., and Weber, J. E. (1984) Immobilization by Polyurethane of *Pseudomonas dacunhae* Cells Containing l-Aspartate beta-Decarboxylase Activity and Application to l-Alanine Production. *Appl Environ Microbiol* 48, 694-698.
- (7) Yamakatsu, F., Kiyokazu, Y. (1983) Pressurized Reaction Method for Continuous Production of L-Alanine by Immobilized *Pseudomonas dacunhae* Cells. *J. Ferment. Technol.* 61, 587-591.

- (8) Rosenberg, R. M., and O'Leary, M. H. (1985) Aspartate beta-decarboxylase from *Alcaligenes faecalis*: carbon-13 kinetic isotope effect and deuterium exchange experiments. *Biochemistry* 24, 1598-603.
- (9) Chang, C. C., Laghai, A., O'Leary, M. H., and Floss, H. G. (1982) Some stereochemical features of aspartate beta-decarboxylase. *J Biol Chem* 257, 3564-9.
- (10) Dimroth, P., and Schink, B. (1998) Energy conservation in the decarboxylation of dicarboxylic acids by fermenting bacteria. *Arch Microbiol* 170, 69-77.
- (11) Abe, K., Ohnishi, F., Yagi, K., Nakajima, T., Higuchi, T., Sano, M., Machida, M., Sarker, R. I., and Maloney, P. C. (2002) Plasmid-encoded asp operon confers a proton motive metabolic cycle catalyzed by an aspartate-alanine exchange reaction. *J Bacteriol* 184, 2906-13.
- (12) Richard, H., and Foster, J. W. (2004) *Escherichia coli* glutamate- and arginine-dependent acid resistance systems increase internal pH and reverse transmembrane potential. *J Bacteriol* 186, 6032-41.
- (13) Kakimoto, T., Kato, J., Shibatani, T., Nishimura, N., and Chibata, I. (1969) Crystalline L-aspartate beta-decarboxylase of *Pseudomonas dacunhae*. I. Crystallization and some physicochemical properties. *J Biol Chem* 244, 353-8.
- (14) Mehta, P. K., and Christen, P. (2000) The molecular evolution of pyridoxal-5'-phosphate-dependent enzymes. *Adv Enzymol Relat Areas Mol Biol* 74, 129-84.
- (15) Altschul, S. F., Madden, T. L., Schaffer, A. A., Zhang, J., Zhang, Z., Miller, W., and Lipman, D. J. (1997) Gapped BLAST and PSI-BLAST: a new generation of protein database search programs. *Nucleic Acids Res* 25, 3389-402.

- (16) Schaffer, A. A., Aravind, L., Madden, T. L., Shavirin, S., Spouge, J. L., Wolf, Y. I., Koonin, E. V., and Altschul, S. F. (2001) Improving the accuracy of PSI-BLAST protein database searches with composition-based statistics and other refinements. *Nucleic Acids Res* 29, 2994-3005.
- (17) Krissinel, E., and Henrick, K. (2004) Secondary-structure matching (SSM), a new tool for fast protein structure alignment in three dimensions. *Acta Crystallogr D Biol Crystallogr* 60, 2256-68.
- (18) Gibrat, J. F., Madej, T., and Bryant, S. H. (1996) Surprising similarities in structure comparison. *Curr Opin Struct Biol* 6, 377-85.
- (19) Marchler-Bauer, A., and Bryant, S. H. (2004) CD-Search: protein domain annotations on the fly. *Nucleic Acids Res* 32, W327-31.
- (20) Gani, D. (1991) A structural and mechanistic comparison of pyridoxal 5'-phosphate dependent decarboxylase and transaminase enzymes. *Philos Trans R Soc Lond B Biol Sci* 332, 131-9.
- (21) Cleland, W. W. (2000) Low-barrier hydrogen bonds and enzymatic catalysis. *Arch Biochem Biophys* 382, 1-5.
- (22) Alexander, F. W., Sandmeier, E., Mehta, P. K., and Christen, P. (1994) Evolutionary relationships among pyridoxal-5'-phosphate-dependent enzymes. Regio-specific alpha, beta and gamma families. *Eur J Biochem* 219, 953-60.
- (23) Yano, T., Kuramitsu, S., Tanase, S., Morino, Y., Hiromi, K., and Kagamiyama, H. (1991) The role of His143 in the catalytic mechanism of *Escherichia coli* aspartate aminotransferase. *J Biol Chem* 266, 6079-85.

- (24) Hayashi, H., Mizuguchi, H., Miyahara, I., Islam, M. M., Ikushiro, H., Nakajima, Y., Hirotsu, K., and Kagamiyama, H. (2003) Strain and catalysis in aspartate aminotransferase. *Biochim Biophys Acta* 1647, 103-9.
- (25) Graber, R., Kasper, P., Malashkevich, V. N., Strop, P., Gehring, H., Jansonius, J. N., and Christen, P. (1999) Conversion of aspartate aminotransferase into an L-aspartate beta-decarboxylase by a triple active-site mutation. *J Biol Chem* 274, 31203-8.
- (26) Palekar, A. G., Tate, S. S., and Meister, A. (1970) Inhibition of aspartate beta-decarboxylase by aminomalonate. Stereospecific decarboxylation of aminomalonate to glycine. *Biochemistry* 9, 2310-5.
- (27) Guirard, B. M., and Snell, E. E. (1980) Purification and properties of ornithine decarboxylase from *Lactobacillus* sp. 30a. *J Biol Chem* 255, 5960-4.
- (28) Sabo, D. L., and Fischer, E. H. (1974) Chemical properties of *Escherichia coli* lysine decarboxylase including a segment of its pyridoxal 5'-phosphate binding site. *Biochemistry* 13, 670-6.
- (29) Sabo, D. L., Boeker, E. A., Byers, B., Waron, H., and Fischer, E. H. (1974) Purification and physical properties of inducible *Escherichia coli* lysine decarboxylase. *Biochemistry* 13, 662-70.
- (30) Boeker, E. A., and Snell, E. E. (1968) Arginine decarboxylase from *Escherichia coli*. II. Dissociation and reassociation of subunits. *J Biol Chem* 243, 1678-84.
- (31) Rodrigez, B. R., Carroll, D. W., Mitchell, D., Momany, C., and Hackert, M. L. (1994) Crystallization of biosynthetic arginine decarboxylase from *Escherichia coli*. *Acta Crystallogr D Biol Crystallogr* 50, 175-7.

- (32) Momany, C., Ernst, S., Ghosh, R., Chang, N. L., and Hackert, M. L. (1995) Crystallographic structure of a PLP-dependent ornithine decarboxylase from *Lactobacillus* 30a to 3.0 Å resolution. *J Mol Biol* 252, 643-55.
- (33) Momany, C., and Hackert, M. L. (1989) Crystallization and molecular symmetry of ornithine decarboxylase from *Lactobacillus* 30a. *J Biol Chem* 264, 4722-4.
- (34) Luft, J. R., Collins, R. J., Fehrman, N. A., Lauricella, A. M., Veatch, C. K., and DeTitta, G. T. (2003) A deliberate approach to screening for initial crystallization conditions of biological macromolecules. *J Struct Biol* 142, 170-9.
- (35) Chayen, N. E., Shaw Stewart, P. D., and Blow, D. M. (1992) Microbatch crystallization under oil—a new technique allowing many small-volume crystallization trials. *J. Crystal Growth* 122, 176-180.
- (36) Use of the Advanced Photon Source was supported by the U. S. Department of Energy, O. o. S., Office of Basic Energy Sciences, under Contract No. W-31-109-Eng-38.
- (37) Otwinowski, Z., and W., M. (1997) Processing of X-ray Diffraction Data Collected in Oscillation Mode. *Methods in Enzymology* 276, 307-326.
- (38) Schneider, T. R., and Sheldrick, G. M. (2002) Substructure solution with SHELXD. *Acta Crystallogr D Biol Crystallogr* 58, 1772-9.
- (39) Uson, I., and Sheldrick, G. M. (1999) Advances in direct methods for protein crystallography. *Curr Opin Struct Biol* 9, 643-8.
- (40) Collaborative Computational Project, N. (1994) The CCP4 Suite: Programs for Protein Crystallography. *Acta Cryst D* 50.
- (41) Terwilliger, T. C. (2003) Automated main-chain model building by template matching and iterative fragment extension. *Acta Crystallogr D Biol Crystallogr* 59, 38-44.

- (42) Lamzin, V. S., Perrakis, A., and Wilson, K. S. (2001) The ARP/WARP suite for automated construction and refinement of protein models. In *Int. Tables for Crystallography*, Vol. F, Dordrecht, Kluwer Academic Publishers, The Netherlands.
- (43) Murshudov, G. N., Vagin, A. A., and Dodson, E. J. (1997) Refinement of macromolecular structures by the maximum-likelihood method. *Acta Crystallogr D Biol Crystallogr* 53, 240-55.
- (44) McCoy, A. J., Grosse-Kunstleve, R. W., Storoni, L. C., and Read, R. J. (2005) Likelihood-enhanced fast translation functions. *Acta Crystallogr D Biol Crystallogr* 61, 458-64.
- (45) Davis, I. W., Leaver-Fay, A., Chen, V. B., Block, J. N., Kapral, G. J., Wang, X., Murray, L. W., Bryan Arendall, W., 3rd, Snoeyink, J., Richardson, J. S., and Richardson, D. C. (2007) MolProbity: all-atom contacts and structure validation for proteins and nucleic acids. *Nucleic Acids Res.*
- (46) Ohashima, T., and Soda, K. (1979) Purification and properties of alanine dehydrogenase from *Bacillus sphaericus*. *Eur J Biochem* 100, 29-30.

**Table 3.1.** Summary of crystallographic analysis.

Space group	I23
Resolution range (outer shell), Å	50-2.3 (2.41-2.34)
No of reflections (outer shell)	22531 (1634)
R <sub>factor</sub> (outer shell)	0.18479 (0.21)
<sup>a</sup> R <sub>free</sub> (outer shell)	0.24123 (0.28)
R <sub>sym</sub> (outer shell)	0.076 (0.57)
Redundancy (outer shell)	10.6 (7.1)
Mean B value	46 Å <sup>2</sup>
r.m.s delta. from ideal geometry:	
Bond angles	1.223°
Bond distances	0.010 Å
Ramachandran plot residues in favored/allowed/disallowed (%) regions	97.2/2.4/0.4

<sup>a</sup>R<sub>free</sub> calculated with 5.1 % of data excluded from refinement

**Figure 3.1.** ABDC monomer with successive secondary structure elements labeled. Each ABDC monomer binds one pyridoxal-5'-phosphate molecule and is composed of a large, small, and oligomerization domains. The large domain is composed of a seven stranded anti-parallel  $\beta$ -sheet containing  $\beta$  strands S1, S7, S6, S5, S4, S2, and S3. The small domain contains a two stranded anti-parallel  $\beta$ -sheet composed of strands S8 and S9, and the oligomerization domain is composed by  $\alpha$ -helices H2-H4.

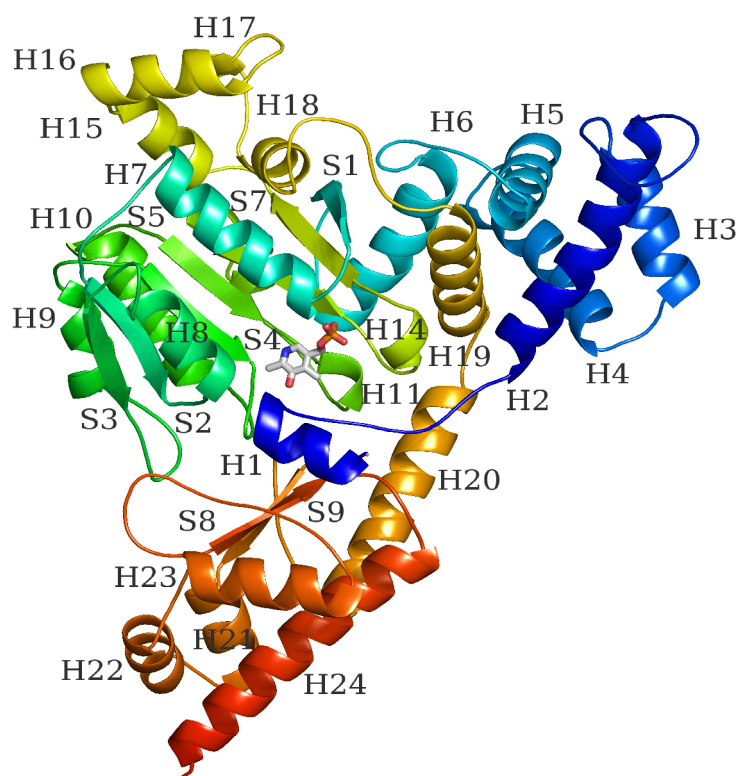


**Figure 3.2.** The ABDC active site is composed of residues contributed from two monomer chains related by a 2-fold axis of symmetry. Each active site contains one pyridoxal-5'-phosphate molecule covalently bound to an active site Lys-315 via a Schiff base linkage. Tyr-134 is contributed from the symmetry related monomer.

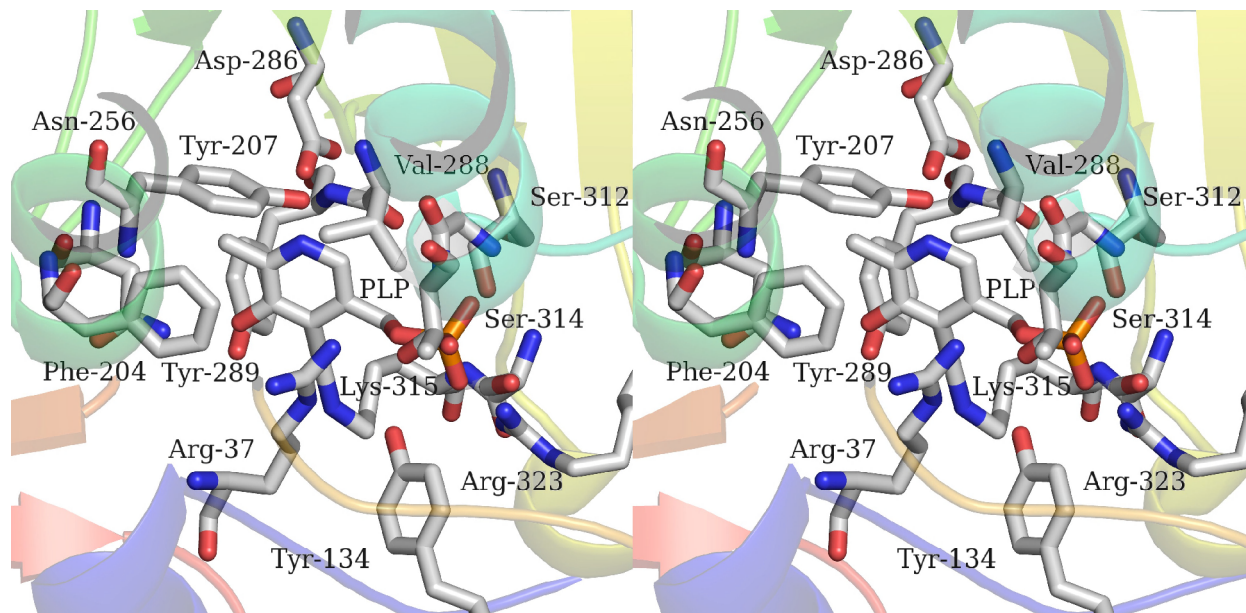


**Figure 3.3.** Active sites of structurally superposed ABDC and *E. coli* AAT (PDB accession no. 1X2A). ABDC residues are colored with white carbons, blue nitrogens, orange phosphorous, and red oxygens. AAT are colored with green carbons and green labels, blue nitrogens, orange phosphorous, and red oxygens. The following ABDC/AAT residues were omitted for clarity: Asp-286/Asp-222, Val-288/Ala-244, Ser-311/Ser-253, Lys-315/Lys-258. Note the large conformational differences between the side chains of ABDC residues Arg-375/Arg-292 and Arg-497/Arg-386.

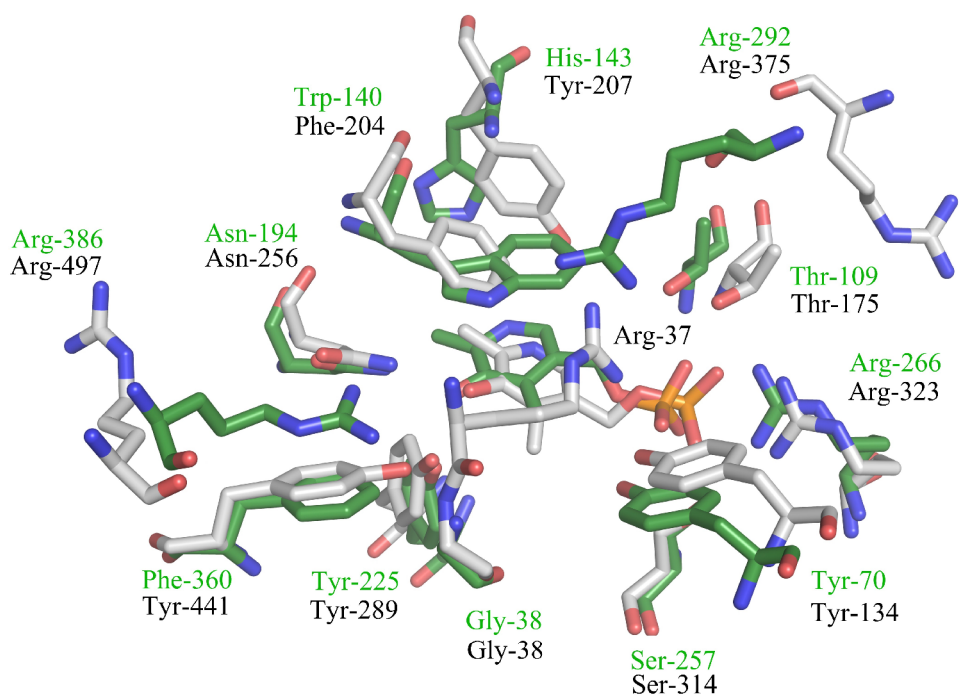


**Figure 3.4.** Ribbon representation of the ABDC dodecamer with each monomer labeled. Dimers forming the dodecamer are A-B, C-D, E-F, G-H, I-J, K-L. Monomers I and J are at the back of the molecule and cannot be seen.

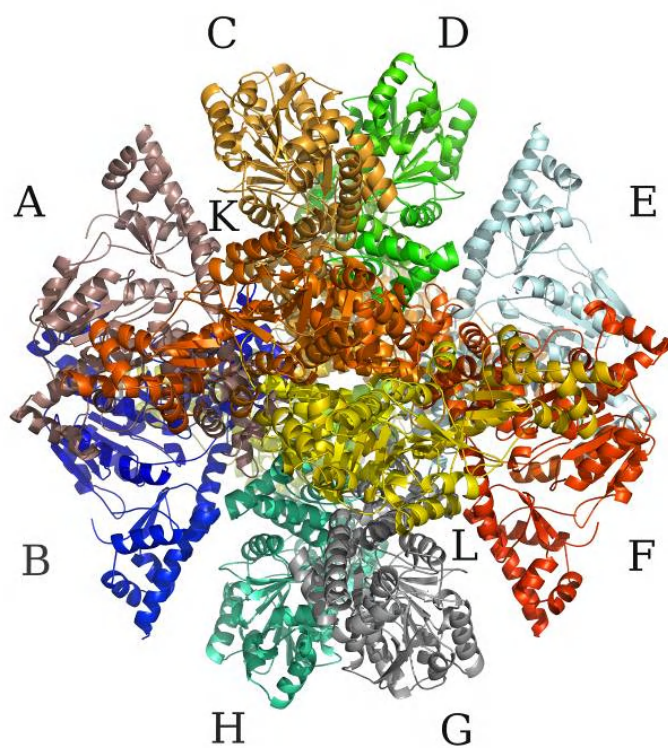
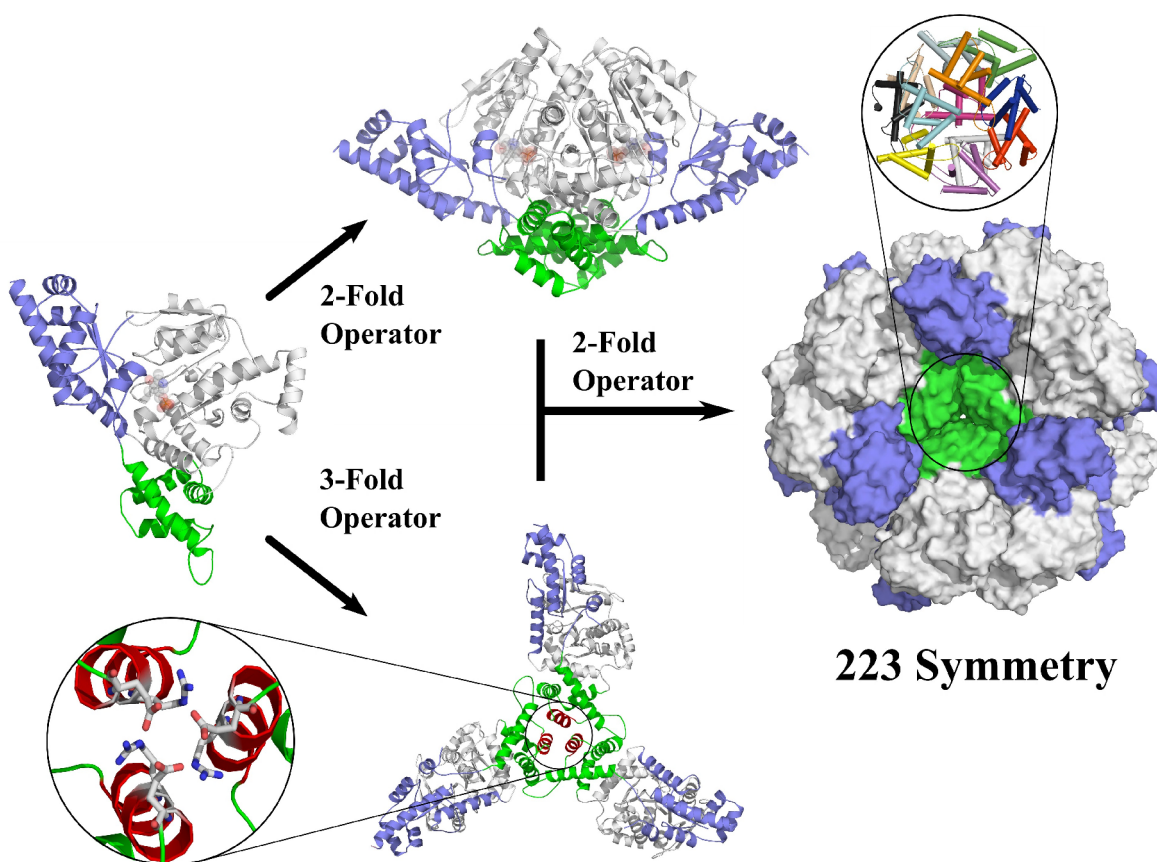


**Figure 3.5.** Schematic illustrating the symmetry relationships between monomers in the ABDC particle. Each monomer is colored by domains with the small domain colored blue, the large domain colored white, and the oligomerization domain colored green. The ABDC dodecamer can be generated by applying a 2-fold and 3-fold symmetry operator to a monomer, which generates a hexamer composed of three dimers (not shown). A subsequent 2-fold symmetry operation completes the dodecamer particle. The bottom left inset illustrates the interactions that stabilize a three helix bundle at the interface of the oligomerization domains in three monomers related by a 3-fold axis of symmetry. Residues in the inset are Arg-89 and Glu-93. The top right inset displays only the oligomerization domains (residues 45-130) individually colored for each monomer in the dodecamer.



## CHAPTER 4

ATOMIC STRUCTURE AND SUBSTRATE SPECIFICITY OF THE *PYROCOCCUS**FURIOSUS* TRYPTOPHAN SYNTHASE B SUBUNIT HOMOLOG

---

<sup>4</sup> Santiago Lima, Christopher Schlett, Francis E. Jenney, Cory Momany, Michael Kaufmann, Boris Striepen, Michael W.W. Adams, and Robert S. Phillips. Manuscript in preparation for submission to *Proceedings of the National Academy of Sciences*.

## Abstract

Tryptophan synthase is a pyridoxal-5'-phosphate dependent enzyme that catalyzes the last step in the L-tryptophan biosynthetic pathway. The canonical tryptophan synthase  $\alpha_2\beta_2$  (TrpAB1) complex produces L-tryptophan from indole-3-glycerophosphate and L-serine (L-ser). Yet, *Pyrococcus furiosus* and many other Archaea, hyperthermophilic Bacteria, and some plants possess two tryptophan synthase  $\beta$ -subunit genes that encode two phylogenetically distinct yet closely related enzymes: the canonical tryptophan synthase  $\beta$ -subunit (TrpB1) and a tryptophan synthase  $\beta$ -subunit homolog (TrpB2). Some effort has been dedicated to elucidate the physiological role of these enzymes and TrpB2s are thought to function as either L-ser deaminases or indole scavengers. In this report, we characterize the atomic structure and kinetic properties of the *P. furiosus* TrpB2 (PfTrpB2). Our results indicate that the PfTrpB2 can catalyze the condensation of L-cysteine + indole to yield tryptophan, in addition to the canonical L-ser reaction. In order to better understand the significance of these findings we characterized the L-cysteine (L-cys) binding affinities and catalytic efficiencies of the *Salmonella typhimurium* TrpAB1 complex, the *P. furiosus* TrpAB1 complex, the *S. typhimurium* TrpB1, and the *P. furiosus* TrpB1. Based on a comparison of substrate specificities in these enzymes with PfTrpB2 we suggest that these enzymes function as tryptophan synthases, yet do so in a manner that does not differentiate between L-cys and L-ser as substrates.

## Introduction

Tryptophan synthase is a pyridoxal-5'-phosphate dependent enzyme that catalyzes the last step in the L-tryptophan biosynthetic pathway. For the most part, tryptophan synthases from mesophilic organisms form a quaternary  $\alpha_2\beta_2$  complex (TrpAB) and they are encoded as the last two genes in the *trp* operon. Much of our understanding of allosteric and conformational protein

regulation stems from decades of studying this enzymatic complex (1). The canonical tryptophan synthase reaction produces L-tryptophan from indole-3-glycerophosphate and L-serine (L-ser). Yet, the  $\alpha_2\beta_2$  complex can also utilize L-cysteine (L-cys) as a substrate to produce tryptophan (2), but the reaction is much slower than that with L-ser (2, 3). L-cys binding affinities for the mesophilic TrpAB or tryptophan synthase  $\beta$ -subunit (TrpB1) have not been reported in the literature.

*Pyrococcus furiosus* and many other Archaea, hyperthermophilic Bacteria, and some plants (4) possess two tryptophan synthase  $\beta$ -subunit genes that encode two distinct (5) but closely related enzymes: the canonical tryptophan synthase  $\beta$ -subunit (TrpB1) and a tryptophan synthase  $\beta$ -subunit homolog (TrpB2) (5). In *P. furiosus*, the *trpB2* gene is located outside of a full set *trp* operon genes (6) but some *Crenarchaeota*, *Pyrococcus horikoshii*, and several hyperthermophilic Bacteria possess only *trpB2* and none of the other *trp* operon genes (5). Sequence-based comparisons reveal that these enzymes are moderately homologous (28 % identity between *P. furiosus* TrpB1s and TrpB2s), but TrpB1 proteins are on average 50 residues shorter than TrpB2s (5) (PfTrpB2 is 58 residues larger than PfTrpB1). Also, the regulatory residues involved in allosteric interactions with the tryptophan synthase  $\alpha$ -subunit (*S. typhimurium* Arg-141 and Lys-167) are not conserved (5, 7). Thus, it is thought that TrpB2s have lost the ability to interact with tryptophan synthase  $\alpha$ -subunits (TrpA). In fact, a study with recombinant TrpA and TrpB2 from *Thermotoga maritima* and *Sulfolobus solfataricus* revealed that these proteins do not associate to form an  $\alpha_2\beta_2$  complex, nor does TrpA increase the activity of TrpB2 (7, 8), as is seen between mesophilic TrpA and TrpB1.

Some effort has been dedicated to elucidate the physiological role of these enzymes, yet a clear function has not emerged. Studies with a recombinant *Thermotoga maritima* TrpB2

(TmTrpB2) and *Sulfolobus solfataricus* TrpB2 (SsTrpB2) have shown that these enzymes catalyze the canonical tryptophan synthase reaction  $\text{L-ser} + \text{indole} \rightarrow \text{H}_2\text{O} + \text{L-tryptophan}$  with  $K_{\text{mS}}$  for L-ser of 50.2 mM (TmTrpB2) and 151 mM (SsTrpB2), respectively (7, 8). Based on the low Michaelis constant for indole and low substrate specificity for L-ser it was concluded that the TmTrpB2 and SsTrpB2 are scavenging proteins used to salvage indole escaping from the putative tryptophan synthase  $\alpha_2\beta_2$  reaction (7). Other studies have predicted that these enzymes function as L-ser deaminases on the basis of genomic analysis in which the presence of *trpB2* genes was correlated with the absence of L-ser deaminase genes (5).

Several observations suggest that further investigation of the properties of TrpB2 is needed to understand the physiological role of these enzymes. First, intracellular concentrations of L-ser have been measured in bacteria and found not to exceed 5 mM (9). Thus, the high L-ser  $K_{\text{mS}}$  of 50.2 mM (7) and 151 mM (8) observed in TmTrpB2 and SsTrpB2 implies that catalytic turnover into tryptophan would rarely occur. Second, a sequence based phylogenetic analysis revealed that although *Methanothermobacter thermoautotrophicus* TrpB1 and TrpB2 are closely related, they each represent a distinct family of proteins (5, 7). Third, studies involving the non-coding region upstream of the *M. thermoautotrophicus* TrpB2 (MtTrpB2) revealed the presence of a tryptophan repressor protein (TrpY in *M. thermoautotrophicus*) consensus binding site (10). *In vitro* transcription experiments involving the intergenic region immediately upstream of the MtTrpB2 gene showed that *M. thermoautotrophicus* TrpY regulates the transcription of MtTrpB2 in direct response to L-tryptophan concentrations (10). Thus, direct regulation of TrpB2 expression by tryptophan suggests that these proteins are likely to be involved in the tryptophan biosynthetic pathways.

In this work, we characterized the kinetic and structural properties of a recombinant PfTrpB2. Our data suggest that PfTrpB2 is a tryptophan synthase that non-preferentially utilizes either L-cys or L-ser to produce tryptophan in a TrpA-independent manner. We base this assertion on a contextual characterization of the L-cys and L-ser substrate specificities among the *Salmonella typhimurium*  $\alpha_2\beta_2$  tryptophan synthase complex (StTrpAB1), the *S. typhimurium* tryptophan synthase  $\beta$  subunit (StTrpB1), and the *P. furiosus*  $\alpha_2\beta_2$  tryptophan synthase (PfTrpAB1). The results of this analysis allow the construction of a detailed account of the substrate specificities among tryptophan synthases, and indicate that StTrpAB1, PfTrpAB1, StTrpB1, and PfTrpB1 have a higher specificity for L-ser than for L-cys, whereas the PfTrpB2 does not differentiate between substrates.

## **Materials and Methods**

### **Cloning, Expression, and Purification**

A single colony of *E. coli* BL21 (DE3) cells transformed with the recombinant plasmid was inoculated into 1L of ZYP-5052 medium (31) containing 35 mg L<sup>-1</sup> kanamycin and grown at 38 °C for 25 hrs with shaking at 300-325 rpm. The culture was harvested by centrifugation at 2500 × g for 15 min at 25 °C. The cell pellet was resuspended in 30 mL buffer A (0.3 M NaCl, 0.05 M potassium phosphate pH 7.0, and 0.1 mM PLP) and sonicated for four cycles of 1 min intervals followed by 2 min rest at room temp. Cell debris was removed by centrifugation for 20 min at 25,000 × g at 25 °C. Four mL of a 4% protamine sulfate solution (in resuspension buffer) were added to the supernatant, and the resultant cloudy solution was centrifuged for 40 min at 25,000 × g at 25 °C. The supernatant was applied to column containing Ni-CAM (Sigma) resin pre-equilibrated with buffer A (0.3 M NaCl, 0.05 M KPi pH 7.0, 0.1 mM PLP, 25 °C) at a rate of 0.5 mL min<sup>-1</sup> at 25 °C. After a 90 min wash with buffer A (0.5 mL min<sup>-1</sup>), TrpB2 was eluted

from the column with a 420 min 0 % to 100 % buffer B (0.3M NaCl, 0.05M KPi pH 7.0, 0.1 mM PLP, 70 mM imidazole, 25 °C) linear gradient (0.5 mL min<sup>-1</sup>). SDS-PAGE analysis of fractions eluting from the column was used to determine appropriate samples to be pooled and concentrated. Pooled fractions were dialyzed twice for 3.5 hours at 25 °C in a 1 L solution containing 0.05 M KPi pH 7.0, 0.1 mM PLP. Following dialysis, the protein solution was filter sterilized by passage through a 0.22 µm pore membrane. PfTrpB2 was stored at room temperature shielded from any light source. Protein concentration was determined using a Bradford (Bio-Rad) assay.

### **PfTrpB2 Crystallization, data collection, and molecular replacement**

For crystallization purposes, PfTrpB2 was further purified from the method described above by applying the dialyzed and concentrated solution (45 mg mL<sup>-1</sup>) to a 40 x 2.5 cm column containing Sephacryl S-200 resin (GE Biosciences) pre-equilibrated with buffer F (50 mM bicine, 0.1 mM EDTA, pH 7.8, and 0.1 mM PLP) and eluted at a flow rate of 0.1 mL min<sup>-1</sup>. SDS-PAGE analysis of fractions eluting from the column was used to determine appropriate samples to be pooled and concentrated. High-throughput crystallization trials were conducted at the Hauptman-Woodward Institute (<http://www.hwi.buffalo.edu/>) (32) with an 11 mg mL<sup>-1</sup> PfTrpB2 solution in buffer F. PfTrpB2 crystals were grown at 23.5 °C using the microbatch under-oil method (33) by mixing, in a 1:1 ratio, a 11 mg mL<sup>-1</sup> PfTrpB2 solution in 50 mM bicine, 0.1 mM EDTA, pH 7.8, and 0.1 mM PLP with a solution containing 0.1 M Tris pH 8 and 30 % PEG 6000. Dark yellow PfTrpB2 crystals (0.2 x 0.2 x 0.2 mm) appeared after 4-6 weeks. Crystals were flash-frozen in liquid nitrogen with cryoprotectant containing 0.06 M Tris (pH 8), 0.025 M bicine, 0.005 M EDTA, pH 7.8, 0.1 mM PLP, and 35 % PEG 6000. These crystals belonged to spacegroup C2 and had cell constants  $a = 151.816 \text{ \AA}$ ,  $b = 58.541 \text{ \AA}$ ,  $c = 102.465 \text{ \AA}$ ,

and  $\beta = 108.02^\circ$ . X-ray synchrotron data were collected (detector distance 230 mm, 190 frames,  $1^\circ$  oscillations, 5 sec. exposure,  $\lambda = 1.000 \text{ \AA}$ ) at the Advanced Photon Source SER-CAT beamline 22-BM in Argonne, IL (34). Data were processed, scaled, and merged using HKL2000 (35). The merged SCALEPACK intensities were used as input for the Phaser (36-38) module in the CCP4i crystallographic suite (39) and a suitable molecular replacement solution was identified using the *P. furiosus* tryptophan synthase  $\beta$ -subunit (11) (PDB accession no. **1V8Z**) as the phasing model. All water molecules, hetero atoms, and pyridoxal-5'-phosphate coordinates were deleted from the molecular replacement phasing model. The return of electron density for the PLP cofactor was used to evaluate the success of phasing methods. The PfTrpB2 sequence was threaded into the molecular replacement solution with XtalView/Xfit (40). The resulting model was rigid body refined for 30 cycles using Refmac5 (41) and then subjected to solvent flattening with DM (42). The refined phases were used as input for the automated building package RESOLVE (43) with default set parameters and no input model. Manual rebuilding of the remainder of the model and pyridoxal-5'-phosphate docking was performed using COOT (44).

### **PfTrpB1 Cloning, Expression, and Purification**

The *P. furiosus* tryptophan synthase  $\beta$ -subunit (PF1706) gene was PCR amplified from genomic *P. furiosus* DNA and cloned into a pET D-TOPO vector (Invitrogen). The PCR amplification primers used were: forward: 5'-CACCTTTGTAAGGAGGGCCAAAA-3', and reverse: 5'-GAGAACCATCCTTAAACATTTCCA-3'. The resulting plasmid was sequenced to confirm identity with genomic DNA. A single colony of *E. coli* BL21 (DE3) cells transformed with a recombinant plasmid containing the *P. furiosus* ORF PF1706 was inoculated into 1L of ZYP-5052 medium containing 100 mg/L ampicillin and grown at 38 °C for 25 hrs with shaking

at 300-325 rpm. PfTrpB1 was purified by the method described for the purification of non-crystallization purity grade PfTrpB2.

### **PfTrpA Expression and Purification**

A single colony of *E. coli* BL21 (DE3) cells transformed with the recombinant plasmid containing the *P. furiosus* ORF PF1705 was inoculated into 1L of ZYP-5052 medium containing 35 mg/L kanamycin. Cells were grown at 38 °C for 25 hrs with shaking at 300-325 rpm. PfTrpA was purified by the method described for non-crystallization purity PfTrpB2 with the exception that PLP was excluded from all buffers.

### **StTrpAB1 and StTrpB1 Expression and Purification**

The StTrpAB and StTrpB1 were purified as previously described (45, 46).

### **Steady-State Kinetics**

Spectrophotometric assays were performed by following the absorbance change at  $\lambda_{\max} = 290$  nm ( $\Delta\epsilon = 1890$  M<sup>-1</sup>cm<sup>-1</sup>) (47). All solutions were de-gassed prior to use, and all L-cys assays contained 10 mM TCEP (pH 8). PfTrpB2 activity was measured at 95 °C and contained 50 mM KPi (pH 8), 100 mM LiCl, 0.5 mM indole, and varying concentrations of L-ser and L-cys. PfTrpB1 and PfTrpAB1 activity was measured at 80 °C and contained 50 mM KPi (pH 8), and 0.5 mM indole. For PfTrpAB1 activity measurements, a four-fold molar excess of PfTrpA to PfTrpB1 was used to ensure PfTrpAB1 complex formation. This was further verified by increasing the PfTrpA concentration until no rate change could be measured. StTrpAB1 and StTrpB1 activity measurements were carried out at 37 °C and contained 50 mM KPi (pH 8), 0.5 mM indole, and varying concentrations of L-cys and L-ser. All data were fit using Prism (GraphPad).

Measurement of PfTrpB2 and PfTrpB1 activity by analytical HPLC was performed by incubating each enzyme in a solution containing 50 mM KPi (pH 8), 0.5 mM indole, and varying concentrations of L-ser and L-cys at 95 °C for 10 minutes. Reactions were quenched by the addition of acetic acid. The resulting samples were applied to a reverse phase C-18 column pre-equilibrated with a solvent system composed of 5% methanol and 0.095% acetic acid. A linear gradient to 40% methanol 0.065% acetic acid was used to elute L-trp. Prior to each initial rate measurement, reactions were monitored by HPLC to ensure a linear rate over the course of 10 min. Enzyme concentration was adjusted accordingly to satisfy these criteria.

## **Results and Discussion**

### **PfTrpB2 Subunit Structure**

The final PfTrpB2 model was refined to an  $R_{\text{factor}}$  of 0.19219,  $R_{\text{free}}$  of 0.23108, and contained two monomers in the C2 asymmetric unit forming the biologically active dimer. The structure had excellent geometry with 100% of residues in the allowed regions of the Ramachandran plot (see Table 1 for crystallographic statistics). Each monomer was modeled to 96% (A) and 97% (B) of the predicted amino acid sequence. Electron density for PLP atoms was well ordered, and density could be clearly seen extending between the  $\epsilon$  nitrogen of Lys-110 and the C-4' carbon of PLP, which is consistent with the presence of an internal aldimine covalent adduct. Each PfTrpB2 monomer (Fig. 4.1A) covalently binds one PLP molecule and is composed of N-terminal (residues 1-73 and 109-236) and C-terminal (residues 74-108 and 236-446) domains. The organization of secondary structure elements in the central six stranded antiparallel  $\beta$ -sheet ( $\beta$ -strands S3, S4, S14, S9, S10, S13) and surrounding  $\alpha$ -helices (H5, H8, H13, H14, H15, H16) is similar to that of PfTrpB1 (11). The N-terminal domain four stranded antiparallel  $\beta$ -sheet ( $\beta$ -strands S7, S6, S5, S8) was found to be surrounded by five  $\alpha$ -helices (H8-

H12) in PfTrpB2 as opposed to four in PfTrpB1. This additional  $\alpha$ -helix (H11, Fig.4.1B) makes the COMM (12) domain (PfTrpB2 residues 125-225) 13 residues longer in PfTrpB2. As expected, a PDB-wide structure similarity search with SSM (13) revealed that PfTrpB2 is most similar to tryptophan synthase  $\beta$ -subunits. Yet, the top scoring match (*Z*-score) was not the dimeric form of PfTrpB1, but rather the  $\beta$ -subunit in the tetrameric form of the *P. furiosus*  $\alpha_2\beta_2$  TrpAB1 (14) complex (PDB accession no. **1WDW**, r.m.s.d. 1.38 Å). The PfTrpB2 monovalent cation binding (MVC) is formed between side chain and main chain atoms of Gly-261, Ala-294, Ser-296, Leu-335, Tyr-337, and Gly-339. Electron density clearly indicated the presence of a bound cation and the site was modeled to contain a penta-coordinate potassium ion.

Most PfTrpB2 active site residues participating in the stabilization of the PLP cofactor are conserved with those of PfTrpB1 and StTrpB1 (11, 15). As such, an extensive account of these interactions will not be presented here. Instead, a description focusing on active site substitutions that are conserved among each class of tryptophan synthase  $\beta$ -subunits will be provided. Also, since the vast majority of site-directed mutagenesis studies have been conducted on StTrpB1, the analysis will center on a direct comparison between PfTrpB2 and StTrpB1 active site residues. The structural superposition between PfTrpB2 and StTrpB1 ( $\beta$ -subunit of PDB accession no. **1QOQ**, r.m.s.d. 1.50 Å) reveals a number of amino acid differences (Fig 4.2 left). Furthermore, a sequence alignment (Fig. 2 right) shows that these differences are strictly conserved among each  $\beta$ -subunit class. Among these, several studies (16) have shown that the StTrpB1 Asp-305 (Arg-336 in PfTrpB2) is a catalytically and dynamically important residue involved in substrate binding and  $\alpha\beta$  subunit allosteric signaling (17). Furthermore, mutations at this position alter the L-ser binding affinity, destabilize bound  $\alpha$ -aminoacrylate species, change the nucleophile specificity of the  $\beta$ -reaction, and increase the production of pyruvate in the

presence of  $\text{NH}_4^+$  and  $\text{Cs}^+$  or in the absence of MVCs (17). In StTrpB1, mutations that affect Lys-382 (Leu-415 in PfTrpB2) have been shown to cause complete loss of catalytic activity (18-20) and altered substrate specificity towards L-ser (19).

### **Comparison with PfTrpAB1 and StTrpAB1**

A structural superposition between PfTrpB2, StTrpAB1 (PDB accession no. **1QOQ**), and PfTrpAB1 (PDB accession no. **1WDW**) reveals that many of the additional amino acids found in PfTrpB2 form extensions of secondary structure elements that interfere with normal TrpAB1 dimerization contacts. Specifically, the PfTrpB2 loop interconnecting  $\alpha$ -helices H1 and H2 (residues 31-36) extends beyond the dimerization interface of the StTrpB1 to superpose directly over StTrpA residues 131-133 (not shown). Other PfTrpB2/StTrpA dimerization interface clashes would occur between PfTrpB2 residues on a loop interconnecting  $\beta$ -strand S12 and  $\alpha$ -helix H16 (residues 308-314) with StTrpA residues 56-58. Although longer in length (six residues), this loop extension in PfTrpB2 is the equivalent of the StTrpB1 loop that contains Tyr-279 and Phe-280, which delimits the C-terminal domain side of the StTrpAB1 intramolecular tunnel (Fig. 4.3A). Thus, in PfTrpB2, residues 308-311 block the  $\beta$ -subunit channel entrance (Fig. 4.3B). Although not as drastic, an analogous closure mechanism is seen by the occlusion of the tunnel (Fig. 4.3C) by Asn-171 and Tyr-279 in some StTrpAB1 structures (PDB accession no. **1A5S**).

### **PfTrpB2 Substrate Specificity**

Our initial approach to characterizing the kinetic properties of PfTrpB2 was to investigate if other L-amino acids could be used by this enzyme for the biosynthesis of L-tryptophan. Our results (not shown) indicate that PfTrpB2 will deaminate amino acids such as L-histidine, L-ornithine, L-arginine, and N-acetyl-glutamine. We also evaluated whether PfTrpB2 could use L-

cys as a substrate as had previously been reported for TrpB1 (2, 3). These experiments revealed that L-cys (5 mM) causes a spectral change (Fig. 4.4) within instrumental and mixing dead time (20 seconds), and results in a broad peak centered around 470 nm that resembles that of an  $\alpha$ -aminoacrylate species observed in O-acetylserine sulfhydrylases (21) and tryptophan synthase (17). This spectrum remained stable over a period of 30 min. When indole was added (0.4 mM) to this reaction the 470 nm species disappeared within the dead time and red shifted to resemble that of a tryptophan external aldimine (425 nm). Interestingly, a similar experiment with L-ser (5 mM) showed no appreciable spectra change until the L-ser concentration exceeded 70 mM (not shown). An HPLC and LC-MS analysis of the PfTrpB2 L-cys + indole and L-ser + indole reactions confirmed that tryptophan had indeed been produced in these assays. Since the reaction that yields tryptophan from L-ser and indole has been previously examined in *T. maritima* and *S. solfataricus* TrpB2s (7, 8), we conducted experiments to characterize the PfTrpB2 L-ser reaction and make a comparison of the catalytic efficiencies and binding affinities with those reported. Yet, during our analysis we noted a divergence from classic initial rate vs [S] behavior at high concentrations of L-ser (Fig. 4.5A). In these experiments we observed that reaction rates continued to increase in a linear fashion at substrate concentrations that exceeded 1M (Fig. 4.5A), a behavior characteristic of substrate activation kinetics. Indeed, these data showed a non-linear trend in a  $v$  vs.  $v/[S]$  plot (Fig. 4.5A inset), suggesting that a Michaelis-Menten equation could not be accurately used to fit these data. To confirm these observations we applied the Michaelis-Menten treatment and found an estimated  $K_m$  for L-ser of  $432 \pm 38$  mM. Yet, as can be seen in Fig. 4.5A (dashed line), this strategy does not provide an accurate fit for data measured in the PfTrpB2 L-ser reaction. Instead, a better fit is obtained when a substrate

activation equation is used (eq. 1) (22, 23). This results in a decrease of the estimation in  $K_m$  for L-ser to a value of  $6.0 \pm 1.7$  mM.

$$v = \frac{V_{\max} [A](1 + \beta[A]/K_A)}{K_m(1 + \beta[A]/K_A) + [A](1 + [A]/K_A)} \quad (1)$$

In an analogous manner, the PfTrpB2 L-cys + indole reaction displays substrate activation kinetics and requires the utilization of eq. 1 to satisfactorily fit these data (Fig 4.5B). In these assays, high L-cys concentrations had to be measured using the HPLC analytical method since the spectrophotometric assay shows a large background change in UV absorbance without the addition of enzyme. We speculate that this is due to the formation of a disulfide bond from the oxidation of L-cys into cystine. A similar background absorbance change is observed if DTT is used as a reducing agent and thus cannot be used in these assays. At low L-cys concentrations (Figure 4.5B inset) this problem can be averted by the addition of TCEP (tris(2-Carboxyethyl) phosphine), yet because TCEP must be pH adjusted prior to use with the appropriate base (LiOH in these assays), addition of a stoichiometric amount (to one half of L-cys concentration in assay) inevitably adds large amounts of the corresponding salt. For this reason, only the low L-cys concentrations can be measured with the UV method, whereas the HPLC method is more accurate for high L-cys concentrations. Unlike the L-ser experiments, the highest concentration of L-cys that can be measured is largely limited by the solubility of this amino acid. Thus, the highest L-cys concentration for which rates were obtained is 128 mM. Data obtained by both methods correlates to within 8% in the estimation of  $V_{\max}$  and  $k_{\text{cat}}$  (not shown). The estimated L-cys  $K_m$  calculated by fitting these data with a Michaelis-Menten equation was  $29.3 \pm 2$  mM, and when the substrate activation equation was used this value was estimated at  $7.1 \pm 0.6$  mM. As the

results in Table 4.2 suggest, PfTrpB2 has no appreciable preference (within experimental error) for L-cys or L-ser.

### **L-Cys Binding Affinities in TrpB1 and TrpAB1**

Based on our observations of the L-ser/L-cys substrate specificity and catalytic efficiencies in PfTrpB2, and considering that no reports regarding the L-cys binding affinities in other TrpB1s were available at the time this manuscript was prepared, we deemed it necessary to establish a contextual L-ser/L-cys specificity profile among StTrpB1, StTrpAB1, PfTrpB1, and PfTrpAB1. In these experiments, all L-cys and L-ser initial rate vs [S] data could be satisfactorily fit with a Michaelis-Menten equation (Fig. 4.6). Yet, in an effort to ensure that the L-cys profiles were not undergoing substrate activation we also fit these data to eq. 1. Although these results (not shown) showed that  $K_m$  and  $V_{max}$  values calculated with either method were similar, the statistics for substrate activation treatment had poor statistics and were thus not used for any calculations.

The results of the kinetic analysis of these reactions, summarized in Table 4.2, show that the StTrpAB1 complex has a binding affinity for L-cys (1.57 mM) that is comparable to that of L-ser (0.9 mM). Yet, overall turnover for the L-cys dependent reaction is 31-fold slower, equating to a difference in catalytic efficiency ( $k_{cat}/K_m$ ) of more than 52-fold in favor for L-ser as a substrate. The primary contribution to this large difference in substrate specificity appears to be stimulation of the L-ser reaction by StTrpA. This can be more clearly seen by comparing the overall activation ratios for L-cys and L-ser between StTrpB1 and StTrpAB1. In the presence of StTrpA, StTrpB1 has an overall 22-fold activation for the L-ser reaction, whereas that for L-cys is only increased three-fold. This is further reflected by a comparison of the L-ser and L-cys catalytic efficiencies among StTrpB1 and StTrpAB1. In the case of L-ser, the StTrpAB1

complex is 70-fold more efficient than StTrpB1 alone, yet the L-cys reaction shows only 30-fold ratio difference. Similarly, the PfTrpAB1 complex shows an overall catalytic efficiency for the L-ser reaction 71-fold larger than that for L-cys. Yet, in this complex the primary contribution originates from a 100-fold higher binding affinity for L-ser than for L-cys. Unlike StTrpA which greatly enhances the catalytic efficiency of the StTrpB1 reaction, PfTrpA only increases that of PfTrpB1 by a factor of seven. PfTrpA slightly (3-fold) stimulates the PfTrpB1 L-ser turnover, and increases the binding affinity by a factor of two. Individually, PfTrpB1 is ten times more efficient than StTrpB1 for both L-ser and L-cys reactions.

### **Conclusion**

The PfTrpB2 structure reveals that many of the features important for the allosteric communication between subunits in the canonical tryptophan synthase are not structurally conserved in PfTrpB2. For example, an important aspect of the allosteric communication that has been observed to occur between  $\alpha$  and  $\beta$  subunits in these enzymes is the formation of salt bridges and hydrogen bonds (24, 25) that stabilize open and closed forms of the tetrameric complex. These conformational states appear to be tightly regulated in order to limit the amount of indole that is released into the solvent environment and increase the catalytic efficiency of the reaction (26-28). In StTrpB1, Lys-167 has been identified as one of the primary protagonists in this role by forming a salt bridge with the TrpA Asp-56 that stabilizes the closed conformation of the  $\alpha$ -subunit (16, 28, 29), and stimulates a conformational change of the  $\beta$ -subunit into an open state. Although sequence analysis had revealed the absence of a conserved lysine at this position in PfTrpB2 (5), the structure of PfTrpB2 reveals that a structurally homologous residue is not present at this position. Furthermore, analysis of the contacts at this region reveals that the residue occupying the position analogous to Lys-167 in StTrpB1, Gly-205, is in fact involved in

a hydrogen bond interaction with the side chain of Ser-309 (3.66 Å). Thus, the hydrogen bond between Gly-205 and Ser-309 effectively maintains the “closed” tunnel conformation in PfTrpB2. Yet, a structural superposition with a known closed conformation of TrpB1 (PDB accession no. 1A5S) reveals a 3.8 Å difference between the  $\alpha$ -carbons of Lys-167 and Gly-205, as well as most COMM domain residues (25, 30) involved in closing the TrpB1 tunnel. This suggests that it is likely that PfTrpB2 has an alternative closure mechanism not linked to an external signal, but rather one that is internal in origin. This is consistent with the observation that these enzymes do not form complexes or are activated by TrpA subunits (7, 8).

The characterization of the kinetic properties of PfTrpB2 reveals a previously unidentified reaction among tryptophan synthases in which L-cys is used with the same catalytic efficiency as serine for the biosynthesis of tryptophan. Also, this work has shown that this reaction is unique to TrpB2s since TrpAB1s and TrpB1s have at least a ten fold preference for L-ser as substrate in this reaction. Additionally, we have characterized a novel behavior among tryptophan synthases that displays substrate activation with both L-ser and L-cys. This observation has allowed us to accurately measure the binding affinities of these substrates and gain a better understanding of the function of these enzymes. Our results indicate that the PfTrpB2 is a tryptophan synthase that can non-preferentially catalyze the condensation of indole with L-ser or L-cys.

## References

1. Miles, E. W. (2001) *Chem Rec* 1, 140-51.
2. Crawford, I. P. & Ito, J. (1964) *Proc Natl Acad Sci U S A* 51, 390-7.
3. Kayastha, A. M. & Miles, E. W. (1991) *Anal Biochem* 193, 200-3.
4. Sato, S., Kotani, H., Nakamura, Y., Kaneko, T., Asamizu, E., Fukami, M., Miyajima, N. & Tabata, S. (1997) *DNA Res* 4, 215-30.
5. Xie, G., Forst, C., Bonner, C. & Jensen, R. A. (2002) *Genome Biol* 3, RESEARCH0004.
6. Xie, G., Keyhani, N. O., Bonner, C. A. & Jensen, R. A. (2003) *Microbiol Mol Biol Rev* 67, 303-42, table of contents.
7. Hettwer, S. & Sterner, R. (2002) *J Biol Chem* 277, 8194-201.
8. Leopoldseder, S., Hettwer, S. & Sterner, R. (2006) *Biochemistry* 45, 14111-9.
9. Clark, V. L., Peterson, D. E. & Bernlohr, R. W. (1972) *J Bacteriol* 112, 715-25.
10. Xie, Y. & Reeve, J. N. (2005) *J Bacteriol* 187, 6419-29.
11. Hioki, Y., Ogasahara, K., Lee, S. J., Ma, J., Ishida, M., Yamagata, Y., Matsuura, Y., Ota, M., Ikeguchi, M., Kuramitsu, S. & Yutani, K. (2004) *Eur J Biochem* 271, 2624-35.
12. Schneider, T. R., Gerhardt, E., Lee, M., Liang, P. H., Anderson, K. S. & Schlichting, I. (1998) *Biochemistry* 37, 5394-406.
13. Krissinel, E. & Henrick, K. (2004) *Acta Crystallogr D Biol Crystallogr* 60, 2256-68.
14. Lee, S. J., Ogasahara, K., Ma, J., Nishio, K., Ishida, M., Yamagata, Y., Tsukihara, T. & Yutani, K. (2005) *Biochemistry* 44, 11417-27.
15. Hyde, C. C., Ahmed, S. A., Padlan, E. A., Miles, E. W. & Davies, D. R. (1988) *J Biol Chem* 263, 17857-71.

16. Ferrari, D., Niks, D., Yang, L. H., Miles, E. W. & Dunn, M. F. (2003) *Biochemistry* 42, 7807-18.
17. Ferrari, D., Yang, L. H., Miles, E. W. & Dunn, M. F. (2001) *Biochemistry* 40, 7421-32.
18. Yanofsky, C., and Crawford, I. P. (1972) *The Enzymes*, Academic Press, New York).
19. Yang, L., Ahmed, S. A., Rhee, S. & Miles, E. W. (1997) *J Biol Chem* 272, 7859-66.
20. Murdock, D., Ensley, B. D., Serdar, C. & Thalen, M. (1993) *Biotechnology (N Y)* 11, 381-6.
21. Tai, C. H., Nalabolu, S. R., Simmons, J. W., 3rd, Jacobson, T. M. & Cook, P. F. (1995) *Biochemistry* 34, 12311-22.
22. Eriksson, H. & Augustinsson, K. B. (1979) *Biochim Biophys Acta* 567, 161-73.
23. Tormos, J. R., Wiley, K. L., Seravalli, J., Nachon, F., Masson, P., Nicolet, Y. & Quinn, D. M. (2005) *J Am Chem Soc* 127, 14538-9.
24. Rhee, S., Parris, K. D., Ahmed, S. A., Miles, E. W. & Davies, D. R. (1996) *Biochemistry* 35, 4211-21.
25. Bahar, I. & Jernigan, R. L. (1999) *Biochemistry* 38, 3478-90.
26. Dunn, M. F., Aguilar, V., Brzovic, P., Drewe, W. F., Jr., Houben, K. F., Leja, C. A. & Roy, M. (1990) *Biochemistry* 29, 8598-607.
27. Brzovic, P. S., Sawa, Y., Hyde, C. C., Miles, E. W. & Dunn, M. F. (1992) *J Biol Chem* 267, 13028-38.
28. Brzovic, P. S., Ngo, K. & Dunn, M. F. (1992) *Biochemistry* 31, 3831-9.
29. Brzovic, P. S., Hyde, C. C., Miles, E. W. & Dunn, M. F. (1993) *Biochemistry* 32, 10404-13.

30. Rhee, S., Parris, K. D., Hyde, C. C., Ahmed, S. A., Miles, E. W. & Davies, D. R. (1997) *Biochemistry* 36, 7664-80.
31. Studier, F. W. (2005) *Protein Expr Purif* 41, 207-34.
32. Luft, J. R., Collins, R. J., Fehrman, N. A., Lauricella, A. M., Veatch, C. K. & DeTitta, G. T. (2003) *J Struct Biol* 142, 170-9.
33. Chayen, N. E., Shaw Stewart, P. D. & Blow, D. M. (1992) *J. Crystal Growth* 122, 176-180.
34. Use of the Advanced Photon Source was supported by the U. S. Department of Energy, O. o. S., Office of Basic Energy Sciences, under Contract No. W-31-109-Eng-38.
35. Otwinowski, Z. & Minor, W. (1997) *Methods Enzymol* 276, 307-326.
36. McCoy, A. J., Grosse-Kunstleve, R. W., Storoni, L. C. & Read, R. J. (2005) *Acta Crystallogr D Biol Crystallogr* 61, 458-64.
37. Storoni, L. C., McCoy, A. J. & Read, R. J. (2004) *Acta Crystallogr D Biol Crystallogr* 60, 432-8.
38. Read, R. J. (2001) *Acta Crystallogr D Biol Crystallogr* 57, 1373-82.
39. Potterton, E., Briggs, P., Turkenburg, M. & Dodson, E. (2003) *Acta Crystallogr D Biol Crystallogr* 59, 1131-7.
40. McRee, D. E. (1999) *J Struct Biol* 125, 156-65.
41. Murshudov, G. N., Vagin, A. A. & Dodson, E. J. (1997) *Acta Crystallogr D Biol Crystallogr* 53, 240-55.
42. Cowtan, K. (1994) 31, 34-38.
43. Terwilliger, T. C. (2003) *Acta Crystallogr D Biol Crystallogr* 59, 38-44.
44. Emsley, P. & Cowtan, K. (2004) *Acta Crystallogr D Biol Crystallogr* 60, 2126-32.

45. Miles, E. W. & McPhie, P. (1974) *J Biol Chem* 249, 2852-7.
46. Wilson, D. A. & Crawford, I. P. (1965) *J Biol Chem* 240, 4801-8.
47. Faeder, E. J. & Hammes, G. G. (1970) *Biochemistry* 9, 4043-9.

**Table 4.1.** Summary of Crystallographic Analysis

space group	<i>C</i> 2
resolution range (outer shell) Å	50-2.25 (2.33-2.25)
no. of reflections (outer shell)	36262 (2289)
R <sub>factor</sub> (outer shell)	0.1921
R <sub>free</sub> <sup>a</sup> (outer shell)	0.23108
R <sub>sym</sub> (outer shell)	0.083 (0.027)
mean <i>B</i> value (Å <sup>2</sup> )	43.72
rmsd from ideal geometry	
bond angles (deg)	1.4°
bond distances (Å)	0.012
Ramachandran plot residues (%)	98.2/1.8/0
in favored/allowed/disallowed regions	

<sup>a</sup>R<sub>free</sub> calculated with 5.1% of the total data that were excluded from refinement.

**Table 4.2.** Summary of kinetic constants measured for the tryptophan synthases from *S.typhimurium* and *P. furiosus*. Assays were performed as described in Materials and Methods.  $K_m$  and  $V_{max}$  for PfTrpB2 L-ser and L-cys reactions were calculated using eq. 1 described in the text. All other data were fit to a Michaelis-Menten equation. All fits were performed with prism (GraphPad).

Enzyme	L-Ser			L-Cys			Ratio	Preference
	kcat ( $s^{-1}$ )	$K_m$ (M)	kcat/ $K_m$ ( $M^{-1} s^{-1}$ )	kcat ( $s^{-1}$ )	$K_m$ (M)	kcat/ $K_m$ ( $M^{-1} s^{-1}$ )		
StTrpAB1	3.17	$0.9 \times 10^{-3}$	3254	0.1	$1.59 \times 10^{-3}$	62	52	Serine
StTrpB1	0.14	$3 \times 10^{-3}$	46	0.03	$8.68 \times 10^{-3}$	3.4	11	Serine
PfTrpAB1	0.48	$0.14 \times 10^{-3}$	3428	0.67	$14.06 \times 10^{-3}$	48	71	Serine
PfTrpB1	0.15	$0.32 \times 10^{-3}$	468	0.31	$6.9 \times 10^{-3}$	44	11	Serine
PfTrpB2	0.13	$6 \times 10^{-3}$	16	0.11	$7 \times 10^{-3}$	15	1	None

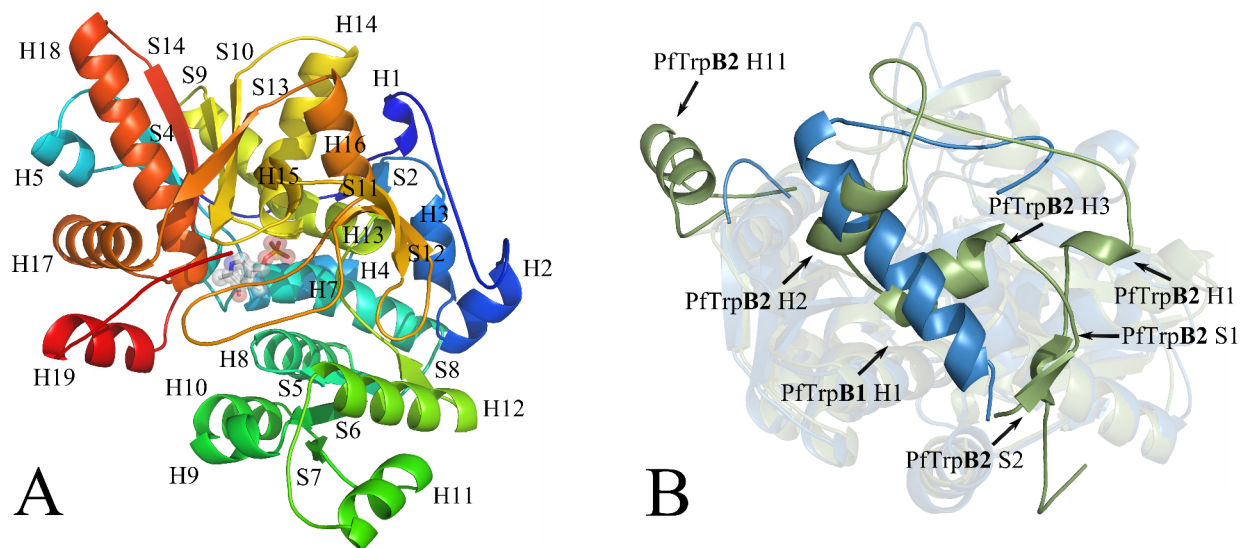


**Figure 4.1.** **A)** PfTrpB2 monomer with secondary structure elements labeled. **B)** Secondary structure differences between the PfTrpB2 (colored dark green) and the StTrpB1 (colored navy blue, PDB accession no. **1QOQ**). The PfTrpB2 H11  $\alpha$ -helix is an extension of residues between the S7 and H12 secondary structure elements of the COMM (12) domain.

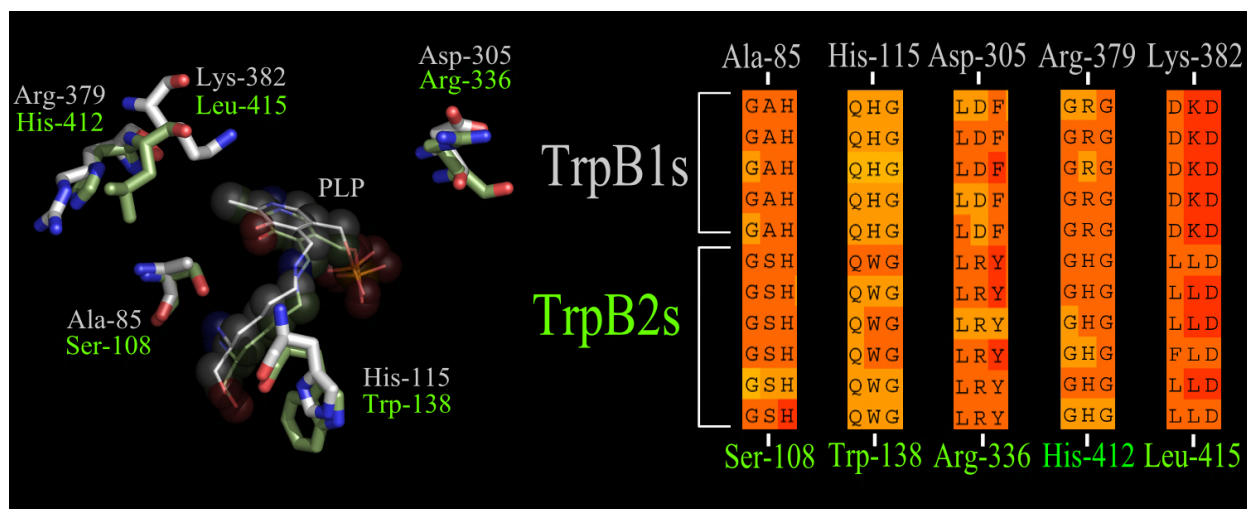


**Figure 4.2.** A structural superposition between the PfTrpB2 (bonds and labels green) and PfTrpB1 (bonds and labels white, PDB accession no. **QOQ**) identifies substitutions among residues surrounding the PLP cofactor. On the right hand side, a sequence alignment between TrpB2s and TrpB1s reveals that these substitutions are strictly conserved among each tryptophan synthase  $\beta$ -subunit subclass.

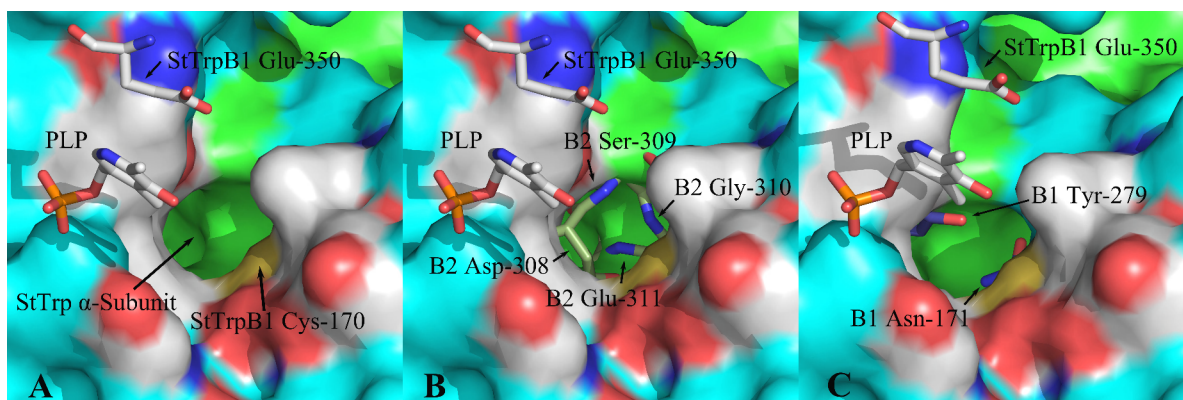


**Figure 4.3.** **A)** The StTrpAB1 complex has an intramolecular tunnel through which indole is diffused from the  $\alpha$ -subunit (electrostatic surface colored green) to the  $\beta$ -subunit (electrostatic surface colored CPK and blue) active sites (only PLP and StTrpB1 Glu-350 are shown, sticks, white bonds, surfaces for residues 86-125 and 359-433 have not been calculated for clarity). **B)** Upon superposition of StTrpAB1 and PfTrpB2, the StTrpB1 tunnel entrance is occluded by PfTrpB2 residues 308-311(residues labeled with prefix B2, sticks, green bonds). **C)** In this panel, StTrpAB1 in a closed conformation (PDB accession no. **1A5S**) was structurally superposed with **1QOQ** to illustrate the tunnel closure by the side chains StTrpAB1  $\beta$ -subunit residues Asn-171 and Tyr-279 (labeled with prefix B1, sticks, blue bonds).

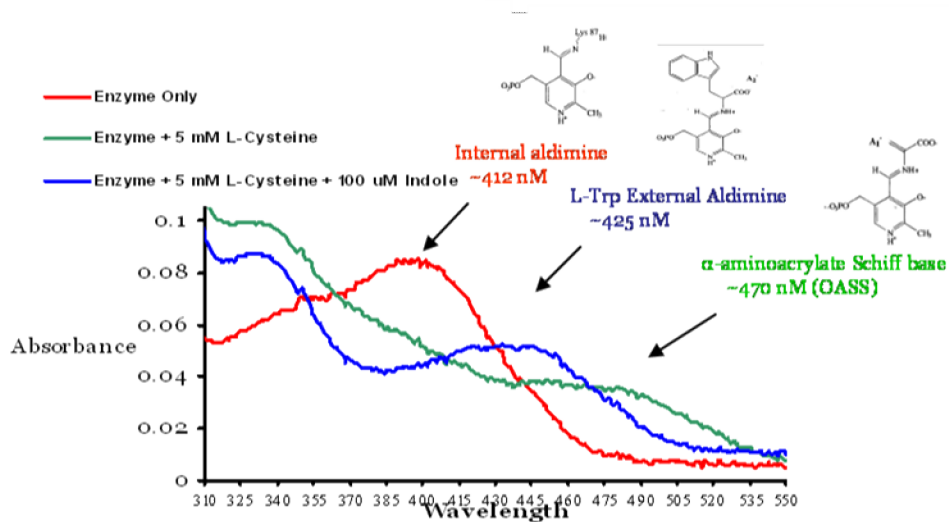


**Figure 4.4.** Spectral changes associated with the sequential addition of 5 mM L-L-cys, and 0.1 mM indole, to a solution containing PfTrpB2 (4  $\mu\text{M}$ ) and 50 mM KPi pH 8.0 at 95° C. Intermediates associated with the spectroscopic features observed after the addition of L-cys and indole are marked.

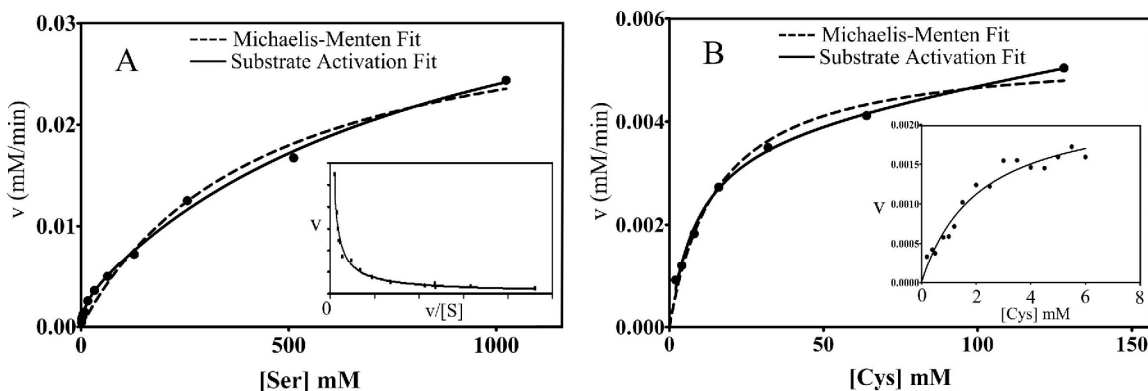


**Figure 4.5.** **A)** Initial rate vs  $[S]$  plot of a reaction containing PfTrpB2, indole (0.2 mM), and varying concentrations of L-ser (UV assay, 95 °C, 50 mM KPi, 100 mM LiCl). High L-ser concentrations (>15 mM) showed significant substrate activation and an overall non-linear  $v$  vs  $v/[S]$  plot (inset), which indicate deviation from classic Michaelis-Menten behavior. Data were fit to Michaelis-Menten (dashed line) and substrate activation equations (non-dashed line). **B)** Initial rate vs  $[S]$  plots for a reaction containing PfTrpB2, indole (0.2 mM), and varying concentrations of L-cys (HPLC method, 95 °C, 50 mM KPi, 100 mM LiCl). Data were fit to Michaelis-Menten (dashed line) and substrate activation equations (non-dashed line). The inset in this panel contains data for initial rates measured at L-cys concentrations below 6 mM by the UV assay method and were performed under similar conditions (95 °C, 50 mM KPi, 100 mM LiCl).

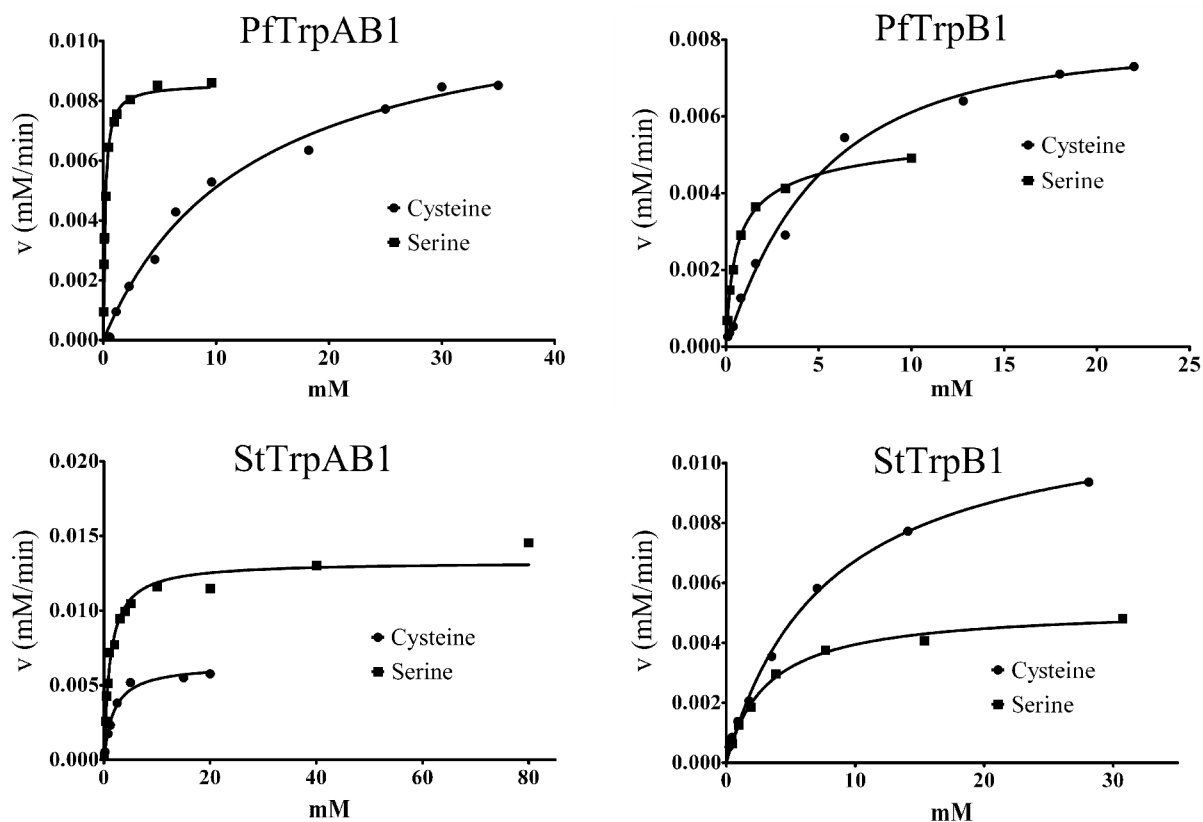


**Figure 4.6.** Initial rate  $v$  vs  $[S]$  profiles for the L-ser/L-cys + indole condensation catalyzed by PfTrpB1, PfTrpAB1, StTrpAB1, and StTrpB1. The PfTrpAB1 and PfTrpB1 reactions were characterized by the UV method at 80 °C and contained 50 mM KPi (pH 8), 0.5 mM indole, and L-cys reactions contained 10 mM TCEP. The StTrpAB1 and StTrpB1 reactions were characterized by the UV method at 37 °C and contained 50 mM KPi (pH 8), 0.5 mM indole, and L-cys reactions contained 10 mM TCEP.

## CONCLUSIONS

### **Kynureninase**

Like other members of the PLP-dependent  $\alpha$ -family, kynureninase appears to undergo conformational changes during catalysis. In this work, two regions in the small and large domains are identified that could play a role in opening and closing the active site cavity: the small domain S20-S21  $\beta$ -hairpin, and the large domain S15-S16loop. The S20-S21  $\beta$ -hairpin in particular emerges as a dynamic region since a structural superposition between Hkyn and several aminotransferases reveals that the difference in the S20-S21  $\beta$ -hairpin conformational states observed between kynureninases is also clearly visible with other members of the  $\alpha$ -family (Figure 1.7). Based on the structural superposition, it appears that the conformation of the conserved Arg-434 in Hkyn is a function of the positioning of the small domain, in particular that of the S20-S21  $\beta$ -hairpin. Furthermore, the conformational changes required to position the Hkyn S20-S21  $\beta$ -hairpin, Arg-434, and small domain elements closer to active site residues would be very similar to the movements observed between aspartate aminotransferase open and closed conformational states. Indeed, the conformation of Arg-434 in the kynureninase-3-hydroxyhippuric acid inhibitor complex (Figure 2.1 and 2.2) resembles that seen in ligand bound aspartate aminotransferases. Although the small domains of kynureninases and aspartate aminotransferases do not superimpose well, in part due to a difference in length between the small-large domain linker  $\alpha$ -helix, the relative motion that must be undertaken by the entire small domain is very similar between the AAT open/closed and Pkyn/Hkyn pairs (Figure 1.8). Even though the small domain movements in aspartate aminotransferase are much more pronounced, it

is possible that neither the Pkyn or Hkyn structures demonstrate a fully closed/open state, but rather an intermediate between them. Thus, the investigation of new kynureninase conformational states presents an interesting avenue of research.

The kynureninase-3-hydroxyhippuric acid inhibitor complex allowed the identification of residues involved in conveying substrate specificity to these enzymes. The primary residues in this mechanism appear to be His-102 and Asn-333. Characterization of the kynureninase mutant H102W/N333T revealed only a small increase in binding affinity for L-kyn, yet a sufficiently large change in  $k_{\text{cat}}/K_m$  for 3-OH-kyn which resulted in the lack of any measurable activity with this substrate. Thus, removing the hydrogen bonding partner at the  $\gamma$  position of Asn-333, increasing the local non-polar environment, and introducing a large bulky side chain (Trp-102) effectively act to exclude any 3-OH-kyn binding at the concentrations measured. This suggests that these residues (Asn-333 and His-102) are the primary substrate specificity contacts for the 3' substituent on the kynurenine aromatic ring. In order to further probe which residues contribute to catalytic efficiency, a third mutation was introduced, S332G, a residue showing a conserved pattern among orthologs utilizing L-kyn or 3-OH-kyn similar to that of His-102 and Asn-333. The residue at this position hydrogen bonds through the backbone amide nitrogen with one of the PLP phosphate moiety oxygens, and in the complex presented in Chapter 2 it does not hydrogen bond or have electrostatic contacts with atoms in 3-HHA. H102W/S332G/N333T mutants had the strongest binding affinity and catalytic efficiency towards L-kyn of all mutants studied, and showed no activity with 3-OH-kyn. From these results, it can be inferred that the increased backbone elasticity provided by Gly-332 imparts flexibility to the interaction between Thr-333 and the bulky side chain of Trp-102, allowing a better fit of L-kyn within the mutant Hkyn active site cavity. Furthermore, this suggests that two shells of residues surrounding ligand atoms

determine catalytic efficiency; one directly contacting ligand atoms, and another contributing to the geometrical arrangement of the active site and playing a dynamic role in catalysis as opposed to a mechanistic one.

### **L-Aspartate- $\beta$ -Decarboxylase**

A number of studies have shown that the ABDC catalyzed decarboxylation of L-aspartate inverts the configuration of L-aspartate C- $\beta$  protons while retaining absolute configuration about C- $\alpha$ , suggesting that two bases are involved. One required for the removal/addition of the  $\alpha$ -proton on the *si*-side of the external aldimine/quinonoid intermediate, and the second base adding a proton to C- $\beta$  on the *re*-side of the enamine. Assuming, as do other members of the PLP-dependent aminotransferase family, that the Schiff base forming lysine abstracts the  $\alpha$ -proton and reprotonates at C-4' to form the ketimine intermediate, the identity of the second base remains unknown.

In the crystal structure presented in this work, the *re*-side of the PLP cofactor and the aldimine nitrogen are closely flanked by the side chain of the strictly conserved Arg-37, making Arg-37 a likely candidate for the second catalytic base. The kinetic analysis showed that R37A mutants have a 24-fold reduction in  $k_{\text{cat}}/K_m$  for L-aspartate as compared to Wt ABDC, which indicates that this residue plays some role in catalysis. Yet, a number of different scenarios can be considered which are consistent with these results: **1)** Arg-37 is not directly involved in reprotonating the L-aspartate enamine and thus a very large change in catalytic efficiency is not observed, **2)** the mutation affects the catalytic cycle at a non-rate limiting step, or **3)** protonation at the enamine C- $\beta$  is much faster than the rate-limiting step, and the mutation does not affect this rate sufficiently to be observed in the steady state. Further characterization of ABDC is needed to confirm these possibilities.

Structure-structure and sequence based comparisons reveal that ABDC is most closely related to aspartate aminotransferase-like enzymes. However, no PLP-dependent transferase contains a domain homologous to the ABDC oligomerization domain, nor does any transferase use an oligomerization scheme similar to that used by this enzyme.

Conformational and structural details in this crystal structure do not clearly reveal the functional role of the dodecameric assembly with respect to catalysis. Although it has been previously determined that ABDC will partially dissociate into a mixture of dodecamer/dimers and lose activity as the pH increases, it is not clear whether this effect is primarily due to a pH dependence on catalytic activity, or if the effect is due to a structural rearrangement of the particle into a low activity conformational state. It is also possible that the modular assembly/disassembly of ABDC in response to pH changes is a form of regulation by intracellular proton concentrations- all controlled by interactions between residues within the oligomerization domain.

### ***P. furiosus* Tryptophan Synthase $\beta$ -Subunit Homolog**

The PfTrpB2 structure reveals that many of the features important for the allosteric communication between subunits in the canonical tryptophan synthase are not structurally conserved in PfTrpB2. For example, an important aspect of the allosteric communication that has been observed to occur between  $\alpha$  and  $\beta$  subunits in these enzymes is the formation of salt bridges and hydrogen bonds that stabilize open and closed forms of the tetrameric complex. These conformational states appear to be tightly regulated in order to limit the amount of indole that is released into the solvent environment, and increase the catalytic efficiency of the reaction. In StTrpB1, Lys-167 has been identified as one of the primary protagonists in this role by forming a salt bridge with the TrpA Asp-56 that stabilizes the closed conformation of the  $\alpha$ -

subunit, and stimulates a conformational change of the  $\beta$ -subunit into an open state. Although sequence analysis had revealed the absence of a conserved lysine at this position in PfTrpB2, the structure of PfTrpB2 reveals that a structurally homologous residue is not present at this position. Furthermore, analysis of the contacts at this region reveals that the residue occupying the position analogous to Lys-167 in StTrpB1, Gly-205, is in fact involved in a hydrogen bond interaction with the side chain of Ser-309 (3.66 Å). Thus, the salt bridge between Gly-205 and Ser-309 effectively maintains the “closed” tunnel conformation in PfTrpB2. Yet, a structural superposition with a known closed conformation of TrpB1 reveals a 3.8 Å difference between the  $\alpha$ -carbons of Lys-167 and Gly-205, as well as most COMM domain residues involved in closing the TrpB1 tunnel. This suggests that it is likely that PfTrpB2 has an alternative closure mechanism not linked to an external signal, but rather one that is internal in origin. This is consistent with the observation that these enzymes do not form complexes or are activated by TrpA subunits.

The characterization of the kinetic properties of PfTrpB2 reveals a previously unidentified reaction among tryptophan synthases in which L-cys is used with the same catalytic efficiency for the biosynthesis of tryptophan. Also, this work has shown that this reaction is unique to TrpB2s since TrpAB1s and TrpB1s have at least a ten-fold preference for L-ser as substrate in this reaction. Additionally, a novel behavior among tryptophan synthases that displays substrate activation with both L-ser and L-cys has been characterized in this work. This observation has allowed to accurately measure the binding affinities of these substrates and gain a better understanding of the function of these enzymes. The results of this analysis indicate that the PfTrpB2 is a tryptophan synthase that can non-preferentially catalyze the condensation of indole with L-ser or L-cys.